

Old Dominion University

ODU Digital Commons

Electrical & Computer Engineering Theses & Dissertations

Electrical & Computer Engineering

Summer 2004

Fuzzy Modeling of Electromagnetic Emissions from Portable Electronic Devices Onboard Commercial Aircraft

Madiha Jamil Jafri
Old Dominion University

Follow this and additional works at: https://digitalcommons.odu.edu/ece_etds



Part of the [Electrical and Electronics Commons](#), [Electromagnetics and Photonics Commons](#), and the [Programming Languages and Compilers Commons](#)

Recommended Citation

Jafri, Madiha J.. "Fuzzy Modeling of Electromagnetic Emissions from Portable Electronic Devices Onboard Commercial Aircraft" (2004). Master of Science (MS), Thesis, Electrical & Computer Engineering, Old Dominion University, DOI: 10.25777/hydw-zq56
https://digitalcommons.odu.edu/ece_etds/380

This Thesis is brought to you for free and open access by the Electrical & Computer Engineering at ODU Digital Commons. It has been accepted for inclusion in Electrical & Computer Engineering Theses & Dissertations by an authorized administrator of ODU Digital Commons. For more information, please contact digitalcommons@odu.edu.

**FUZZY MODELING OF ELECTROMAGNETIC EMISSIONS FROM
PORTABLE ELECTRONIC DEVICES ONBOARD COMMERCIAL AIRCRAFT**

by

Madiha Jamil Jafri

B.Sc. December 2003, Old Dominion University, Norfolk, Virginia

A Thesis Submitted to the Faculty of
Old Dominion University in Partial Fulfillment of
the Requirement for the Degree of

MASTER OF SCIENCE

ELECTRICAL ENGINEERING

OLD DOMINION UNIVERSITY

August 2004

Approved by: _____

Dr. Linda Vahala (Director)

Dr. Ravindra Joshi (Member)

Dr. Frederic McKenzie (Member)

Mr. Jay J. Ely (Member)

ABSTRACT

FUZZY MODELING OF ELECTROMAGNETIC EMISSIONS FROM PORTABLE ELECTRONIC DEVICES ONBOARD COMMERCIAL AIRCRAFT

Madiha Jamil Jafri
Old Dominion University, 2004
Director: Dr. Linda Vahala

The use of Portable Electronic Devices (PEDs) is prohibited during take-off and landing of an aircraft because PEDs may emit signals that can interfere with the aircraft's navigation and communication systems. The electromagnetic interference (EMI) on the aircraft's electronics due to PEDs emissions is examined for Boeing 737 and 747 aircraft. This work, funded by the NASA Graduate Researchers Program, uses Interference Path Loss (IPL) data, collected by researchers from NASA Langley Research Center, Eagles Wings Inc. and United Airlines on several out-of-service United B737 and B747 airplanes.

B737 and B747 IPL data has been analyzed using a graphical analysis of the EMI patterns. Graphical comparisons of horizontal and vertical polarizations as well as comparison of the EMI patterns from Biconical versus Dipole antennas are made. Data accuracy is measured by comparing graphs from B737 (#1989) versus B737 (#1997). The necessity of taking IPL data on the entire plane, instead of just the windows is proven by a graphical and statistical comparison of the results. Statistical analysis on the data is also performed using MATLAB and Arena. Aircraft symmetry is tested in terms of EMI patterns. The graphical analysis of mitigation techniques, which consists of sealing the door and exit seams as well as taping of windows, is performed. Following the graphical and statistical analysis, a detailed model involving Fuzzy logic is examined.

This thesis is dedicated to my parents Jamil Jafri and Ghazala Jafri.
I couldn't have come this far without their prayers, love, guidance and tremendous support.

ACKNOWLEDGMENTS

There are many people who have contributed to the successful completion of this thesis. I would like to extend a special thanks to my advisor, Dr. Linda Vahala for her support, guidance and patience throughout my research. I would also like to thank Dr. Ravindra Joshi and Dr. Frederic McKenzie for being an important part of my defense committee. This research could not have progressed this far without the hard work and tremendous support by Mr. Ely. I would like to sincerely thank him for all his time spent in editing the conference papers, and for having the patience to teach me the fundamental concepts behind this research. Mr. Ely, who served as my mentor at NASA, was instrumental in defining the research problems on which I have concentrated.

I would also like to extend a special thanks to the following HIRF Lab Team at NASA Langley Research Center for their continuous support: Mr. Truong Nguyen, Mrs. Sandra Koppen, Dr. John Beggs, Miss. Teresa Salud, Mr. Daniel Koppen, and Ms. Laura Smith. I specifically wish to thank Mr. Rudy Williams for not only his guidance, but also for making this research possible by providing the necessary funding as well as fulfilling the computer equipment and software needs.

I am grateful to the personnel in United Airlines, Eagles Wings Inc. and NASA's Aviation Safety Program whose joint partnership enabled me to obtain the useful data analyzed throughout this thesis. I thank Mr. Gerald L. Fuller for his previous analysis of the data upon which this work builds. I also thank Mr. Brain Eppic and other Engineers from Delta Airlines for providing me with the necessary schematics for research purposes.

Last but not least, I would like to thank my family for their belief in my abilities that kept me determined, and for their immense assistance, love and support in all other aspects of life: Jamil and Ghazala Jafri, Faiza, Mehdi, Faraz, Anika, Osman, Amber, and Reda. I also appreciate the support provided by my aunts, uncles and cousins. A special thanks to my college friends, Rob Shell, Bryan Robinson and Fatemah Al-Douli for being incredibly supportive in times of stress. And finally, I am very grateful for the help, patience and support from my fiancé, Hamid, and his family.

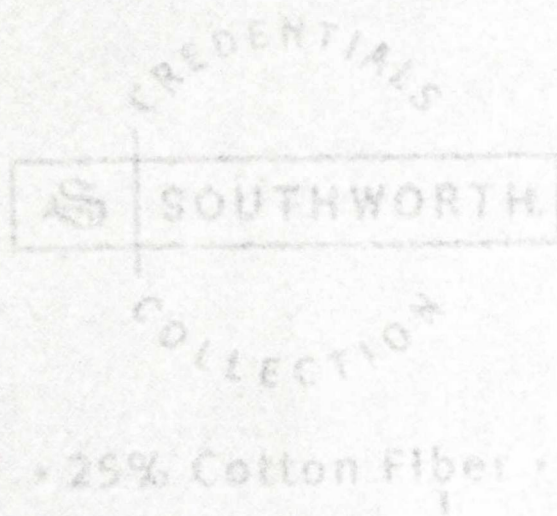


TABLE OF CONTENTS

Page

1	RESEARCH MOTIVATION AND OVERVIEW	1
1.1	INTRODUCTION TO PROBLEM	1
1.2	CLASSIFICATION OF PORTABLE ELECTRONIC DEVICES	3
1.3	GOVERNING REGULATIONS AND ADVISORY MATERIALS.....	6
1.4	AIRLINE REGULATIONS ON PEDS	10
1.5	STATISTICS AND REPORTS OF ACCIDENTAL PED USAGE	15
1.6	RESEARCH OVERVIEW	24
2	INTRODUCTION TO AIRCRAFT SYSTEMS AND TESTING METHODOLOGIES.....	26
2.1	REASONS FOR VULNERABILITY OF AIRCRAFT SYSTEMS DUE TO PED-RELATED EMISSIONS	26
2.2	FREQUENCY BAND INFORMATION OF AIRCRAFT SYSTEMS OF CONCERN.....	29
2.3	SIGNAL LEAKAGE FROM PEDS AND COUPLING TO AIRCRAFT SYSTEMS.....	31
2.4	DB TUTORIAL	33
2.5	INTERFERENCE PATH LOSS TESTING METHODOLOGY.....	36
3	DETAILED AIRCRAFT SCHEMATICS AND DATA INTERPOLATION FOR LATER ANALYSIS	55
3.1	INTRODUCTION TO AIRCRAFT SCHEMATICS AND DETAILS.....	55
3.2	HYPOTHESIZING REGIONS OF GREATEST COUPLING:	58
3.3	SOFTWARE SELECTION FOR IPL DATA INTERPOLATION:.....	62
3.4	IPL DATA INTERPOLATION FOR MISSING TEST LOCATIONS.....	63
3.5	IPL PLOT GENERATION IN MATLAB.....	68
4	GRAPHICAL ANALYSIS OF IPL DATA ON MAJOR AIRCRAFT SYSTEMS AND TESTING AIRCRAFT SYMMETRY.....	73
4.1	INTRODUCTION TO IPL DATA ON AIRCRAFT SYSTEMS OF B737-200, #1989.....	73
4.1.1	<i>Glideslope (GS) Analysis</i>	73
4.1.2	<i>TCAS Analysis</i>	76
4.1.3	<i>GPS Analysis</i>	78
4.1.4	<i>VHF Com. Analysis</i>	81
4.1.5	<i>LOC Analysis</i>	83
4.2	TESTING AIRPLANE SYMMETRY ON GPS	85
5	IPL VALIDATION AND COMPARISON	89
5.1	DATA VALIDATION BY USING DIFFERENT AIRCRAFT: #1989 vs. #1997.....	89
5.2	DATA VALIDATION BY USING DIFFERENT TRANSMITTING ANTENNAE: DIPOLE vs. BICONICAL.....	95
5.3	DATA VALIDATION BY TAKING DATA ON WINDOWS ONLY: FULL PLANE vs. WINDOWS	99

6	STATISTICAL ANALYSIS OF IPL DATA.....	102
6.1	STATISTICAL ANALYSIS ON IPL DATA ON ENTIRE AIRCRAFT.....	102
6.1.1	<i>GS Measurement Distribution Plot.....</i>	<i>103</i>
6.1.2	<i>TCAS Measurement Distribution Plot.....</i>	<i>104</i>
6.1.3	<i>VHF Measurement Distribution Plot.....</i>	<i>106</i>
6.1.4	<i>LOC Measurement Distribution Plot.....</i>	<i>107</i>
6.2	STATISTICAL ANALYSIS ON IPL DATA ON WINDOW LOCATIONS ONLY	109
6.2.1	<i>GS Measurement Distribution Plot for window data</i>	<i>109</i>
6.2.2	<i>TCAS Measurement Distribution Plot for window data.....</i>	<i>109</i>
6.2.3	<i>VHF Measurement Distribution Plot for window data.....</i>	<i>112</i>
6.2.4	<i>LOC Measurement Distribution Plot for window data.....</i>	<i>112</i>
7	AIRCRAFT COUPLING MITIGATION TECHNIQUES USING CONDUCTIVE TAPE AND WINDOW FILMS.....	116
7.1	CONDUCTIVE SEALING OF DOORS AND EXIT SEAMS.....	117
7.1.1	<i>Analysis of Shielding of Exit Seams on GPS.....</i>	<i>118</i>
7.1.2	<i>Analysis of Shielding of Exit Seams on VHF1</i>	<i>121</i>
7.1.3	<i>Analysis of Shielding of Exit Seams on LOC</i>	<i>123</i>
7.2	PED EMI MITIGATION BY CONDUCTIVE WINDOW FILMS.....	126
7.2.1	<i>Analysis of Window Films on GPS</i>	<i>127</i>
7.2.2	<i>Analysis of Window Films on TCAS</i>	<i>129</i>
8	MODELING EMI PATTERNS USING FUZZY LOGIC	132
8.1	INTRODUCTION TO FUZZY LOGIC.....	132
8.2	ASSUMPTIONS USED FOR MODELING	134
8.3	FORMULATION OF FUZZY RULES	136
8.3.1	<i>Seat Distance from Window.....</i>	<i>137</i>
8.3.2	<i>Seat Distance from Door</i>	<i>138</i>
8.3.3	<i>Seat Distance From Antenna</i>	<i>140</i>
8.4	MODELING RESULTS AND CONCLUSION	142
8.5	INTRODUCTION TO DEFUZZIFICATION	146
9	CONCLUSION	149
9.1	SUMMARY.....	149
9.2	IMPLICATIONS	150
9.3	FUTURE WORK	151
	REFERENCES.....	153
	VITA.....	158

1 RESEARCH MOTIVATION AND OVERVIEW

1.1 Introduction to Problem

“Ladies and gentlemen, we will begin our safety briefing video momentarily. We would appreciate your attention to this important information. Use of portable electronic devices is not permitted during taxi, takeoff, and landing. Your crew will let you know when we reach an altitude where you can begin using an approved electronic device.”

Similar announcements are commonly heard in the welcoming briefings by the flight attendants before an aircraft takes off from the runway. Every year, more and more people travel onboard commercial airliners for business purposes, rather than luxury or leisure. Therefore, the traveling environment today is not conducive to relaxation, and as a result, many passengers want to be entertained by recorded media or games. To ensure quality time while in the air, passengers are likely to have with them one or more Portable Electronic Devices (PEDs), many with wireless capabilities. Most PEDs offer new and personalized entertainment, information and communication services [16]. The business traveler has opted to use the air-time for more productive applications thanks to the capabilities provided by today's computers and personal productivity devices. According to the International Air Transport Association's (IATA) database, most frequently used PEDs on aircraft include laptop computers, electronic games, video camcorders, CD players, audio players-recorders and mobile phones [26].

Regardless of the numerous warnings by the flight attendants, the probability of all passengers turning off their PEDs is very small. According to a Boeing Engineer, Dave Carson, “when it comes to PEDs, ‘people would like to do exactly in the airplane what they do at home or in their cars’” [17]. Therefore, sometimes, the constant persistence of flight crew in asking passengers to turn off their PEDs results in “air rage.” In fact, according to NASA’s Aviation Safety Reporting System (ASRS), of the 152 passenger air rage incidents reported, 15% were attributed to the prohibition on the use of PEDs. This makes prohibited electronic devices the second most likely cause of air rage behind alcohol at 43% but ahead of smoking in lavatories at 9% [21]. With the increasing variety of available PEDs, and the increasing number of rules against the use of PEDs in commercial flights, ‘Airlines are caught in the middle.’ According to an Air Transports Assistant, “flight attendants have had numerous confrontations with passengers about which PEDs can and cannot be used on airline flights.” [17]

With the use of PEDs becoming such a necessity, the question only remains that why are such bans and prohibitions placed on the use of PEDs on commercial aircraft? PEDs are capable of Electromagnetic emissions, which may possibly interfere with the avionics system, most commonly radio navigation and communications. The problem is complicated by the aircraft’s aluminum frame, which can act as a shield, a resonant cavity, or a phased array, and the sensitivities of the avionics. The radiation from the devices can couple to the avionics through the antennas, the wiring, or directly into the receiver [22].

1.2 Classification of Portable Electronic Devices

Most Portable Electronic Devices can be divided into two categories, intentional transmitters and non-intentional transmitters. Intentional transmitters must transmit a signal to accomplish their function; therefore, they are designed to radiate energy. Typically, intentional transmitters radiate electric fields up to 10 to 20 V/m according to the device at a one-meter distance inside their operational frequency band. The values can be even higher in the near field. This type of emission is correlated in frequency and restricted to a narrow band frequency. Although these types of transmitters are restricted in narrow frequency bands, they can generate spurious emissions outside their operational bands that are not well controlled by the civil standards. [27]. A typical intentional transmitter has emission levels in the order of a few volts/meter and are typically 60 dB greater than the undesired emissions allowed in other parts of the spectrum.

The Federal Communications Commission (FCC) specifically forbids the use of cellular phones onboard aircraft while in the air, and the Federal Aviation Administration (FAA) limits the use while on the ground [26]. This prohibition was not done to protect the aircraft's avionics systems from interference from the intentional transmitter. Rather, this prohibition was made to protect the cellular service from interference. As the altitude of a cellular phone increases, so does its transmission range, and consequently, its coverage area. At high altitudes, such as would be achieved from an in-flight aircraft, the handheld unit places its signal over several cellular base stations, preventing other cellular users within range of those base stations from using the same frequency. This would increase the number of blocked or dropped cellular calls. [19].

PEDs with intentional transmitting capability include, but are not limited to, mobile phones, wireless networking technology, handheld radio transceivers, and transmitters that control devices such as toys. Some specific examples are cell phones, pagers, two-way radios, Wi-Fi-equipped laptops, PDAs and wireless gaming devices. [27]

Other types of PEDs are unintentional transmitters. They do not need to transmit a signal to accomplish their function. But like any electrical device, they emit some level of electromagnetic radiation. Therefore, unintentional transmitters only generate spurious emissions at arbitrary frequencies as a result of their electric and electronic parts. The internal RF energy generated by unintentional transmitters is not intended to be radiated nor does it need to be radiated in order for the product to function properly. The radiation of the RF energy is a by-product since the RF energy generated internally cannot be completely shielded from the outside. Examples of unintentional transmitters include compact-disc players, tape recorders, game-boys, laptop computers, palm pilots as well as laser pointers [21]. In the US, the FCC regulates unintentional radiators under Part 15 of the rules. Emission limits are specified in the FCC rules to reduce the probability of causing harmful interference to other radio operations [19].

The undesired emissions from intentional radiators are comparable to the emissions produced by unintentional radiators. In both cases, the FCC or other national regulatory authority requires the undesired emissions to be below a specific limit. This limit is established to minimize the potential for interference between products in the commercial or residential environment in which the product is intended to be used. In a similar manner, RTCA, formerly known as the Radio Technical Commission for

Aeronautics, recommends limits for equipment installed on aircraft but these are not applicable to personal use of unintentional radiators. Therefore, it becomes necessary to determine the levels and frequency ranges critical to operation in an aircraft environment. [26]

Despite increases in microprocessor clock operating speeds, the input power required for PEDs is continuing to decrease. Each new generation of product offers lower operating voltages and increased battery life, which means a reduction in emissions. The design factor has to do with the physical construction of the products. Once again, market factors have resulted in the miniaturization of products to the point where the majority of electronics are reduced to a minimal number of integrated circuits. This reduction in the number of discrete components and the corresponding reduction in the interconnecting wiring further reduce the potential for emissions, particularly at low frequencies although there may be an increase in high frequency emissions.

During product manufacturing, shielding is one factor that has the most potential for being compromised. A product that is well designed and properly shielded at the time of manufacture may have its integrity violated through normal wear and tear, damage and improper repair procedures. On the positive side, even though proper shielding implies the potential for added weight to the product, the miniaturization of the product reduces the volume that has to be shielded. Even though the numbers, operating speeds and types of personal electronic devices that might be carried onboard an aircraft have increased, the design enhancements favor a reduction in overall emissions. [26]

A third classification of PEDs, not considered in this research, includes a particular case of pulsed type transmissions called ultra wideband (UWB) transmission.

UWB technology is being adopted for commercial communication devices, that transmit at very low power levels, but emit signals across other licensed and restricted frequency bands. The main characteristics of each PED category are summarized in Table 1.1:

Table 1.1: Brief Description of the three main PED Categories [27].

Type of PED	Type of Emission
Intentional Radiators	<ul style="list-style-type: none"> - Useful signals are stable, band limited signals - Wide range of emission levels (from low level up to 10 to 20 V/m at 1 m) in operational range. - Restricted to identified and licensed frequency bands. - Spurious emissions of low level can occur outside the useful frequency band, with the above characteristics.
Unintentional Radiators	<ul style="list-style-type: none"> - Emissions that can occur at arbitrary frequencies, covering a large frequency band. - Low level, less than 0.1 V/m at 1 m. - Emissions can be pulse-like signals or broadband noise. - Some radiated spikes, stable or modulated, can occur due to poorly filtered transmitter circuitry.
Ultra Wideband Devices	<ul style="list-style-type: none"> - Type of intentional transmitters using very low-level emissions. - Due to pulsed technology used, emissions may occur in restricted frequency bands.

1.3 Governing Regulations and Advisory Materials

Specific rules have been formed to regulate the use of intentional and unintentional transmitters onboard commercial aircraft due to the possibilities of Electromagnetic interference (EMI) from the transmitted emissions. The following few

sections, which summarize some of the regulations used through out the United States as well as in the rest of the world, are from a manual prepared by the RTCA's special committee (SC-177). The RTCA recommends standards and offers guidance to the aviation industry. Currently, most airlines in the United States and elsewhere voluntarily follow an RTCA recommendation issued on September 16th, 1988, that prohibits the use of PEDs during takeoff and landing. That recommendation was issued mostly to lessen any possibility of interference with aircraft avionics, but also to reduce the chance of passengers being injured by PEDs that might bounce around on a flight and prevent passengers from being distracted from safety announcements. [22]

1.1.1 Federal Communication Commission (FCC) Regulation

The FCC, which forbids the use of cellular phones onboard aircraft while in the air, is an independent United States government agency directly responsible to Congress. The FCC was established by the Communications Act of 1934 and is charged with regulating interstate and international communications by radio, television, wire, satellite and cable. The FCC's jurisdiction covers the 50 states, the District of Columbia, and U.S possessions. The Commission's primary goals are to promote competition in communications, protect consumers, and support access for every American to existing and advanced communication services [19]. FCC Regulations, Section 22.911, paragraph (a)(1) on "Prohibition on airborne operation of cellular telephones" states the following:

"(a) Mobile Stations in this service are authorized to communicate with and through base stations only...

(1) Cellular telephones shall not be operated in airplanes, balloons or any other aircraft capable of airborne operation while airborne. Once the aircraft is airborne, all cellular telephones on board such vehicles must be turned off. The term airborne means the aircraft is not touching the ground. Cellular telephones may be installed in the aircraft. A cellular telephone which is installed in an aircraft must contain a posted notice which reads: 'The use of cellular telephones while this aircraft is airborne is prohibited by FCC rules, and the violation of this rule could result in suspension of service and/or fine. The use of cellular telephones while aircraft is on the ground is subject to FAA regulations.'"

Following the regulations above, many airlines now install special aeronautical public correspondence phones that can be operated while the aircraft is airborne. Although similar in operation, it should be noted that these correspondence phones are not the same as cellular phones [26].

1.1.2 Federal Aviation Regulations (FAR)

The emissions of portable electronic devices used on aircraft are regulated by the Federal Aviation Regulations in Section 91.21 ("Portable Electronic Devices"), stated below:

- (a) "Except as provided in paragraph (b) of this section, no person may operate, nor may any operator or pilot in command of an aircraft allow the operation of, any portable electronic device on any of the following US.-registered civil aircraft:
 - (1) Aircraft operated by a holder of an air carrier operating certificate or an operating certificate; or

- (2) Any other aircraft while it is operated under IFR. [Instrument Flight Rules]
- (b) Paragraph (a) of this section does not apply to:
- (1) Portable Voice Recorders;
 - (2) Hearing Aids;
 - (3) Heart Pacemakers;
 - (4) Electric Shavers; or
 - (5) Any other portable electronic device that the operator of the aircraft has determined will not cause interference with the navigation or communication system of the aircraft on which it is to be used.
- (c) In the case of an aircraft operated by the holder of an air carrier operating certificate or an operating certificate, the determination required by paragraph (b)(5) of this section shall be made by that operator of the aircraft on which the particular device is to be used. In the case of other aircraft, the determination may be made by the pilot in command or other operator of the aircraft.”

Paragraph (b) of the FAR makes the aircraft operator permitting the operation of a portable device responsible for determining that a device will not cause interference with the navigation and communication systems of the aircraft [26], [9].

1.1.3 International Civil Aviation Organization (ICAO)

According to the RTCA/DO-233 documentation of rules on PEDs, the ICAO does not have contain specific standards or practices that pertain to the use of portable electronic devices onboard aircraft. However, the following paragraph from Chapter 8 of Doc 9376-AN/914 (under the topic of passenger cabin briefings, instructions and communications) includes a few statements about portable electronic devices:

“In addition, the operation manual should give guidance ... Guidance should also be given in the manual on the use of electronic devices in the passenger cabin and on the need to include instructions in the passenger briefing. Certainly the use of radios, radio-controlled toys, portable telephones and portable television sets should be forbidden as these may interfere with the airplane navigation systems. Other electronic devices such as personal computers, calculators, etc., may also interfere, but the range of possibilities is such that it is impracticable to give guidance here and the operators will, depending on the type of airplane and navigation equipment involved, have to develop their own instructions.” [26]

1.1.4 Joint Aviation Authority Regulation (JAR)

Sections 1.110 and 1.285 include the JAR requirements for portable devices.

According to JAR-OPS 1.110 on “Portable electronic devices”:

“An operator shall not permit any person to use and no person shall use, onboard an airplane a portable electronic device that can adversely affect the performance of the airplane’s systems and equipment.”

Also, JAR-OPS 1.285 on “Passenger Briefing” states:

“(a) An operator shall establish procedures to ensure that all passengers are familiar with:

(4) The restrictions on the use of portable electronic device.” [26]

1.4 Airline Regulations on PEDs

1.4.1 Delta Airlines

The following devices may not be operated at any time on Delta aircraft:

- Cellular telephones
- Commercial two-way transmitters (i.e. Walkie-talkies)
- Amateur transmitters (i.e. Ham radios)
- Citizen band (CB) transmitters

- 49 MHz transmitters
- Devices designed to radiate RF energy on a specific frequency
- Peripheral devices for computers or games connected by cable (i.e. Printers)
- Am/fm radios and portable TV sets
- Remote-control toys.

The following may not be operated when the aircraft is at the gate, in the taxi, take-off, initial climb, approach, and landing phases:

- Personal computers (cable-connected peripheral devices such as printers, external disc drives, etc, are not authorized)
- Personal computer games
- VHF scanner receivers
- Compact-disc players
- Digital/ cassette-tape player-recorders
- Video recorders/playback systems
- Calculators

The following may be operated at all times:

- Hearing aids
- Heart pacemakers and other implanted medical devices
- Electronic watches
- Electronic nerve stimulators
- Properly certified operator-installed and -maintained equipment, such as the public passenger-telephone equipment

Personal life-support systems may be operated during all phases of flight, provided that the equipment conforms to the criteria established by the administrator of the FAA.

1.4.2 United Airlines

On June 22, 1993, United Airlines announced that effective July 1, it will prohibit the use of PEDs onboard its aircraft during takeoffs and landings. The policy was

developed to address the possibility of such devices causing EMI with cockpit navigation or communications systems when aircraft are on the ground or flying below 10,000 feet, the most critical phase of aircraft operation. According to Ed Soliday, United's director-corporate safety and security, "we have not experienced any safety problems with these devices, but enough questions have been raised in the industry to prompt us to implement this policy as a precautionary measure until further study determines if any safety hazard exists." Excluded from the new policy are electronic medical devices, such as hearing aids, pacemakers and electronic watches, which may be used onboard an aircraft at any time.

According to the rules by United, when an aircraft is flying at or above 10,000 feet, which normally occurs within 10 minutes of takeoff and until 10 minutes before landing, passengers may use the following devices:

- Compact disc players;
- Electronic cameras (film or video);
- Electric shavers;
- Hand-held electronic calculators;
- Hand-held electronic games;
- Portable audio tape players;
- Portable video players (tape playback only);
- Portable voice recorders (dictation equipment);
- Portable computers with accessory printers and tape or disk drives.

1.4.3 American Airlines

The Engineers at American Airlines agree that although scientific studies have been inconclusive, there is mounting anecdotal evidence of sporadic and poorly understood problems. When safety is at stake, taking avoidable risk is simply unacceptable. American Airlines announced recently that it will no longer permit the use of such devices during takeoff and landing, and while flying at altitudes lower than

10,000 feet, the phases of flight during which cockpit instruments are used most intensively.

1.4.4 Atlantic Southeast Airlines

The Atlantic Southeast Airlines has detailed rules for PEDs, much similar to Delta Airlines. According to their rules on PEDs in section 3.13:

The FAA prohibits use of electronic devices such as AM/FM radios, cellular telephones, etc. during flight. These transmitters have circuits which can radiate signals strong enough to interfere with the aircraft's navigational systems. Non-transmitting portable electronic devices shall not be used during takeoff and landing when the seat belt sign is on, or when directed by a crew member, or during operations below 10,000 feet. However, non-transmitting portable electronic devices may be used at other times. If interference from the portable electronic device is suspected, the captain may prohibit operation of the device.

The following may not be operated at any time on ASA aircraft:

- Cellular telephones.
- Commercial two-way radios (i.e. Walkie Talkie).
- Personal two-way radios (i.e. Ham operators).
- Citizen Band (CB) radio.
- 49 MHz Transmitters.
- Peripheral devices for computers or computer games (i.e. printers, external mouse, "joy sticks").
- AM/FM radios and televisions.
- Remote controlled toys.
- Devices designed to radiate radio frequencies (RF) energy on specific frequencies.
- Cassette tape players with AM/FM radio capability.
- Compact Disc players.

The following may be operated when there is not a sterile cockpit in effect. The devices must be turned off when the seat belt sign is turned on for approach.

- Personal computers (see restriction above).
- Personal computer games
- VHF scanner receivers.
- Digital cassette tape player-recorders.
- Video recorders/internal playback systems.
- Calculators.

The following devices may be operated at all times.

- Hearing aids.
- Heart pacemakers or other implanted medical devices.
- Electronic watches.
- Electronic nerve stimulators.
- Electric shavers.
- ASA installed equipment.
- Pagers.
- Acceptable personal life support systems.

1.4.5 Southwest Airlines

According to the "Ground Operations Customer Service Manual" of Southwest Airlines:

The FAA allows inflight use of headsets, portable computers, calculators, and electronics games, provided they can be stowed properly in accordance with this rule. Customers should be requested not to use these devices during takeoffs and landings. The FAA does not allow inflight use of walkie-talkies, radio controlled toys, AM/FM radios, portable telephones, or portable television sets, all of which may affect aircraft radio and navigation equipment.

Portable Electronic Devices Not Acceptable [6]:

- Telephones
- Radios
- AM/FM
- VHF
- Battery or cord operated

- TV sets -- battery or cord operated
- Electronic games or toys with remote controls
- Computer, calculators, or typewriters larger than a briefcase and cannot be stored under the seat
- Data entry pad, hand held with umbilical cord attached.

1.5 Statistics and Reports of Accidental PED Usage

According to the rules and guidelines summarized in the sections above, the FAR and JAR regulations prohibit the use on board aircraft of PEDs designed to transmit and the FCC prohibits the use and operation of cellular telephones while airborne. Regardless of these rules and regulations above, numerous reports indicate that passengers use these devices during flight. Usually, passengers are unaware of the potential problems involved in the use of transmitters inside the cabin and of the rules applicable to the use of the devices. On the other hand, it becomes more and more difficult for the crew to detect the use of intentional radiators by passengers. Therefore, the interference risk and the possible operational consequences in the case of interference linked to the use of intentional and unintentional radiators onboard an aircraft must be investigated [26].

According to a report, the number of people boarding airplanes with electronic devices has grown significantly since the 90s and the low-voltage operation of modern aircraft digital electronics has become more susceptible to EMI. Also, during the last few years, investigation shows that the number of events relating to computers, compact disc players, and phones has dramatically increased and these devices have been found to more likely cause interference with systems which control the flight of the aircraft. [22]

The ASRS Summary of reports from 1986 to June 1994 includes the synoptic analysis of passenger electronic devices incidents (at the request of the FAA). There were a total of 46 passenger electronic devices related incidents in the ASRS database covering the period Jan 1, 1986 thru June 30, 1994. This number is in contrast to the 51,337 full form reports covering all types of incidents reported to the ASRS during the same period. These statistics make Passenger electronic devices incidents comprise .08 percent of the total full form reports in the ASRS database.

Out of the 45 incidents involving passenger carrying operations, 33 of the incidents involved aircraft in the 60,000-300,000 lbs. weight classifications. Also, 33 of the incidents referenced alleged aircraft systems interference from an onboard passenger electronic device, while 10 of the incidents referenced alleged interference from an unknown onboard source. The breakdown of aircraft systems {reported} affected by passenger electronics devices interference included: nav equipment (37 incidents), aircraft communications equipment (9 incidents), radar altimeter equipment (1 incident) and fly-by-wire throttle controls (1 incident). On the other end, 21 passenger electronic devices were specifically identified to be the sources of the aircraft systems interference. The reporters noted the interference ceased after the devices were turned off. The identified passenger electronic devices included:

- Cell phones (4)
- Laptop computers (4)
- Portable AM/FM Radio
- Cassette Players (4)
- Portable CD Players (3)
- Electronic Games (3)
- HF Radio (1)
- Heart Monitor (1)

One report cited interference from 23 passengers using AM/FM radio cassette players. While another report cited unknown onboard interference causing ILS signal interference resulting in two missed approaches. Two reports cited passenger use of cell phone as a cause of dual VOR nav failure. None of the passenger electronic devices incidents had a critical impact on the safety of the flight. [9]

There were also 40 PED related reports collected by the International Air Transport Association (IATA). The PED most frequently suspected as a source of interference was laptop computers, 16 times out of 40 or 40%. The most frequent aircraft system affected by a suspected PED interference source was navigation, 27 times out of 40 or 68%. In three of these cases, the suspected PED was turned off to verify that the aircraft system anomaly went away and then turned on to confirm that the PED was actually the source of the interference. [21]

Table 1.2 summarizes the NASA's ASRS reports from search request on passenger PEDs from 1986 to 1994 tabulation [26]:

Table 1.2: Summary of NASA's ASRS Reports from 1986 to 1994 Tabulation.

PEDs cited and Frequency		Aircraft System Affected		Level of Correlation Confirmation	
Audio Players/Recorders	10	Navigation	30	PED On-Off	20
Cellular Phones	9	Communication	4	None	13
Laptop Computers	7			PED On-Off-On	1
Unknown	6				
Electronic games	5				
CD Players	1				
Portable TVs	1				
HF Marine Band Receiver	1				
Heart Pace Monitor	1				

Some of the incidents attributable to PEDs are set forth below [21]:

“In October of 1998, a Boeing 757, flying from Seattle to Covington/Cincinnati, experienced loss of all three of its autopilot systems. Flight attendants checked for a passenger using a portable electronic device and discovered a man wearing headphones, which were part of a hearing aid. The passenger was allowed to continue using the device, but was moved forward several rows. The autopilot system then regained full operational capabilities and was later checked by maintenance, with no problems being found.”

“In March of 1997, a Cessna 340/A pilot experienced erroneous readings when attempting to determine his location because of a passenger using a cellular phone. After the passenger turned off the phone, the pilot was able to locate his position and continue on with no problems.

In January of 1997, a regional jet was flying from Salt Lake City to Eugene. The flight crew received three separate warning messages stating that there were disagreements between the captain's and the first officer's instruments. The three warnings were for discrepancies in heading, airspeed, and altitude indicators. After flight attendants checked the cabin for passengers using portable electronic devices and had the devices turned off, all problems ceased."

"In August 1995, an aircraft making its approach to George Bush Intercontinental Airport in Houston was advised that it was 4 miles off course. Because the course director indicators had been scalloping left and right of center, the captain ordered the flight attendant to check the cabin for any passengers using a portable electronic device. Within 15 seconds, problems with the course director indicators disappeared. The captain later learned that a passenger had been using a portable computer.

In May of 1995, the electric compass indicators of the first officer of a Boeing 737 gave erratic readings. After a sweep of the cabin was made for portable electronic devices, which resulted in flight attendants asking a passenger to turn off a compact disc player, the first officer's instruments returned to normal working order.

Shortly after takeoff from Baltimore, in April 1994, an aircraft was advised by ground control that it was 10 miles off course, though the plane's instruments indicated nothing abnormal. It was found that a passenger in first class was using a portable computer. After the computer was turned off, navigation instruments returned to normal."

"In February 1994, a turboprop aircraft flying government officials from Lake Havasu, AZ to Yuma, AZ experienced trouble with its navigational

radios. Ground control showed that the airplane was off course and gave corrections. However, the plane's navigation system had been checked earlier in the month and was said to have zero error. After the flight, the pilot learned that at least one passenger was using a cellular phone while the plane was in the air."

"In August 1992, a turbojet aircraft was notified three times, by two different control towers, that it looked to be off course. All instruments in the cockpit were showing the plane's position to be correct. Flight attendants searched for portable electronic devices and found a tape machine and a hand-held video game unit in use. The devices were turned off and there were no other navigational discrepancies during the flight.

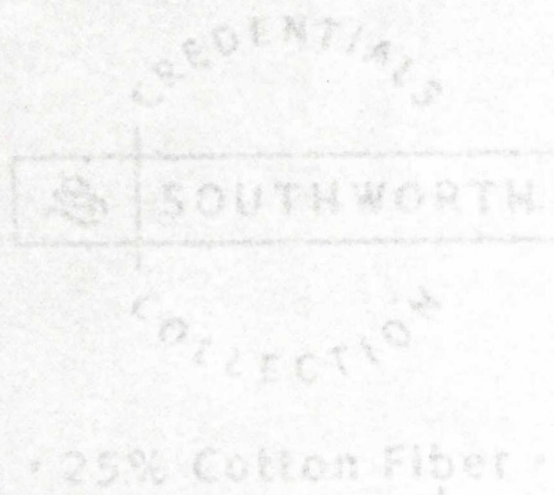
In September of 1990, a plane traveling from Boston to Youngstown/Warren, OH was advised it was off course and was issued a new heading. The plane's navigational instruments showed it to be on course. After checking the cabin for portable electronic devices, the lead flight attendant informed the captain that 23 passengers were using AM/FM cassette players and one passenger was using a personal computer. The passengers were asked to turn off the devices and the flight proceeded without further incident."

Another article reported that a "Slovenian airliner [had to make] an emergency landing after the passenger's mobile phone caused its electronic system to malfunction and indicate there was a fire on board." It was also reported that a "Canadian Regional Jet bound for the Bosnian capital Sarajevo had turned back soon after take-off because of the erroneous fire warning and made an emergency landing in Ljubljana." Another

investigation showed that the alarm had been caused by “a mobile phone in the luggage compartment which had not been switched off” [25].

According to a report by Peter Ladkin, five crashes of Blackhawk helicopters shortly after their introduction into service in the late 1980's were found to be due to electromagnetic interference from very strong radar and radio transmitters with the electronic flight control systems. Therefore, as Ladkin stated, the concern about the phenomenon of electromagnetic interference is not purely the result of speculation; it has actually happened, and it is appropriate to be concerned about the possibility of similar phenomena in transport aircraft. [9]

The following figures summarize the statistics of the interference cited through the use of PEDs onboard aircrafts:



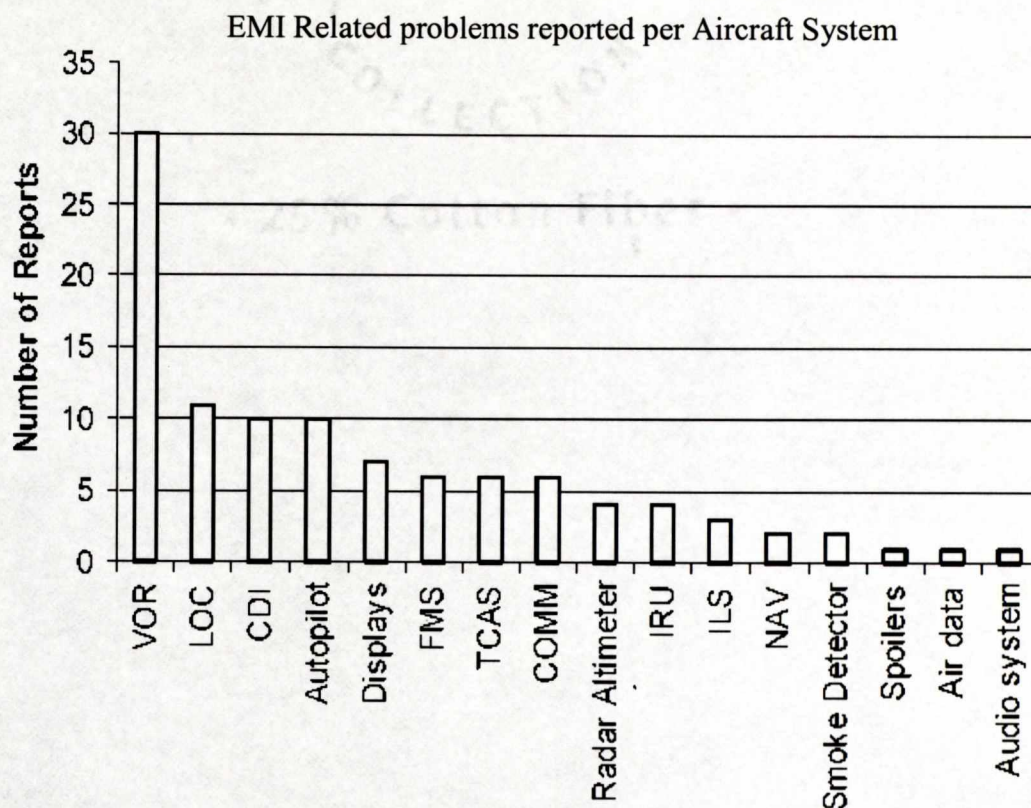


Figure 1.1: Aircraft systems affected by the use of PEDs.

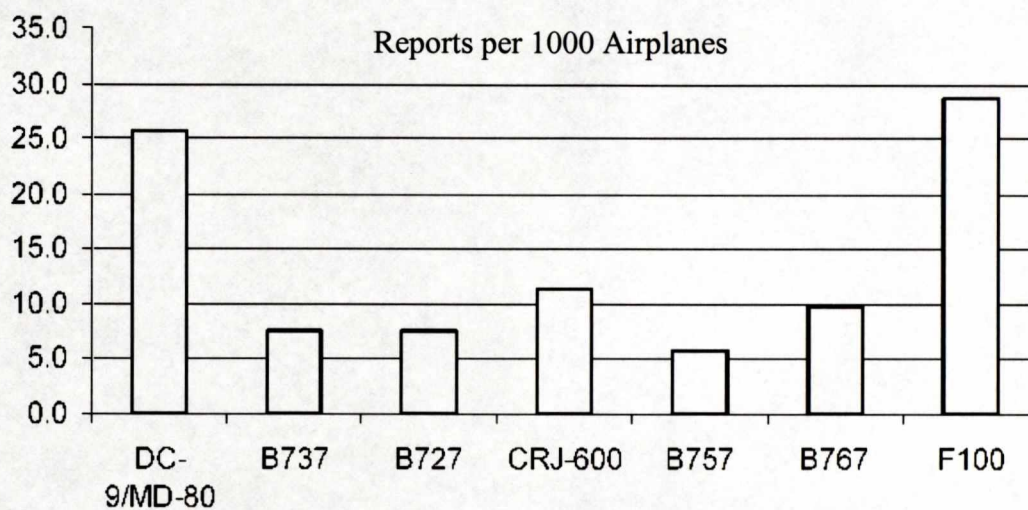


Figure 1.2: Frequency of incidents cited for different types of aircraft.

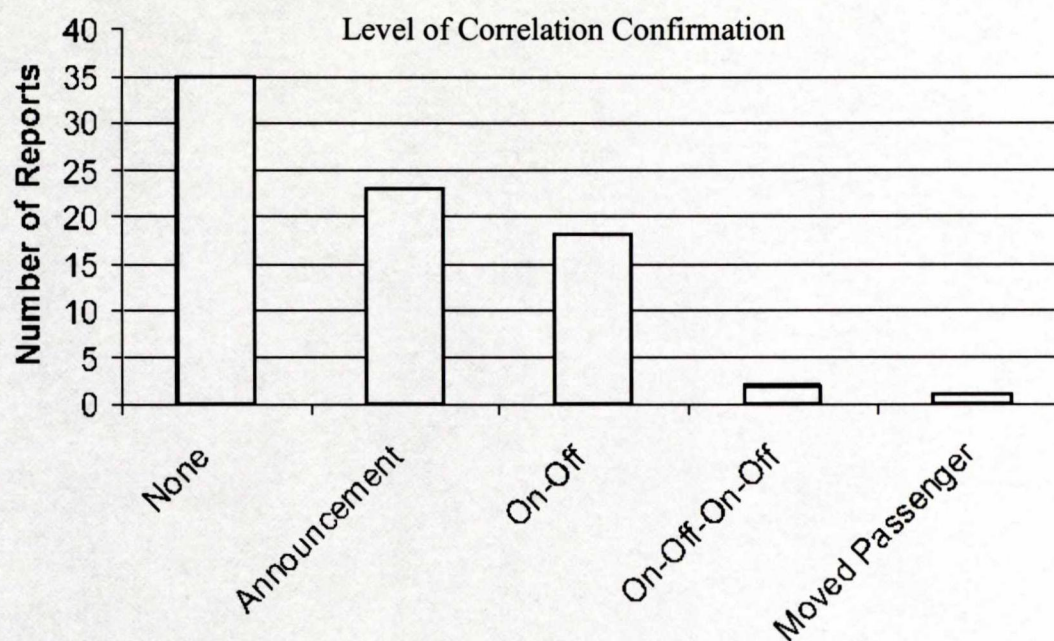


Figure 1.3: Reports of PED interference with confirmation.

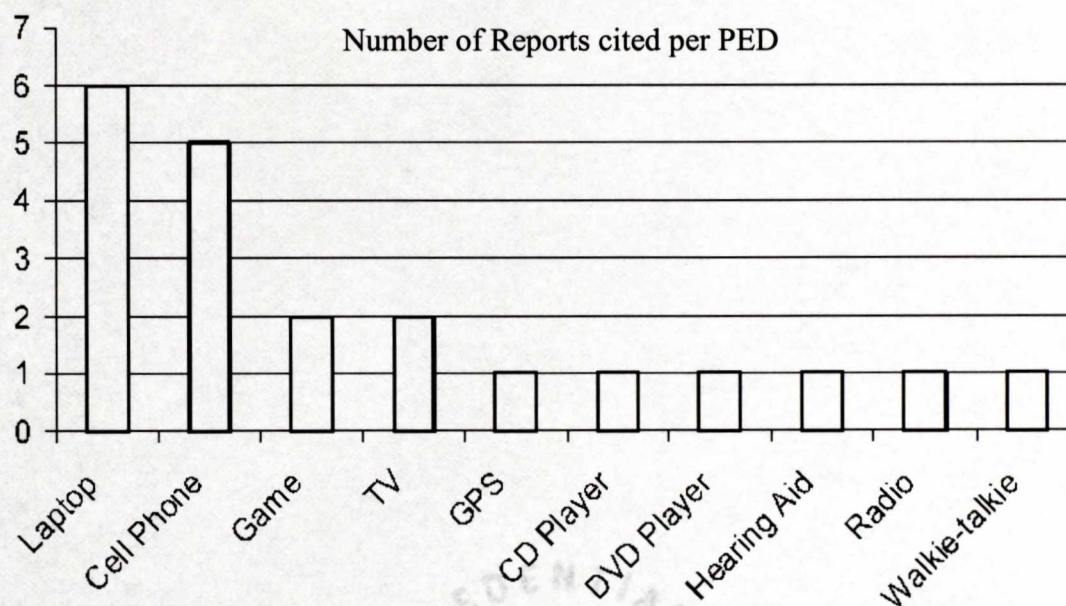


Figure 1.4: PEDs identified in ASRS reports as a possible cause of EMI.

1.6 Research Overview

With so many citations of possible interference due to the use of portable electronic devices onboard aircraft, what is the possible solution? Although several bans are placed on the used of PEDs on aircraft, passengers still sometimes “forget” to turn off their devices, or sometimes, refuse to turn them off. Sometimes passengers are simply not aware of the fact that they may be carrying a PED to begin with. Therefore, passengers frequently use many PEDs surreptitiously or inadvertently on the aircraft. According to Timothy Shaver of United Airlines, “as wireless devices become embedded into other devices, such as laptops, and the antennas for other devices become less conspicuous, it places a greater challenge on [the] flight crew to identify potential interference sources.” [14] Even if airlines place PED detection systems on aircrafts, it is not exactly in their best interest, business-wise, to confront a passenger who is using a PED. As Finbarr O’Conner, electromagnetic compatibility manager of R&B Enterprises and member of SC-177 of RTCA, states it: “If it were up to me, I would shut PEDs down, period” [22]. However, such an easy solution is not preferred by the passengers.

In summary, the problem with the use of PEDs onboard aircraft has many solutions; however, each solution has some support as well as some opposition. If the PEDs are simply banned, it not only makes the passengers upset, but also concerns the manufacturers of the various PEDs. Also, even with a ban, it is very difficult to confirm that all PEDs *have* been turned off or stowed away. As stated in one of the accident reports, sometimes passengers stow away their PEDs as requested, but forget to turn them off first.

The second solution to the problem is to make tougher standards for the PEDs so that the likelihood of interference with the aircraft systems decreases to a minimum. This solution, however, is again a problem with the PED manufacturers as it requires them to invest more money into shielding, which increases the size of their products, thus making the consumers unhappy. The airlines can also install PED detection systems that can pinpoint the exact location of the PED-user in the aircraft; however, such a solution can cause bad relationships between passengers and airline companies, resulting in air-rage. Another solution is to simply ignore the “minute” interference problem and allow the passengers to carry any PED they desire. This however, raises major safety issues by not only the Regulations Agencies, but also for the Airlines that want their passengers to have the safest travel possible.

Therefore, a solution needs to be devised that not only takes into account the safety of the passengers, but also allows the passengers to enjoy the use of their PED while traveling. This solution would not only make the passengers content, but would also benefit the PED manufacturers, the airline companies as well as satisfy the regulation agencies. The following chapters introduce the testing performed in order to understand the behavior of electromagnetic waves in an aircraft due to PEDs. The different analysis performed will be used to propose different solutions possible to overcome the ever-popular problem of the use of PEDs onboard commercial airliners.

2 INTRODUCTION TO AIRCRAFT SYSTEMS AND TESTING METHODOLOGIES

After getting a brief introduction of the functionality of the common Portable Electronic Devices (PEDs) as well the rules and regulations placed by agencies on airlines and PED manufacturers, it is important to understand the relationship between the PEDs relative to the aircraft radio systems that may possibly be affected. As mentioned in the previous chapter, the use of PEDs is prohibited onboard aircrafts due to the electromagnetic emissions from the PEDs, which may interfere with the avionics systems, most commonly radio navigation and communications. The next few sections provide a brief overview of the aircraft structure and why it becomes vulnerable to PED-related emissions.

2.1 Reasons for Vulnerability of Aircraft Systems due to PED-Related Emissions

The radiation from the PEDs can couple to the avionics through the antennas, the wiring, or directly into the receiver of the aircraft [22]. The statistical report in Figure 1.2 of chapter 1 shows that the navigation systems are the most vulnerable to PED-related emissions from within the aircraft's fuselage. The navigation systems are vulnerable for two reasons: they have parts devised to detect and act on signals coming from the 'outside' and they are radio-based systems, which are particularly susceptible to low levels of interference. Since the aircraft control systems are located entirely within the

aircraft, they are shielded from absolutely any signals not coming from one of their own devices. The control systems are also not radio-based, but are based entirely on electrical signals conducted through wires, similar to most computer networks. Navigation avionics, on the other hand, must have some designed sensitivity to environmental radio signals in order to perform their function. [9]

According to Bruce Nordwall, the antennas of radio-based avionics may be affected by electromagnetic field intensities of as small as a microvolt per meter. But being outside the aircraft, the antennas get some protective attenuation from the fuselage of radiation originating inside the aircraft. Non-radio signals generally have higher signal levels, and so are less susceptible to low interference levels [9]. According to Dave Walen, manager of electromagnetic effects for Boeing Commercial Airplane Group, "these are the instruments that we cannot harden because they are built to receive very small signals. We rely on those sensitive receivers to pick up small signals in space and that is the primary concern we have with carry-on electronic devices" [22].

The hull of the metal aircraft forms an effective electromagnetic boundary between the outside and the inside of an aircraft. Electromagnetic signals find it hard to get in, or to get out. For this reason, navigation and the radio antennae on the aircraft need to be placed outside the aircraft hull. But while outside, they must be sensitive. The navigation electronics inside the hull can be in principle just as well and securely shielded as control avionics, because there is no need at all for navigation systems to be sensitive to the electromagnetic signals coming from the inside of the aircraft [9].

Once the antennas have picked up the signals, they run through coaxial cables to communications or navigation receivers generally located below the floor of the cockpit.

The output of those receiver boxes then goes to cockpit indicators or to other computers in the plane, or both. Most navigation signals, for example, go to a cockpit indicator and also to the autopilot computers. The wires that connect the receivers to the indicators or computers are twisted, shielded pairs, or twisted, shielded triples, depending on whether the signal is digital or analogue.

Often the wires from the antennas to the receivers run along the fuselage inside the aircraft skin, passing less than a meter from a PED wielding passenger. The thin sheet non-conducting material that forms the inside of the passenger compartment, typically fibreglass, offers no shielding whatsoever between the PED and the wiring. Boeing's Walen confirmed to IEEE Spectrum ([22]) that wires critical to the functioning of the aircraft are generally shielded. American Airlines' Degner believes that because the cables are so well shielded most of the interference from PEDs is due to radiation that the antennas pick up, and then transmit to the cockpit instruments or the navigation computers [22].

Shielding could be damaged during servicing or could degrade over time. The effectiveness of shielding also depends upon good grounding. This is difficult to maintain over time because of the nature of aluminum's surface chemistry: aluminum oxidizes rapidly in air, thereby increasing the resistance of the electrical connection to ground. In that case, the wires could pick up interfering signals directly. Even with shielding in mint condition, electromagnetic interference can still couple to the aircraft's navigation or communication systems. Although the aluminum skin of the aircraft forms an excellent electromagnetic shield, it has holes through which the radiation can escape. In airliners, the greatest leakage of signals is through the windows as well as the doors. [22]

2.2 Frequency Band Information of Aircraft Systems of Concern

Table 2.1 provides a list of avionics systems that are of concern in the event of interference along with their operational frequencies. Out of the possible aircraft systems mentioned in Table 2.1, most at risk are those that have antennas located at various points outside the skin of the aircraft to pick up the navigation and communication signals. The highlighted systems will be studied in the research.

In general, manufacturers of the systems listed in the table above are responsible for designing immunity into their products. According to Bennett Kobb, editor of Spectrum Guide, “there can be substantial differences in the level of interference immunity between what is technically possible, what is cost effective, and what is reasonable for policy makers to expect from manufacturers.” In terms of functionality of the major systems, OMEGA navigation, at the low end of the frequency spectrum, is used to determine aircraft position through ground-based transmitters. VOR, or the VHF omnidirectional range finder, is a radio beacon that is used to navigate from point to point. The Glide slope system is used during landings. Above 1 GHz is the DME (distance-measuring equipment), which gauges the space between the aircraft and a ground-based transponder and is used throughout the flight, from take-off to landing. Also in the spectrum above 1 GHz are TCAS (Traffic Alert Collision Avoidance System), GPS (Global Positioning System), and cockpit weather radar systems. [22]

Table 2.1: Aircraft systems of Concern in the event of Interference [26].

More Susceptible		Less Susceptible
Glide Slope (329 – 335 MHz)	LORAN-C (100 kHz)	ADF (190 – 2000 kHz)
Localizer (108 – 112 MHz)	MODE-S (1030 MHz)	Autopilot (non-radio)
TCAS (1030, 1090 MHz)	MLS (5031 – 5091 MHz)	EFIS (non-radio)
VOR (108 – 118 MHz)	SATCOM (1) (1545-1555 MHz)	Flux Gate Compass (non-radio)
GPS (1575 MHz)	SATCOM (2) (1610 – 1626.5 MHz)	Low-Freq. Wx Map (50 kHz)
VHF COMM (118 – 137 MHz)	SATCOM (3) (1645.5 – 1655.5 MHz)	NAV Computers (non-radio)
DME, (TACAN) (978-1215 MHz)		Radio Altimeter (GPX) (4.3 GHz)
ATCRBS XPDR (1030 MHz)		Weather Radar (9.375 GHz)
OMEGA (10 – 14 kHz)		HF (2 MHz – 30 MHz)

Among the systems listed above, all avionics systems are susceptible to interference from high levels of electromagnetic radiation. Some systems, however, are more susceptible than others. As mentioned in previous section, for addressing susceptibility, avionics systems can be divided into two broad classifications, radio-based and non-radio. The radio-based systems have an antenna where on-channel field intensities of only microvolts per meter can be a serious interference threat. Non-radio systems do have signals traveling between their components' parts. The signal levels are, however, significantly greater than those received by the radio-based systems and the

susceptibility to low levels of interference is significantly reduced. On the other hand, the radio systems antennas are mounted outside of the aircraft and their susceptibility to interference from radiating devices inside the aircraft benefits from the attenuation of the aircraft fuselage. Interconnecting wires that may serve as ingress points for non-radio systems are inside the fuselage and can be very close to PED radiators and receive much higher field intensity.

The GPS represents a special concern given its emerging importance to civil aviation in all phases of flight. A GPS receiver navigates by estimating certain parameters of the ranging signals received from multiple GPS satellites. Especially important are the arrival time, doppler frequency offset and phase of each ranging signal. The GPS receiver must also demodulate digital data superimposed on these ranging signals. RF noise or interference makes the estimation of these parameters and the demodulation of the digital data more difficult. GPS signal levels are significantly lower than those used in other navigation systems. However, the spread spectrum waveform employed by GPS offers a degree of interference protection; nevertheless, radio frequency interference of sufficient strength can degrade performance and even lead to loss of signal lock on one or more satellite ranging signals. This, in turn, can lead to a loss of required navigation performance. [26]

2.3 Signal Leakage from PEDs and Coupling to Aircraft Systems

The common PEDs operate at frequencies from a few tens of kilohertz for AM radios to 3 GHz for laptop computers. When the harmonics of these signals are taken into account, the emitted frequencies cover almost the entire range of navigation and

communication frequencies used on the aircraft. The frequency and intensity of the radiation also depend on what mode the device is being operated in. Also, different types of avionics have different sensitivities, making the likelihood of interference very random and unpredictable. A radiation source may cause total destruction of a navigation signal one channel while nearby channels are completely unaffected. Another type of signal may be sensitive to the modulation of the signal or to the number of individual radiators. [22]

For example, an FM broadcast receiver commonly use 10.7 MHz IF with LO above the tuned frequency:

$$F_{LO} = f_{Tuned} + f_{IF} \quad (2.1)$$

Where the FM broadcast band ranges from 88 to 108 MHz, while VOR and Localizer systems use 108-118 MHz spectrum. Looking at the overlap of the two frequency spectrums, the FM receiver local oscillator leaking from receiver can be received by VOR/Localizer radios of the aircraft. [25]

Oppositely, the technology of cellular phones poses a threat to the cell phone technology on ground level, as it is based on the small local ground based receptions called cells. The cell phone networks are such that a cell phone user is served by just one cell, and when reaching the boundary of that cell, the signal gets 'handed over' to the next cell which the user is about to enter. The topology of the coverage is based on the assumption that the user is on or near ground, and it is a technical assumption on which the entire system is based that a user will be within 'sight' of just one cell, except when nearing a cell boundary. When in an aircraft, however, the user is within radio 'sight' of many cells, simply because of the very high altitude off the ground. An attempted call or

reception from an aircraft would activate many, if not all cells, in the local area, which 'breaks' the technology. It causes many transmission problems and the network system is disturbed. Therefore, the ban of cell phones onboard aircraft is because it causes the cell phone technology to malfunction, rather than be a significant threat to a particular aircraft radio system. [9]

2.4 dB Tutorial

Before understanding the testing methodology used to obtain data for understanding EMI patterns, the basic terminology of the use of dB scale throughout the report must be understood well. The term dB, or decibel, is a relative unit of measurement used frequently in electronic communications to describe power gain or loss. Decibels are used to specify measured and calculated values in audio systems, microwave system gain calculations, satellite system link-budget analysis, antenna power gain, light-budget calculations and in many other communication system measurements. In each case, the dB value is calculated with respect to a standard or specified reference.

The dB value is calculated by taking the log of the ratio of the measured or calculated power (P_2) with respect to a reference power (P_1). This result is then multiplied by 10 to obtain the value in dB. The formula, commonly referred to as the power ratio form of dB, for calculating the dB value of two ratios is shown below:

$$dB = 10 \log_{10} \frac{P_2}{P_1} \quad (2.2)$$

The equation above can also be modified to provide a dB value based on the ratio of two voltages. By using the power relationship $P = V^2/R$, the relationship shown in the next formula is obtained.

$$dB = 10 \log_{10} \frac{V_2^2 / R_2}{V_1^2 / R_1}; \quad (\text{let } R_1 = R_2) \quad (2.3)$$

$$\therefore dB = 10 \log_{10} \frac{V_2^2}{V_1^2} \quad (2.4)$$

By further simplifying the equation, a dB relationship based on voltage ratios instead of power is obtained, shown below:

$$dB = 20 \log_{10} \frac{V_2}{V_1} \quad (2.5)$$

The dB unit is often used in specifying input and output signal level requirements for different communication systems. An example of specified audio levels can be found in microwave transmitters. It is common for a +8 dBm input level to be specified. Notice that a lower case **m** has been attached to the dB value. This indicates that the specified dB level is relative to a 1 milliwatt reference. In standard audio systems 0 dBm is defined as .001 watt measured with respect to a load termination of 600 ohms. A 600 ohm balanced audio line is the standard for professional audio and telecommunications. Therefore, 0 dBm is defined as 1 mW measured with respect to a 600 ohm termination. [7]

The term dBm also applies to communication systems which have a standard termination impedance other than 600 ohms. For example, video and some RF systems

are terminated with 75 ohms. The 0 dBm value is still defined as 1mW but measured with respect to a 75 ohm termination instead of 600 ohms. Therefore the voltage reference for a 0 dBm system with respect to 75 ohms is:

$$v = \sqrt{P * R} = \sqrt{(.001) * (75)} = .27386 \text{ volts} \quad (2.6)$$

To calculate the voltage gain or loss with respect to a 75 ohm load use equation 2.5 if a voltage is specified and the dB value is needed.

$$dBm(75) = 20 \log_{10} \frac{V}{.27386} \quad (2.7)$$

Therefore, *dBm* relative to 1 milliwatt (.001W) is a typical measurement for audio input/output specifications. It is also used in low power optical transmitter specifications. *dBm(600)* is the standard audio reference power level defined by 1 milliwatt measured with respect to a 600 ohm load. This measurement is commonly used in broadcasting, professional audio applications and is a common telephone communications standard. While, *dBm(50)* is defined by 1 milliwatt measured with respect to a 50 ohm load. This measurement is commonly used in RF transmissions/receiving systems. [7]

Please refer to table 2.2 for a quick relationship between dBm, Volts, and Watts, calculated from the equations derived above: [5]

Table 2.2: Look-up table for dBm, Voltage and Power relationships.

dBm	Volts	Watts
70 dBm	707.11 V	10.00 kW
60 dBm	223.61 V	1.00 kW
50 dBm	70.71 V	100.00 W
40 dBm	22.36 V	10.00 W
30 dBm	7.07 V	1.00 W
20 dBm	2.24 V	100.00 mW
10 dBm	707.11 mV	10.00 mW
0 dBm	223.61 mV	1.00 mW
-10 dBm	70.71 mV	100.00 uW
-20 dBm	22.36 mV	10.00 uW
-30 dBm	7.07 mV	1.00 uW
-40 dBm	2.24 mV	100.00 nW
-50 dBm	707.11 uV	10.00 nW
-60 dBm	223.61 uV	1.00 nW
-70 dBm	70.71 uV	100.00 pW

2.5 Interference Path Loss Testing Methodology

To address the interference issue, NASA entered into a cooperative agreement with UAL and EWI to conduct additional IPL measurements and to address several technical issues. One issue was to measure additional IPL data using a thorough and consistent set of procedures. IPL is the measurement of the radiated field coupling between passenger cabin locations and aircraft communication and navigation receivers, via their antennas and is required for assessing the threat of PEDs to aircraft radios. IPL data is very dependent upon airplane size, the interfering transmitter position within the airplane, and the location of the particular antenna for the aircraft system of concern.

Systems considered were the instrument landing system Glideslope (GS), Traffic Alert and Collision Avoidance System (TCAS), VHF Communication System, instrument landing system Localizer (LOC) and VHF Omnidirectional (VOR) system [28].

Another issue concerned aircraft-to-aircraft repeatability. This repeatability issue resulted in measurements on six similar B737-200 and four similar B747-400 aircraft. The aircraft in each of the two groups were acquired by UAL at approximately the same time, and, therefore were similarly configured. The IPL measurements were performed during three one-week visits to the Southern California Aviation facility in Victorville, California. UAL provided the flight-ready airplanes, along with fuel, engineering and mechanic support for this effort. NASA provided measurement instrumentation, data acquisition and test control software development and support, and staff. EWING was tasked to lead the overall effort and to conduct analysis.

2.5.1 Testing Overview

IPL measurements were conducted on the six B737-200 airplanes for the VOR/LOC, VHF-1 Comm., GS, TCAS, and GPS systems. Please refer to Chapter 3 for the location of the systems studied in this research. The interference source, simulated with dipole and horn antennas, was positioned to radiate toward each of the windows and the door exits on one side of the aircraft. In addition, full IPL measurements were also conducted on two B737s with the transmit antenna positioned at all seat locations including locations between seats (on one side of the aircraft). As a result, each full aircraft (nose number 1989 and 1997) measurement provided approximately 160 locations (times two for two transmit antenna polarizations) rather than about 36 window

and door locations. Please refer to Figure 2.1 for an interior view of a B737-200, along with the locations of measured IPL data in each row.

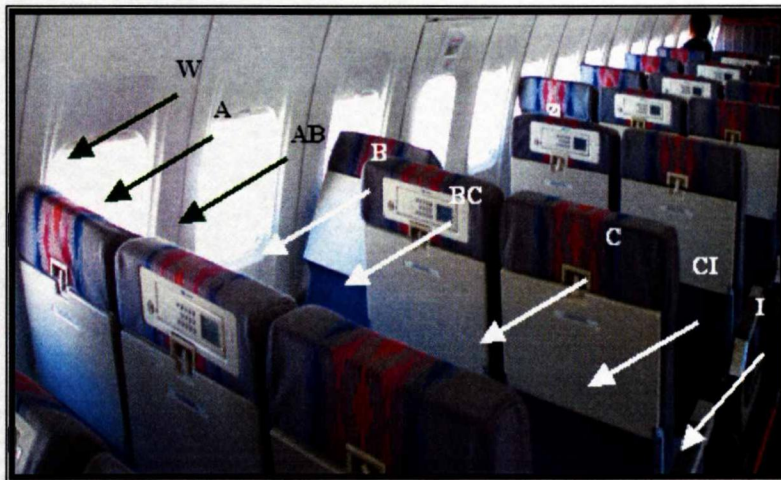


Figure 2.1: B737-200's interior: IPL Measurement Locations.

When taking IPL measurements, it was assumed that for PEDs interference problems, the interference source is located within the passenger cabin, and the victims are aircraft radio receiver systems. A common path of PED interference is through the windows or door seams, along the aircraft body, and into the aircraft antennas. The interference signal picked up by the antennas is channeled back into the receivers to potentially cause interference if they are higher than the receiver interference thresholds. Figure 2.2 shows an illustration of typical radio receiver interference coupling paths. The signals are transmitted through the windows and doors of the aircraft, and creep along the aluminum surface of the fuselage to reach the antenna system of the aircraft.

Figure 2.3 shows a basic setup for conducting IPL measurements. IPL data was taken by radiating a low powered continuous wave (CW) test signal, frequency-synchronized to the spectrum analyzer sweep and fed to the test transmitting Antenna via a double-shielded RF cable. The spectrum analyzer, laptop computer controller, and

preamplifiers were located inside the aircraft. The spectrum analyzer input cable was connected to the aircraft radio receiver rack cable in the avionics equipment bay.

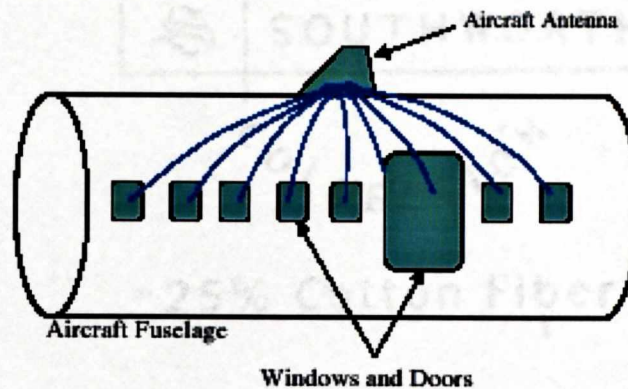


Figure 2.2: Illustration of Typical Radio Receiver Interference Coupling Paths.

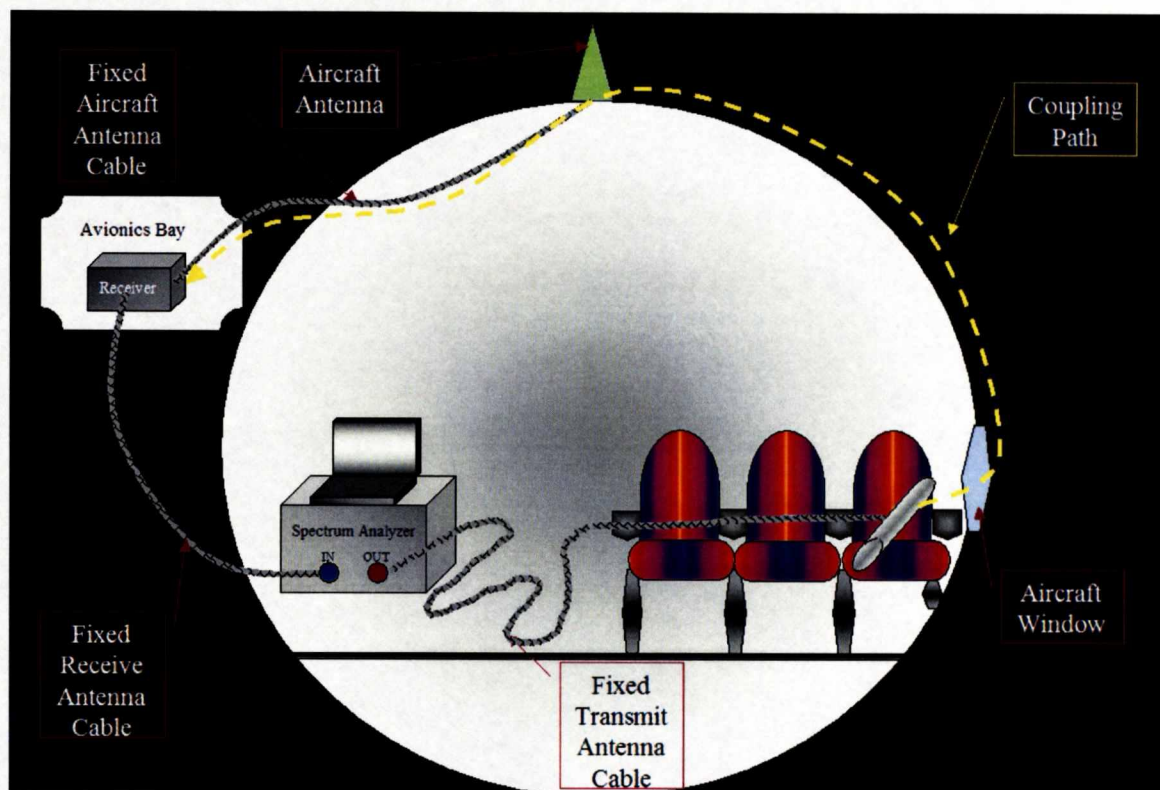


Figure 2.3: Illustration of Instrumentation setup for IPL measurements.

To perform an IPL measurement, the team measured the RF power loss between the calibrated signal source and a spectrum analyzer, via the entire length of test cables plus the aircraft cable, plus the free space loss between the reference antenna and the aircraft antenna. Swept CW was preferred over discrete frequency measurement, according to RTCA/DO-233. A pair of test cables were used to connect the instruments to the aircraft antenna cable and to the transmit antenna. An optional amplifier (optional) was used to increase the signal strength depending upon the capability of the tracking source and the path loss level. Sometimes, a preamplifier is needed in the receive path near the spectrum analyzer for increased dynamic range; however, in this particular setup, the pre-amplifier was internal to the spectrum analyzer.

For most systems, IPL was defined by the ratio (in dBm), or the difference in dB, between the power radiated from the transmit antenna to the power received in the avionics bay's receiver. For GPS testing, however, IPL was defined to be the differences in power between transmit antenna and aircraft antenna only. The antennas used in the measurement include dipoles (a set of dipoles with baluns covering different frequency ranges) for frequencies in the GS band and below, and a dual-ridge horn antenna for the frequencies in the TCAS band and above. Due to obstacles in the plane, such as seats, walls, windows etc, it was considered best not to correct for the free space antenna gain in the definition for IPL. However, free-space antenna gains, as provided by the antenna manufacturers, are shown in Table 2.3 that can be used to factor in the transmit antenna free-space gain, if so desired.

Table 2.3: Aircraft Antennae Characteristics for Testing.

Aircraft Systems	Spectrum (MHz)	Measurement Frequency Range (MHz)	Transmit Antenna Type	Free-Space Antenna Gain (dBi)
VHF-Com	118 – 137	116-138	Dipole	2.1
LOC/VOR	LOC: 108.1 – 111.95 VOR: 108 – 117.95	108-118	Dipole	0.9
GS	328.6 – 335.4	325-340	Dipole	1.9
TCAS	1090	1080 – 1100	Dual-Ridge Horn	7.4
GPS (L1)	1575.42 ± 2	1565 – 1585	Dual-Ridge Horn	9.6
SatCom	1545-1559	1530 – 1561	Dual-Ridge Horn	9.6

As shown in the table 2.3, a transmit antenna was used to simulate an interference source. The tuned dipole transmit antenna was used for measurements in the LOC, VOR and GS bands, and a dual-ridge horn antenna was used for measurements in the TCAS, GPS and SatCom bands.

2.5.2 Testing Details

This section includes a step-by-step procedure of conducting IPL measurements, used by Delta Airlines. The procedure includes the instrumentation needed, as well as the detailed connections and set-up.

2.5.2.1 Parts Required for Measurements

The following instruments and cables are required to perform IPL measurements, please refer to figure 2.4 for the pictures of the parts defined below:

- Laptop Computer with HP VEE Path Loss Measurement Software.
- Spectrum Analyzer. Used Agilent E4407B ESA-E Series Spectrum Analyzer in this write-up.

c. Calibration Cable

d. Power Amplifier with SMA Power-Amp Cable and Power Supply

e. 2 Coaxial cables for Aircraft Antenna and Transmit Antenna

f. Transmitting Antenna (i.e. Biconical, Dipole, Horn etc.)



Figure 2.4: Instrumentation required for IPL Measurements.

2.5.2.2 Instrumentation Hook-up/Set-up

A. Laptop Computer:

In the testing procedure, laptop will be used to capture screen shots from the spectrum analyzer as well as for storing data.

1. After powering up the laptop using the power supply, enter the username and password. (Sticker on computer keyboard)

2. From desktop, launch “PathLossMeas_SA_AutoDownload_ver3.0.1” by double clicking on the icon.

B. Spectrum Analyzer:

1. As shown in Figure 2.5, connect the 120VAC cable to the spectrum analyzer.
2. Using another set of cable, connect laptop’s PCMCIA-GPIB card (National Instruments) with the spectrum analyzer’s HP-IB parallel port. Please refer to figure 2.6.
3. Turn the Spectrum Analyzer on by using the power button on the lower left corner on the front panel.
4. Let the Spectrum Analyzer perform initial alignments automatically.
5. Calibrate the Spectrum Analyzer by using the Calibration cable shown in figure 2.7.
 - a. Connect one end of the calibration cable to “Input 50Ω” while the other end to “AMPTD ref out” connector on the front panel of the spectrum analyzer.
 - b. Go to “Systems”¹ → “alignments”² → “align now” → “All”

¹ Boxed names refer to physical soft buttons found on the *front panel* of the Spectrum Analyzer

² Underlined names refer to options available on the *display screen* of the Spectrum Analyzer.



Figure 2.5: Power Supply for Spectrum Analyzer.

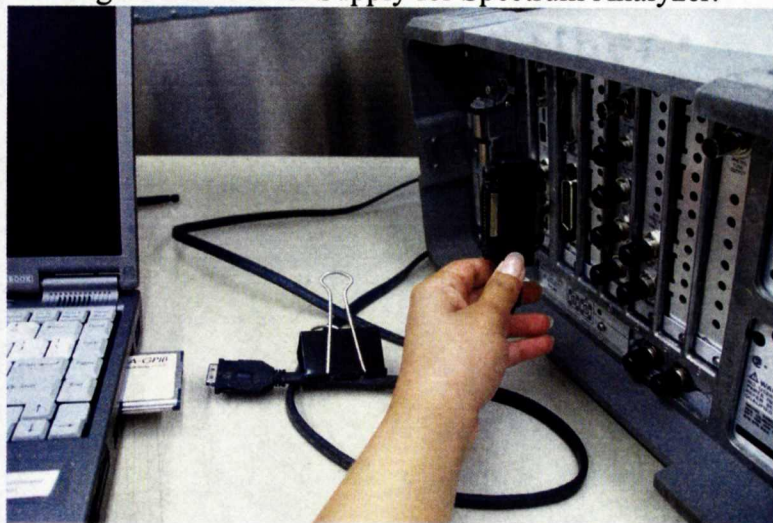


Figure 2.6: Illustration of Laptop to Spectrum Analyzer connection.



Figure 2.7: Illustration for Spectrum Analyzer's Calibration.

2.5.2.3 Test Cable Loss (TCL) Measurements:

After setting up the spectrum analyzer, a TCL measurement needs to be performed for each system tested. TCL Measurements are necessary to observe the power loss incurred in the double shielded RF Cables. This procedure must be performed every time for each system of the aircraft during testing, i.e. VHF, TCAS etc.

- A. Set the Start and Stop frequencies for the system of concern. Please refer to table 2.3 for aircraft systems and their frequency bands.

For example, VOR ranges from 108 MHz to 118 MHz:

- Go to “Frequency” → “Start Freq” → “108” → “MHz” to set starting frequency.
 - Similarly, go to “Stop Freq” → “118” → “MHz” to set the stopping frequency.
- B. Turn the Source on by going to “Source” → “on”. Make sure that the Source “Amplitude” is -10 dBm. If not, then change to “10” → “dBm”
- C. Set the reference to 0 dBm and attenuation to “auto” by going to “Amplitude” and changing the “Ref” to “0” → “dBm”; and “Atten” to “Auto” on the display screen.
- D. Go to “View/Trace” → “ClearWrite” to begin the tracing of the signal on the spectrum analyzer.
- E. Perform peak search to calculate and record the TCL Measurement by pressing “Peak Search”.

$$\text{TCL Measurement} = \text{Source Amplitude} - (\text{result}) \quad (2.8)$$

Where the Source Amplitude was set to -10 dBm in this case, and the “result” is found from the peak search above. Therefore, if the “result” was -11.19 dBm, then TCL = $-10 - (-11.19) = 1.19$ dBm.

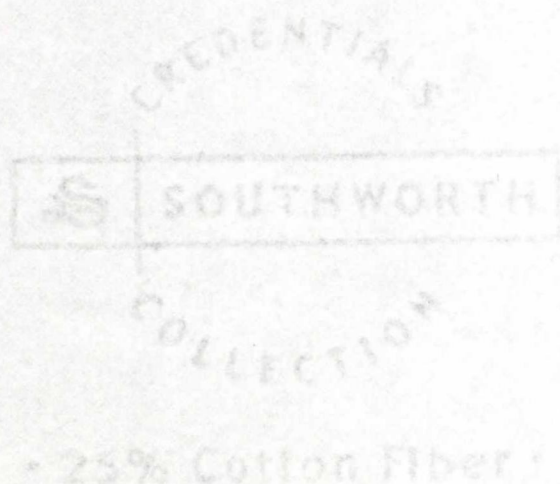
2.5.2.4 IPL Measurements

The following section includes the connections are necessary to perform the IPL measurements:

A. Spectrum Analyzer to Transmitting Antenna using a Power Amplifier:

1. Using Figure 2.8 as a summary, connect an SMA Power-amp cable from “RF out 50Ω ” connector on the spectrum analyzer to the input of the Power Amp.
2. Then connect a double-shielded RF cable from the output of the Power-amp to the transmitting antenna.
3. Connect the power supply to the power-amp***.

*** *Caution: Make sure that steps 1 and 2 above are performed **before** performing this step! ****



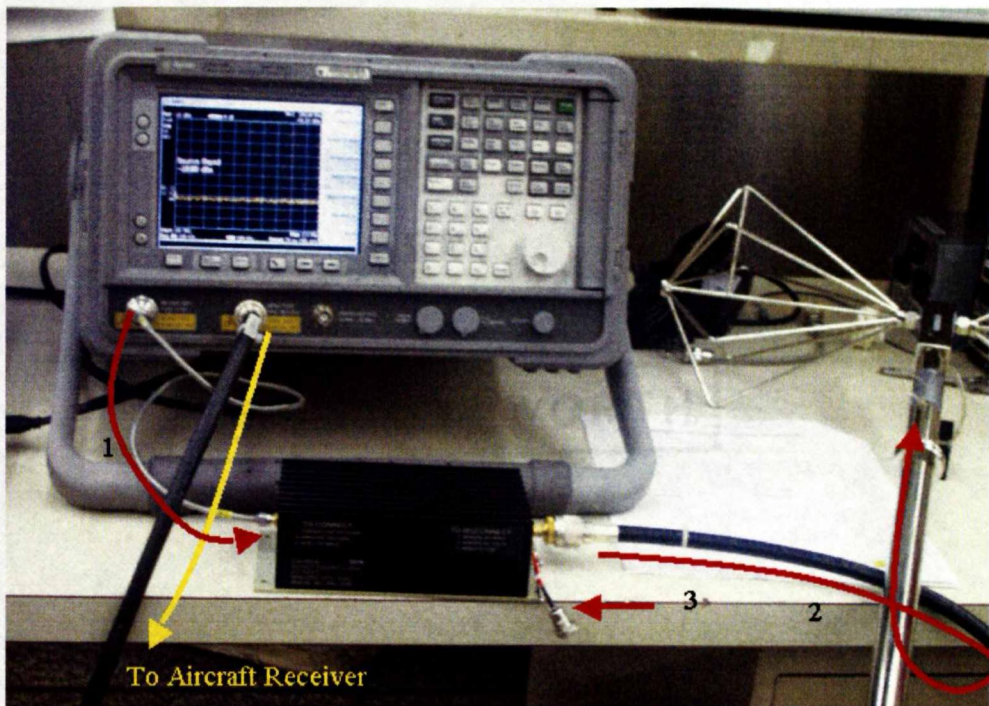


Figure 2.8: Complete hook-up of Spectrum Analyzer with power-amp, coaxial cables, transmitting antenna and laptop computer

B. Spectrum Analyzer to aircraft Receiver in the Avionics Bay:

1. Connect a double-shielded RF cable from the “Input 50 Ω ” connector of the spectrum analyzer to the receiver of the aircraft, usually located in the avionics bay.
2. Before proceeding to measuring and recording IPL Measurements, make sure to change the following settings on the spectrum analyzer:

Go to “Source” → “Amplitude” → “1 0” → “-dBm”. Also make sure that the “Ref” under “Amplitude” is “-10 dBm” while the “Atten” is “0 dBm Manual”.

Side Note: The source amplitude is set to -10 dBm because the power amplifier ZHL-42W (see appendix for spec-sheet”) has a gain of approximately 37 dB across all the frequencies possible. The

power amplifier also only has a Power Output capability of only around 27 dBm. Therefore, to make sure that the actual power output remains less than 27 dBm (which can possibly be as high as 37 dBm), we set the source amplitude to -10 dBm, instead of leaving it at 0 dBm.

3. Take IPL Measurement by going to "View/Trace" → "ClearWrite" and performing "Peak Search"

C. Capturing Data in Laptop:

1. Please refer to the screen shot in figure 2.8. Begin by clicking on the check box next to "Enter Data Dir & Filename Root". In the pop-up directory, find the folder named which will be used to store all data collected during testing. Open the folder, enter test name and click "save". On the original screen (in figure 2.8), observe that the software should have identified the type of spectrum analyzer connected to the system (in this case, "E4407B" on the right hand column).
2. Click on the check box next to "Change File Index Number" whenever it needs to be set. Initially, indexing begins at 1, and automatically increments upon each recording; therefore, use this feature if an erroneous measurement was occurred and data needed to be retaken.
3. Finally, click on the check box next to "Download & Record Trace". This step should result in the capture of the screen currently on the spectrum analyzer (after "View/Trace" → "ClearWrite" → "Peak Search" was performed on the spectrum analyzer). Observe that the software confirms the start and stop

frequency as well as records the maximum frequency measured by the spectrum analyzer, denoted by “Marker Amp” (in this case, -11.16 dBm).

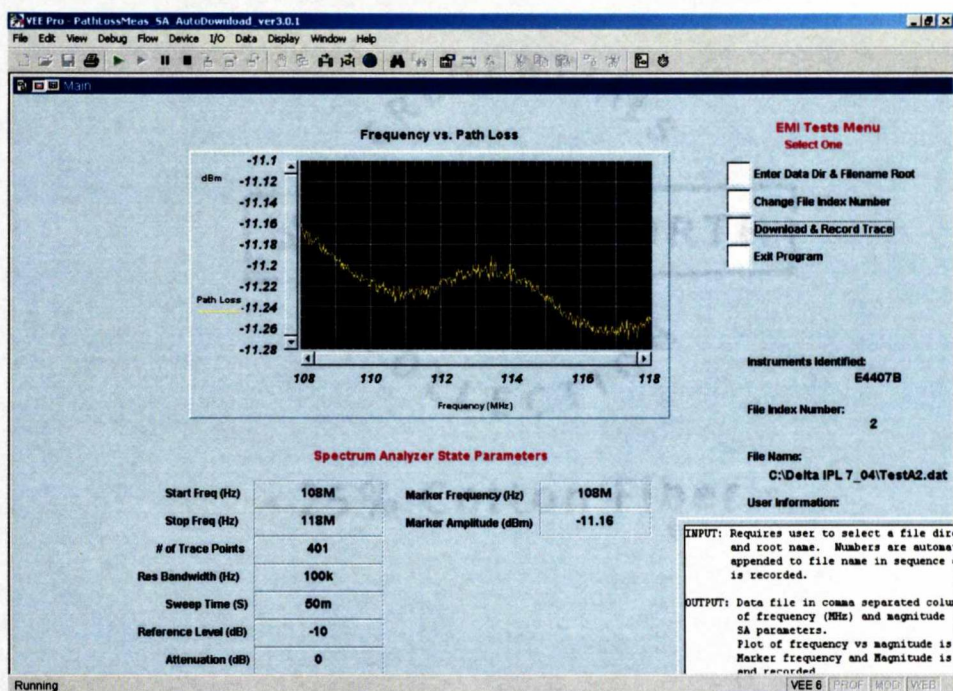


Figure 2.8: Illustration of HP VEE Path Loss Measurement Software.

2.5.3 Summary of Steps for Measuring IPL Data

The measurement process for each system on each aircraft typically involved the following steps:

1. Conduct 1-meter path loss measurement. IPL was measured with the transmit antenna positioned one meter from the aircraft antenna. This simple step established a baseline measurement and helped detect any excessive aircraft antenna cable loss. Excessive cable loss could indicate possible signs of connector corrosion in the path. These data were not needed to compute the IPL.
2. Configure the spectrum analyzer to the proper reference level, resolution bandwidth, attenuation level and desired measurement frequency band. Configure

the tracking source to track the frequency sweep of the spectrum analyzer. Set the tracking source output to desired power level.

3. Measure test cable and aircraft cable “through” losses.
4. Position the transmit antenna at a desired location, typically near a window or door. Point the antenna to radiate toward a window or door seam.
5. Clear spectrum analyzer’s trace. Set spectrum analyzer to “Trace Max Hold” and sweep continuously across the desired measurement band.
6. Scan the transmit antenna slowly along the door seam, while the spectrum analyzer is still set at “Trace Max Hold”. No scanning was needed at the windows due to small window sizes.
7. Record trace and the peak marker value. For systems that experience narrowband peaks caused by strong local transmitters such as LOC, position the marker at the peak of the broadband envelope while avoiding the narrowband peaks. Record data at this marker location.
8. Change polarization and repeat from step 2 so that both vertical and horizontal polarizations of the transmit antenna are included.
9. Relocate the transmit antenna to another window/door and repeat from step 4.

Post processing involved removing the measured system “through” loss from the total path loss data. The system loss includes the effects of test cable losses, amplifier gains, and other types of losses/gains in the measurement path. For step 1 above, please refer to figure 2.9 for an illustration of a 1-meter path loss measurement near a B737 VOR/LOC antenna located in the tail. A 1-meter path loss measurement was conducted

to check the integrity of the aircraft antenna path. The results were not used to calculate IPL and are not reported in this document.



Figure 2.9: Illustration of 1-meter path loss measurement near B737 VOL/LOC Antenna.

Figure 2.10 shows a measurement being conducted with the transmit antenna at a window, and the computer and software used for data acquisition (detailed steps provided in previous sections). Although the testing instruments and computers were located within the passenger cabin, spurious emissions from these equipment were too low to be measurable or to affect the measurement.

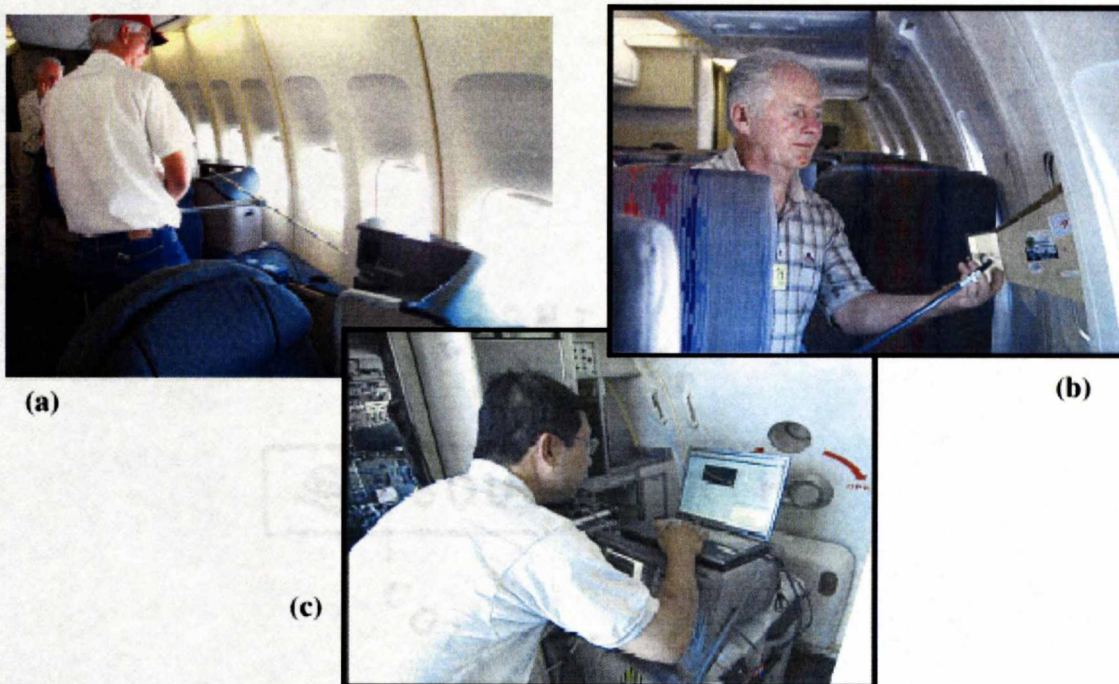


Figure 2.10: Illustration of various phases of testing performed by the test team.

After understanding the details on how IPL measurements are actually taken, the next few chapters summarize the results obtained as a part of this thesis. For good reference, table 2.4 summarizes the antennae tested, as well as their locations. The table also includes the measurement frequency range used by the test team as well as the actual spectrum of the antenna system [10] [27].

Table 2.4: Aircraft Antennae's detailed characteristics for reference.

Aircraft Receiver	Antenna Location	Spectrum (MHz)	# of channels	Channel Bandwidth	Antenna Gain (dBi)	Sensitivity (dBm)	Measurement Freq-range
VHF-Comm1	Top	118-137	2280	8.3 kHz	< 3	-107	116 – 138
LOC	Tail	108- 111.95	40	18 kHz	0	-107	108 – 118
GS	Nose	328.6-335.4	40	34 kHz	0	-99	325 – 340
TCAS	Top	1090	/	9 MHz	+5	-80	1080 – 1100
GPS (L1)	Top	1575.4±2	1	2 MHz	-8	-111	1565 – 1585
SatCom	Top	1545-1559	3 to 6	500 kHz	/	-110	1530 – 1561

3 DETAILED AIRCRAFT SCHEMATICS AND DATA

INTERPOLATION FOR LATER ANALYSIS

3.1 Introduction to Aircraft Schematics and Details

Chapter 2 describes the testing methodology of taking Interference Path Loss (IPL) data on airplanes. For this research, testing was performed on out-of-service, United - Boeing 737, 200 series (B737-200). B737-200 is considered a medium sized aircraft with 4-abreast seating in the first class, and 6-abreast seating in the economy class. Please refer to Figure 3.1 for a cross section of the aircraft. As a standard, the left half of all aircraft, when facing the cockpit of the plane, is referred to as the “port” side of the aircraft as usually the left side is used by passengers for boarding and leaving the plane. The right side of the aircraft is referred to as the starboard side, which is usually not used by passengers for boarding purposes. B737-200 has four exit doors. Two of the doors are located in the front side of the aircraft, referred to as L1 and R1 in this paper. The other two doors are located in the rear of the aircraft near the tail, referred to as L2 and R2. L1 and L2 are located on the port side, while R1 and R2 are located on the starboard side. There are also two emergency exits located near the wings of the aircraft; these are referred as LE and RE for exits on port and starboard side, respectively. The emergency exits are located at window #16 of both port and starboard side of the aircraft on a standard B737-200.

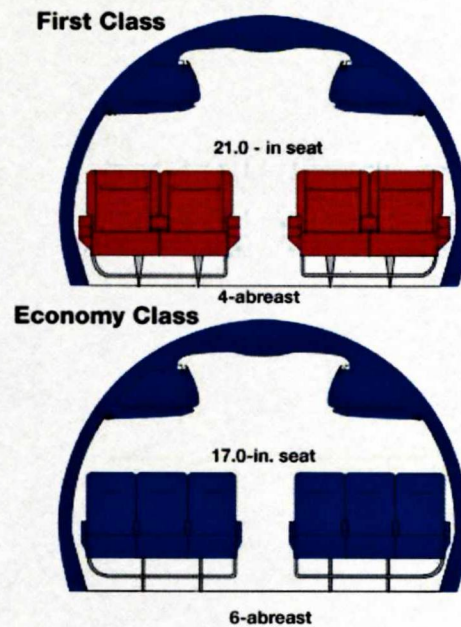


Figure 3.1: Cross-sectional representation of 1st class and coach class seating.

Please refer to figure 3.2 to observe the locations of all the exit doors as well as the emergency exit. Also note that the difference between port and starboard side is also pointed out. B737-200 has 32 windows on each side of the aircraft, including the window for the emergency exit. As explained in chapter 2, the greatest emissions from PEDs is thought to leak out toward the aircraft systems through the doors and windows of the aircraft; therefore, it is necessary to know the exact locations of the doors and windows to analyze the electromagnetic patterns thoroughly.

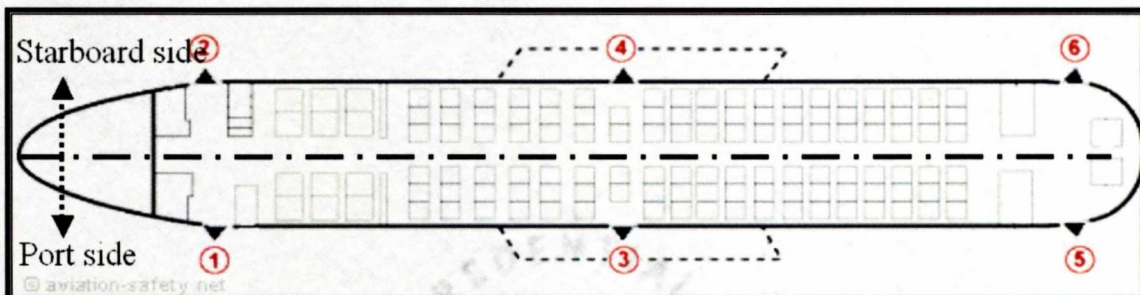


Figure 3.2: Schematic of B737-200, Port vs. Starboard side.

For measuring IPL data, the aircraft systems considered included the instrument landing system Glideslope (GS), Traffic Alert and Collision Avoidance System (TCAS), VHF Communication System #1 (VHF1), instrument landing system Localizer (LOC) and Global Positioning System (GPS). The operating frequencies of the above systems are provided in chapter 2. Figure 3.3 shows the approximate locations of GS, TCAS, VHF and the LOC, while the possible locations of GPS is pointed out in figure 3.4.

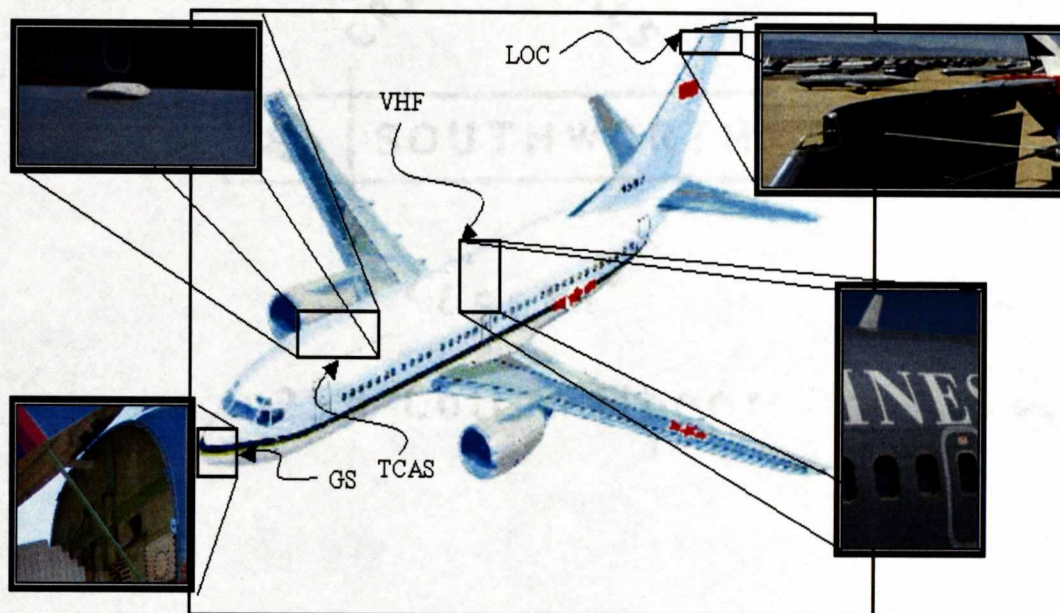


Figure 3.3: Antenna Locations of B737-200.

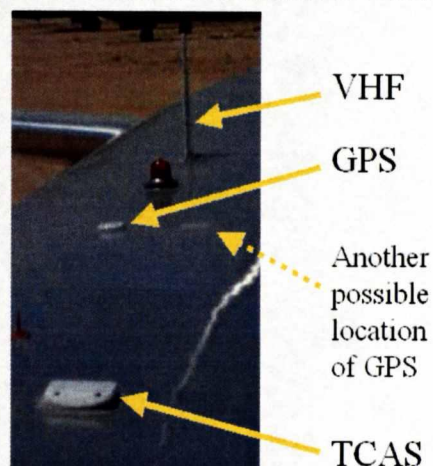


Figure 3.4: Possible antenna locations for GPS on B737.

As shown in figure 3.3, GS is located in the nose of the aircraft; the TCAS is located directly on top of the second window of the aircraft, on the center of the fuselage. Figure 3.4 shows two possible locations of the GPS system, behind the TCAS approximately on top of window #9. As shown in the figure, unlike TCAS, the GPS antenna is not installed along the top centerline of the aircraft, but instead, is slightly offset to the starboard side of the airplane. VHF is located behind the GPS antenna on top of the emergency exit, or window 16. Finally, the LOC system is installed on the tip of the tail of the aircraft. In some aircraft, the LOC is installed in the nose of the aircraft, along with the GS antenna; however, in B737-200, the system is installed in the tail.

3.2 Hypothesizing regions of Greatest Coupling:

As described in previous chapters, PEDs pose particular problems for aircraft because of the relatively high power of their RF emissions. It is hypothesized that there are certain regions of the aircraft where the probability of causing PED-related interference with the aircraft system is greater than other regions. Although the aluminum skin of the aircraft forms an excellent electromagnetic shield, it has holes through which the radiation can escape. In airliners, the greatest leakage of signals is through the windows as well as the doors. Therefore, it is expected that the greatest coupling should occur near the doors and windows of the aircraft, closest to the locations of the antenna.

For example, since the GS is located in the nose of the aircraft, it is hypothesized that the greatest coupling should occur in the front of the plane, with the greatest leakage through L1. Also, the antenna polarizations should play an important

role in the coupling factor as well. Since GS is a horizontally polarized antenna, it can be predicted that the greatest coupling should occur in the IPL data taken for horizontal polarization. Please refer to figure 3.5 for a predicted region of greatest coupling, where the greatest threat of electromagnetic interference exists between a radiating PED and a receiving GS antenna.

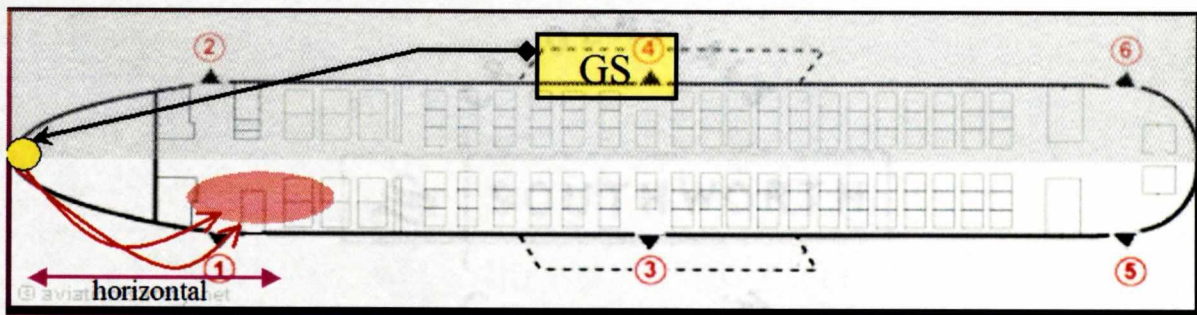


Figure 3.5: Antenna Placement and Coupling prediction for GS.

Using similar method of hypothesizing, since the TCAS is located on top of window #2, it can be predicted that the region with the greatest probability of coupling should be close to window #2 as well as the L1 doorway. Also, since the TCAS is a vertically polarized system, the greater coupling values should occur in the IPL values collected with the transmitting antenna in the vertical position. Please refer to figure 3.6 for a schematic of the above prediction for the TCAS antenna:

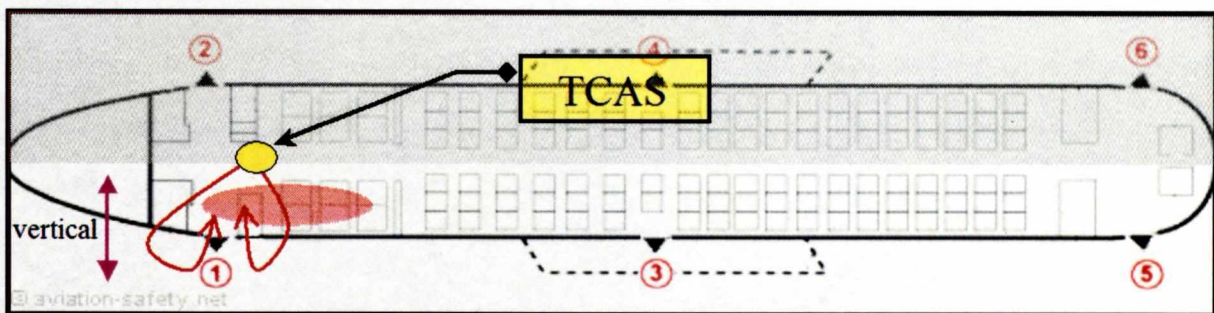


Figure 3.6: Antenna Placement and Coupling prediction for TCAS.

The GPS antenna, which is located on the starboard side's slot on top of window 9 should have the best coupling with the PED located near window 9 in vertical polarization. As described before, since the GPS antenna is not located on the centerline of the fuselage, but is more toward the starboard side, it can also be predicted that the coupling for the location on window 9 on the starboard side should be slightly greater than the coupling levels of the location on the port side. Figure 3.7 shows a schematic for the coupling hypothesis for the GPS antenna:

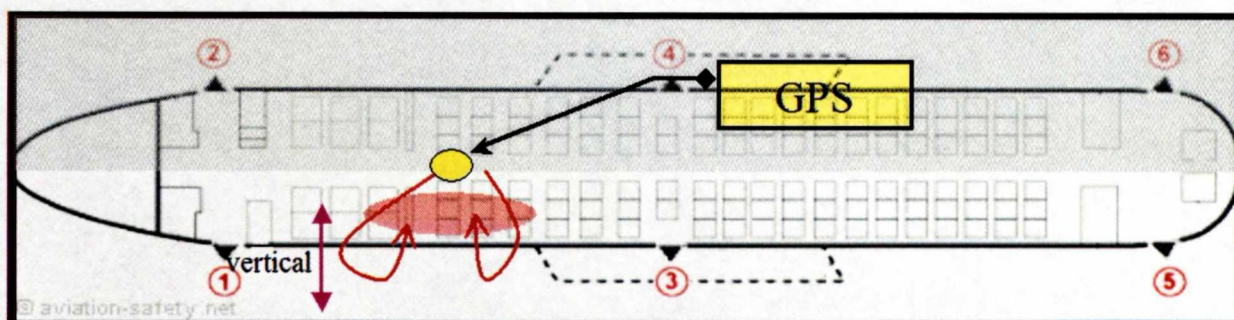


Figure 3.7: Antenna Placement and Coupling prediction for GPS.

The VHF system is located on top of the window 16, which is also an emergency exit. Therefore, it can be predicted that the greatest coupling between a transmitting PED and an aircraft system can occur through leakage from window 16/emergency exit. Also, the VHF system is also vertically polarized, therefore, it can be predicted that the lowest IPL results (or the greatest coupling) should be obtained in vertical polarization of the transmitting antenna as well. Please refer to figure 3.8 for the schematic for a VHF system:

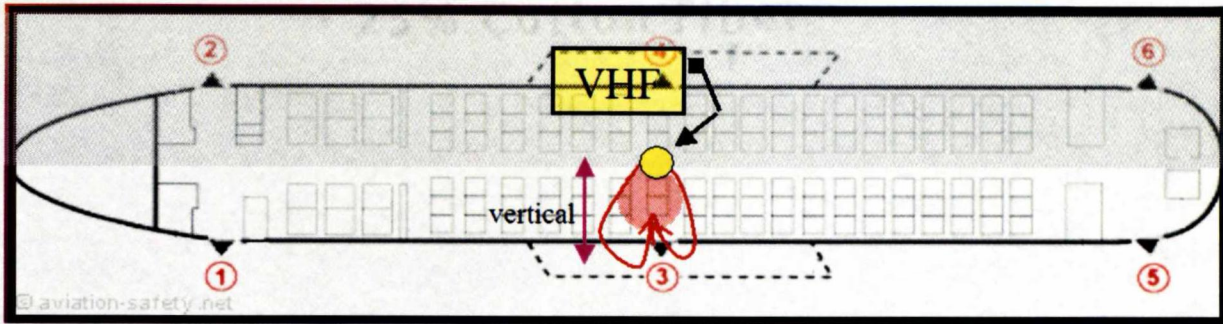


Figure 3.8: Antenna Placement and Coupling prediction for VHF.

The last system to be studied, Localizer, is located on the tip of the tail of the aircraft. Unlike other systems, LOC is horizontally polarized, and it is also not located directly on top of the fuselage, unlike other systems such as TCAS, GPS and VHF. Therefore, the creeping effects of the waves that will leak from the fuselage to the antenna system should be very interesting to observe. However, using the previous methodology of prediction, the greatest coupling should occur near the exit door, which is closest to the LOC system of the aircraft. Therefore, the greatest coupling should occur near the tail of the aircraft near L2 in vertical polarization. The following schematic shows the described prediction for the LOC system:

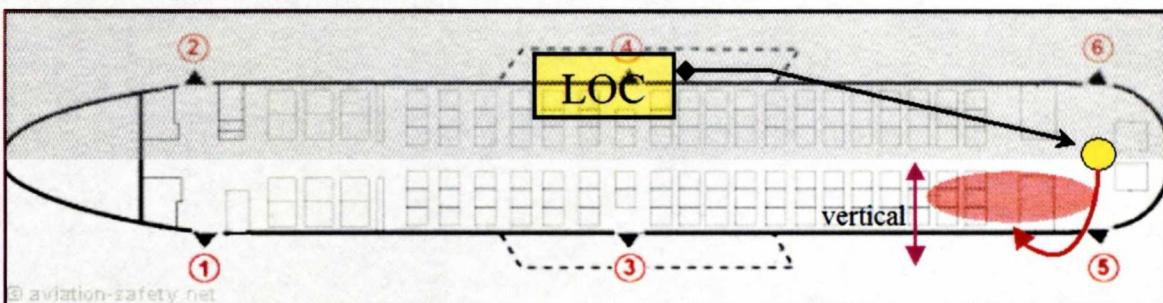


Figure 3.9: Antenna Placement and Coupling prediction for LOC.

3.3 Software Selection for IPL data Interpolation:

IPL data was not only collected along the window locations of the aircraft, but also at each of the seat location, as well as in between two seats. Therefore, with a row of three seats (in coach class), a measurement was taken at the window, then three at seats A, B and C, then three more in between seats A-B, B-C and C-Aisle, and finally one and just the aisle of the row, resulting in a total of 8 measurements at each row of the aircraft. In total, there are 33 windows on B737-200, so 33 rows of data was taken. Moreover, data was not only taken in vertical polarization, but also in horizontal polarization. Therefore, for each aircraft system, a tedious set of IPL data was collected:

$$8 \text{ locations} * 33 \text{ rows} * 2 \text{ polarizations} = 528 \text{ data points!}$$

A creative way was needed to be implemented to ensure that not only all the IPL data was plotted for each system, but also, the regions of greatest coupling could be identified in terms of seat location relative to the location of the windows, doors and antenna system. MATLAB was selected as the software used to display and analyze the collected IPL data. MATLAB is not only a very user-friendly software, but it can also be used to import and export extensive amount of data from other programs, such as EXCEL. This feature was very necessary because overall, about 528 sets of data were collected for each of the five aircraft systems. Then for repeatability and other points of interest, further testing was performed on different B737-200s as well, resulting in an immense amount of data set to be interpreted and analyzed.

Also, MATLAB is one of the most powerful software in vector and matrix manipulations. As described in the next few sections, manipulation had to be performed

on very large matrices to achieve proper results in terms of calibrated IPL data. Furthermore, MATLAB is also very powerful in graphing and plotting of data. Very meaningful 2-D and 3-D plots were obtained using meshing, contouring and surface grids. Other features, such a plot rotation, axis labeling and color maps for legends were also very useful in interpreting the results. Furthermore, MATLAB was also very beneficial in performing the statistical analysis on the extensive set of IPL data.

Since much of the analysis and calculations performed in this research were similar in procedure, another powerful and useful feature of MATLAB included the use of M-Files, designed for small scripts and procedures. The user-friendly software utilizes the basic C-syntax, therefore, commands like 'for', 'while', and 'if' could be used. This helped make the analysis of the data more dynamic and easy to manipulate where necessary. MATLAB is also equipped with many useful toolboxes. In this particular research, the Statistical and Fuzzy Logic toolbox was used extensively in the last few chapters for modeling purposes. With the software selection finalized, the following sections describe the basic approach used to plot the collected IPL data with as much details visible for analysis as possible.

3.4 IPL Data Interpolation for Missing Test Locations

Figure 3.10 (courtesy of Delta Airlines) shows an interior schematic of a B737-200. Observe that the first class seating is in the front of the plane, while the other majority of the seats for coach class are in the back. As described in the beginning of the chapter, the seats in the first class are relatively larger, therefore, only two seats fit in a row on each side of the plane (port and starboard). The seats in the coach class are relatively smaller;

therefore, three seats fit in a row. Also, there are more windows in an aircraft, than seat rows.

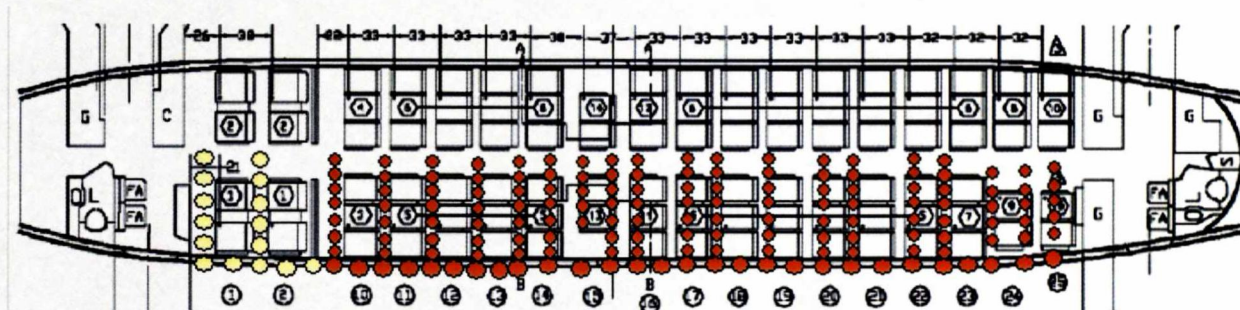


Figure 3.10: Interior Schematic of B737-200 with test locations for IPL measurements.

In the schematic in figure 3.10, yellow circles are used to represent the testing locations in the first class region, while red circles are used for measurement locations in the coach class. Along the walls, observe that there are more windows than seat rows so although every row has a corresponding windows, every window does not have a corresponding row data. This factor is important to understand because the lack of row for every window would create holes in the matrix, designed to be plotted.

Another major observation is that since the number of seats in the first class section differ from that of the seats in the coach class, the number of IPL measurements performed in the First-class rows are less than the measurements on the rows of the coach class. Referring again to figure 3.10, the yellow dots in the first class rows add to up be six measurements for each row: Window, A, A-B, B, B-Aisle, aisle. While the red dots for the measurements along a row of coach class seating add up to 8 measurement locations: Window, A, A-B, B, B-C, C, C-Aisle, aisle. The last three rows of the aircraft, near the tail, also only have two seats, so only six measurements are taken as in the first class. This difference in the number of seats, and therefore data points would also require

some manipulation to the entire matrix of the aircraft. The following figure 3.11 shows an 8 by 33 grid in which the colored region represents locations in which data was collected, while the blank regions represents locations where the measurements were not taken:

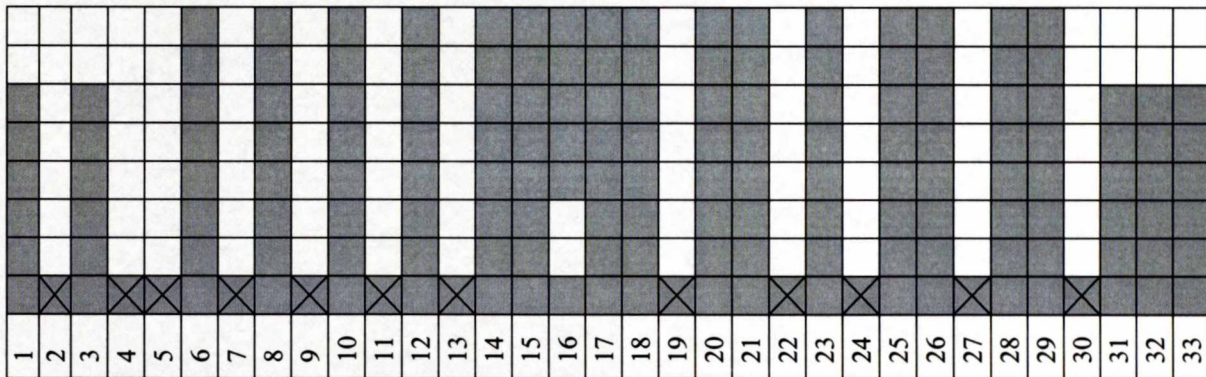



Figure 3.11: 8x33 Matrix Representation of Original Testing Locations.

There were several methods for plotting the data points obtained. One method was to ignore the extra IPL data taken only on the windows, without the corresponding rows (represented by  in the figure); however, this method would result in a loss of valuable data collected. Therefore, it was thought best that to obtain values of the empty rows in figure 3.11 by taking the average of the rows before and after the empty row. The red boxes in figure 3.12 represent the positions of the averaged values of two rows to obtain the middle row.

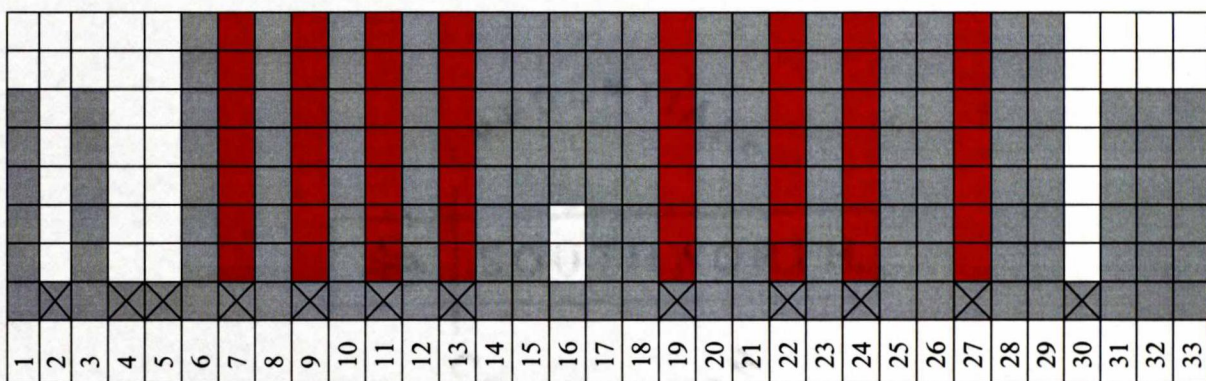


Figure 3.12: Data Interpolation of Entire Rows in 8x33 Matrix.

The next concern taken into consideration was the lack of measurements in a row for first class seating, as well for the rows near the tail of the aircraft. As seen in figures 3.11 and 3.12, rows 1, 3, 31, 32, and 33 only have six measurements recorded, instead of the 8, observed in rows 6 through 29. To make up for the two missing measurements in each row, averaging was performed for between seats W and A, and B-aisle and aisle. Please see figure 3.13 in which the original measurements are still gray, while the new averaged measurements are in yellow, obtained by averaging the measurements taken from the left and right seat locations.

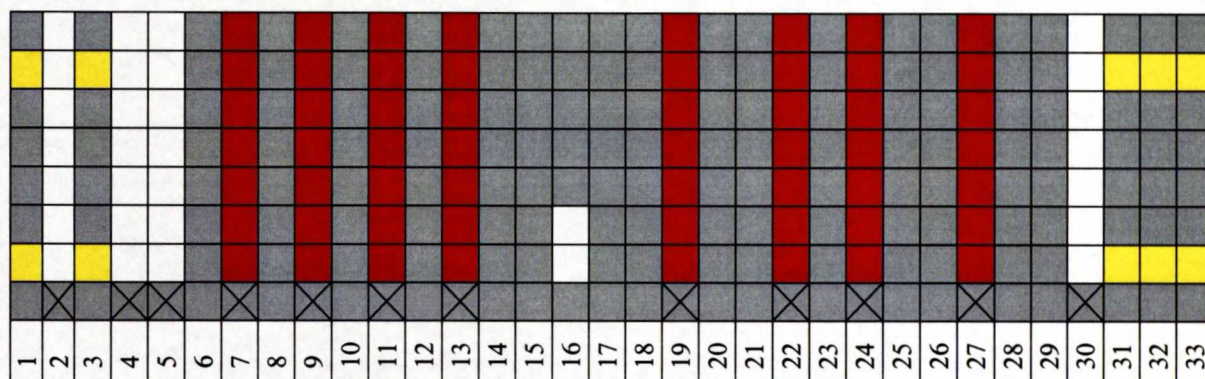


Figure 3.13: Data Interpolation of Missing Seats in First class and Last row seating.

Referring back to figure 3.10, observe that there are only two seats in the emergency exit row of a B737-200. Therefore, on window 16 (emergency exit door), only six set of measurements were recorded, instead of the eight of the other rows in coach class. Since seat 'A' was missing, the following measurements were recorded: window, B, B-C, C, C-aisle and aisle. To make up for the two missing locations, the data was interpolated by averaging the IPL measurement recorded at the window and seat location B of row 16. Figure 3.14 shows the interpolated IPL values obtained for the two missing locations (represented by the green boxes). Finally, rows 2, 4, 5, and 30 could be

obtained using the similar method of averaging entire rows before and after the empty row. Therefore, the values of row 2 are obtained by averaging rows 1 and 3 etc.

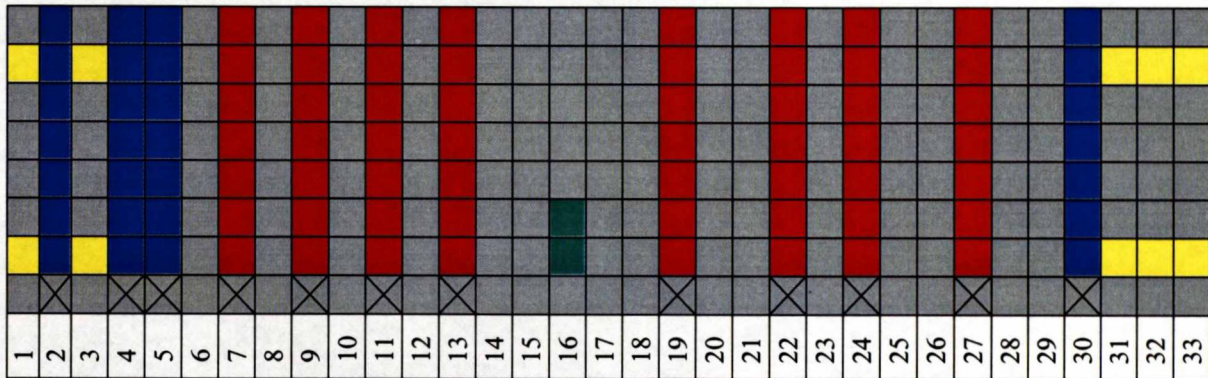


Figure 3.14: Data Interpolation of Missing Seats in Emergency Exit row.

Using the various averaging methodologies above, a complete 8 x 33 matrix was obtain which could be plotted. As a summary, in figure 3.14 above, 33 columns represent the 33 rows of the aircraft, with 1 being close to the nose, while 33 being near the tail of the aircraft. The boxes closest to the numbered locations (bottom most row) represent the IPL measurements taken at the window locations of the aircraft. While the top most row represent the measurements taken at the aisle of the aircraft. Overall, the 8x33 matrix represents the port side of the aircraft. The gray-colored boxes represent the locations where IPL data was actually measured by the test team. The red boxes represent the IPL measurements obtained by averaging the previous and forward rows originally measured (in gray). The yellow boxes represent the values obtained by averaging the IPL measurements taken in the same row on the left and right measurement location of the missing seat. The interpolated values for the missing seat location in the emergency exit row (window 16) are represented by the green boxes. Finally, the blue boxes represent the averaged row obtained by averaging the rows before and after the missing row.

It was assumed that the method of averaging should be valid because major fluctuations in the IPL data were not expected. Therefore, it was assumed that sudden spikes in the data should not exist; rather, the IPL data should increase or decrease gradually from one location to the other. Similar methodology of averaging was used for data collected for all aircraft systems as well as on other B737-200s tested. The next section shows an example of a 3D plot obtained for a system.

3.5 IPL Plot Generation in MATLAB

With the matrices formed with the averaging technique described in the previous section, the IPL data was plotted using the 3-D plotting capabilities in MATLAB. MATLAB provides a variety of functions to display 3-D data. Some plot lines in three dimensions while others draw surfaces and wire frames using pseudocolor to represent a fourth dimension. For the IPL data, the 'mesh' and 'surface' capabilities were used. The command 'mesh' creates 3-D perspective plots of matrix elements, displayed as heights above an underlying plane. MATLAB defines a mesh surface by the z-coordinates of points above a rectangular grid in the x-y plane. It forms a plot by joining adjacent points with straight lines, giving an illusion of a continuous plot, instead of discrete. Mesh surfaces are useful for visualizing matrices that are too large to display in numerical form or for graphing functions of two variables.

The first step in displaying a function of two variables, $z = f(x, y)$, is to generate X and Y matrices consisting of repeated rows and columns, respectively, over the domain of the function. Then use these matrices to evaluate and graph the function. The 'meshgrid' function transforms the domain specified by two vectors, x and y, into

matrices, X and Y . Then these matrices can be used to evaluate functions of two variables. The rows of X are copies of the vector x , and the columns of Y are copies of the vector y .

In addition to the 'mesh' command, 'surf' is also used to better display the IPL data. The functions 'mesh' and 'surf' display surfaces in three dimensions. If Z is a matrix whose elements $Z(i, j)$ define the height of a surface over an underlying (i, j) grid, then `mesh(Z)` generates a colored, wire-frame view of the surface and displays it in a perspective projection. Similarly, 'surf(Z)' generates a colored, faceted view of the surface and displays it in a perspective projection. Ordinarily, the facets are quadrilaterals of constant color, outlines with black mesh lines, but the 'shading' function can be used to eliminate the mesh lines or to select interpolated shading across the facet.

When 'mesh(Z)' and 'surf(Z)' are used with a single matrix argument, that argument specifies both the height and the color of the surface. The 'pcolor' command is used to generate the colors for each value of the data on the z -axis. For each point, $z(i, j)$ is used as an index into a color map to determine the color to display at that point. The color map is a matrix with three columns specifying the intensity of the three video components, red, green and blue. In this case, the color map used maps the data between shades of red, green and blue. This is useful because the continuous range of colors extending from black to white lends itself to representing the contours of the peaks. The function 'rgbplot(Z)' plots the data ranging from red, to green to blue for the values in the z -matrix.

Figure 3.15 shows a sample 3-D plot generated for the IPL data, using the commands described above. The x -axis is used to represent the 33 rows, starting from

row 1 near the nose of the aircraft, to 33 near the tail of the aircraft. The y-axis is used to represent the 8 locations, real or interpolated using the averaging techniques, on which IPL data was measured. The y-axis ranges from W, which represents the window location, to 'I', which represents the aisle location. A, B and C, represent the data taken on the actual seats, while A-B, B-C and C-I represents data taken in between seats and aisle. Finally, the z-axis is used to plot the measured IPL data, which fluctuates smoothly from high to low, representing different levels of coupling.

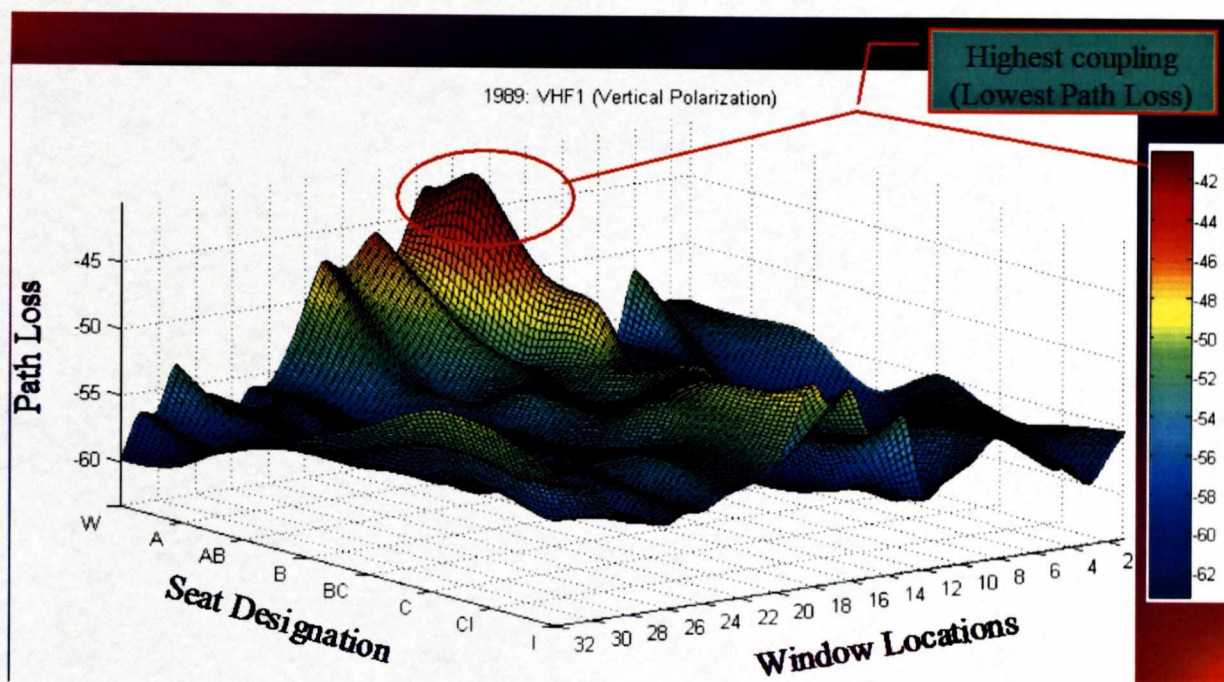


Figure 3.15: 3D Representation of Coupling Patterns.

Figure 3.15 also shows a color bar on the side with shows the IPL values in dBm, corresponding to colors from red to green to blue. The red color, which represents the lowest IPL value, also represents the region where the greatest coupling between a transmitting PED and an aircraft system may exist, while the blue color represents

regions of lowest coupling. Therefore, in the figure, the greatest coupling occurs near the window location on row 16.

When the EMI pattern becomes too complicating in plots, it becomes more complicating to pick out the exact location where the IPL value was the lowest, or where the greatest coupling existed. MATLAB allows the user to specify the angle from which a 3-D graph may be viewed as desired. The 'view' function sets the angle of view in spherical coordinates by specifying the azimuth and elevation of the viewpoint with respect to the axes origin. The azimuth is a polar angle in the x-y plane, with positive angles indicating counter-clockwise rotation of the viewpoint. The elevation is the angle above (positive angle) or below (negative angle) on the x-y plane. Please refer to figure 3.16 below to understand the coordinate system used. The arrows indicate positive directions.

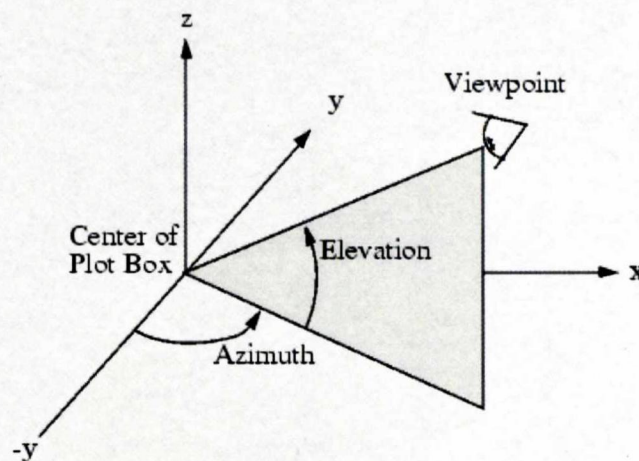


Figure 3.16: Illustration of MATLAB's Co-ordinate System.

Therefore, for the rest of the analysis, it was determined to rotate the 3-D graphs such that the viewpoint is directly above the x-y plane, at an elevation of 90 degrees from

the horizon. This resulted in a 2-D conversion of the 3-D graph in which the color bar would need to be used as the reference to determine the peaks and valleys of the EMI pattern to locate the regions of the lowest and highest couplings. Figure 3.17 shows a rotated version of the graph from figure 3.15. In the figure, it can now clearly, and much easily, be seen that the area of lowest path loss, or the greatest coupling occurs on seat location 'A' of row 16. Again, the areas of concern in this research are where the greatest coupling occurs (red regions, in this case). The next few chapters include the analysis of the IPL data measured and recorded. Much of the plotting techniques used in this chapter are used. Also, the EMI patterns are studies thoroughly so that the hypothesis made in the beginning of this chapter about the relationship of coupling relative to the locations of the aircraft systems, doors and windows, is tested.

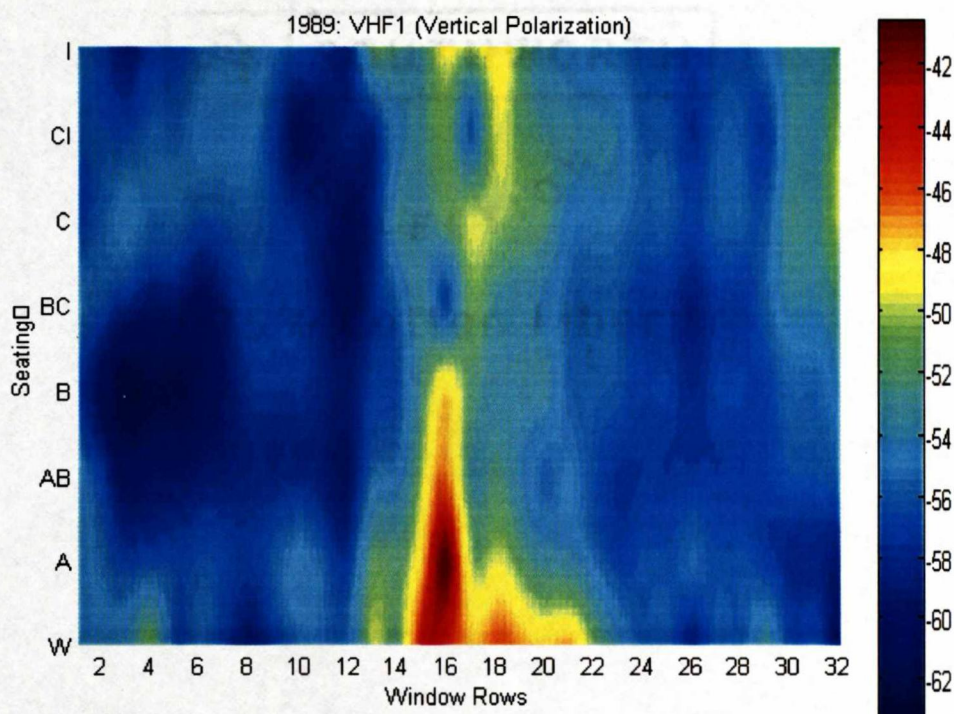


Figure 3.17: Sample IPL Plot Generation for Understanding the Regions of Greatest Coupling.

4 GRAPHICAL ANALYSIS OF IPL DATA ON MAJOR AIRCRAFT SYSTEMS AND TESTING AIRCRAFT SYMMETRY

4.1 Introduction to IPL data on Aircraft Systems of B737-200, #1989

Chapter 3 gives a summary of how the collected IPL data was going to be plotted using MATLAB. In this chapter, the IPL data measured on a B737-200 will be plotted and analyzed using the techniques described previously. Throughout the report, there will be several references to the different 'nose types' of the aircraft. Aircraft are first identified by their model type, i.e. B737, B747, B777 etc. Then they are further classified by their series type, i.e. 200, 300 etc. In this research, the aircraft model and serial numbers were B737-200. However, since several of the airplanes have the same model and serial numbers, it becomes essential to differentiate one plane from the other. Therefore, the numbering sequence is used which is referred to as the 'nose type' of the aircraft. This number is usually visible near the nose, or the tail end of the aircraft. In this particular chapter, IPL results measured on two B737-200s, nose types 1989 and 1997, are analyzed. The next few sections include the analysis of the plotted IPL data from B737-200, #1989 and B737-200, #1997.

4.1.1 Glideslope (GS) Analysis

As mentioned in Chapter 2, the GS system is located in the nose of the aircraft. Due to its location, it was predicted that the greatest coupling would occur at the earlier

rows of the aircraft as well (represented by the red region on the schematic in figure 4.1). It was estimated that the greatest coupling would occur near the first exit door of the aircraft. Figure 4.1 shows the predicted results of coupling patterns for the GS system as well as the actual results plotting using the IPL data. As mentioned in chapter 3, the x-axis represents the seat rows in the aircraft, starting from window location 1 to window 33 in the tail of the aircraft. The y-axis represents the locations at which IPL measurements were performed within each row. In total, 8 sets of measurements existed (actual as well as interpolated), labeled as: Window, A, A-B, B, B-C, C, C-aisle and aisle.

Observe that in figure 4.1, two graphs are cascaded on the same x-axis. One result is when the measurements were taken in vertical polarization (with the transmitting antenna held at a vertical position), while the other plot refers to the measurements with the transmitting antenna held in the horizontal position for horizontal polarization. Also, these measurements were taken on the port side of the aircraft, and not on entire plane, or the starboard side. If the measurements had been taken on the entire plane, the y-axis would've had the following labels: W_{port} , A, A-B, B, B-C, C, C-I, I_{aisle} , I-D, D, D-E, E, E-F, F, $W_{\text{starboard}}$.

As predicted, the graphical results confirm that the lowest IPL was indeed in the front of the aircraft. Therefore, more coupling (represented by the red region) is found in the front sections of the aircraft. The GS system is horizontally polarized, as described in the previous chapters, therefore lower IPL values were expected when the transmitting antenna was held in the horizontal position. According to the plot for the GS system, better coupling does indeed occur between the test antenna and aircraft antenna when the test antenna is horizontally polarized. Observe that in the figure, the plotted results for

horizontal polarization have coupling levels at a greater value than those found in the plot for vertical polarization. Therefore, the greatest coupling is found near the first five window locations of the aircraft. Also, the level of coupling decreases as the distance from the GS system in the nose of the aircraft increases.

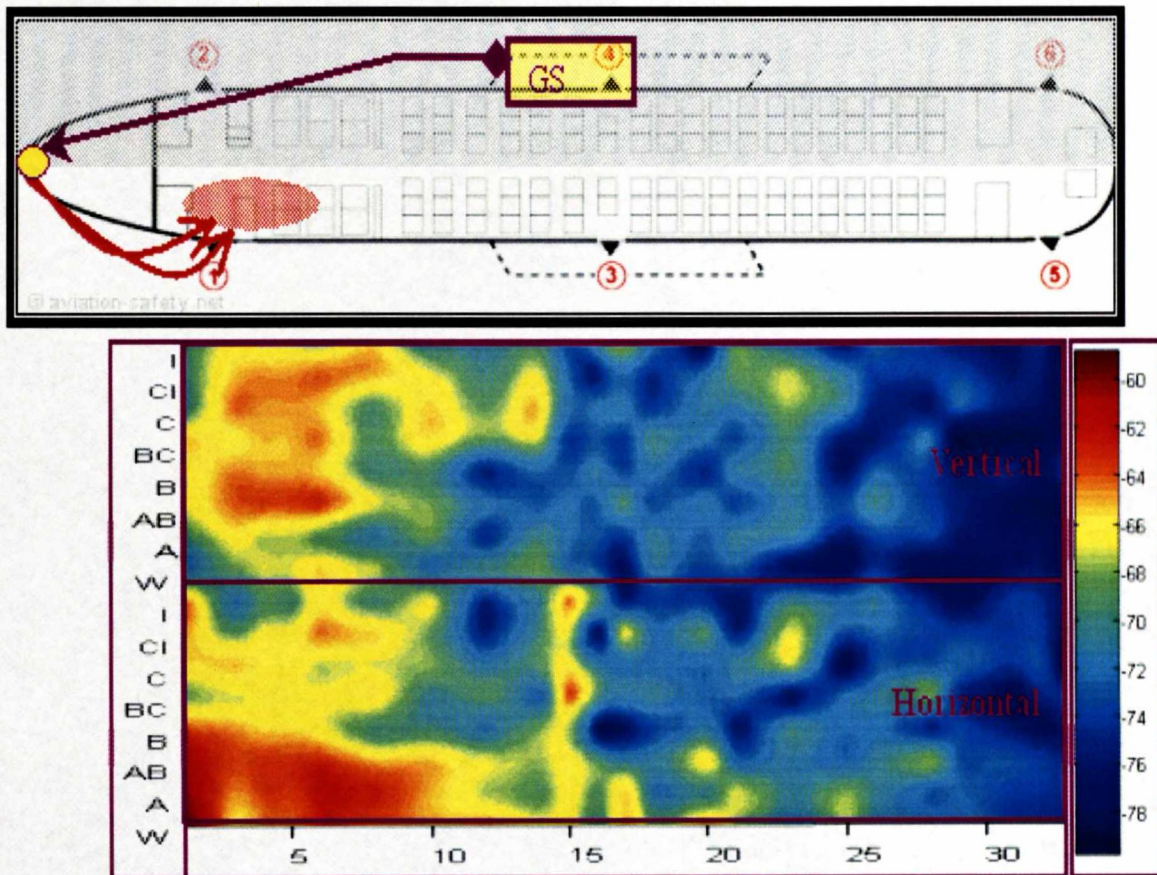


Figure 4.1: GS Prediction and Actual Results.

4.1.2 TCAS Analysis

The Traffic Alert and Collision Avoidance system (TCAS) is located on top of the second window of the aircraft. The estimated and the measured result of the TCAS IPL pattern are shown in Figure 4.2. Due to its location, it was predicted that the greatest coupling would occur near the front exit of the aircraft, as well as near the second window location for TCAS. Unlike the GS system, TCAS is vertically polarized, therefore, it was also predicted that the greatest coupling would occur when the transmitting antenna is held in the vertical position during testing.

Graphical results in figure 4.2 confirm that the lowest IPL was indeed observed at the front end of the fuselage, near the L1 doorway and window location 2. In terms of coupling based on the polarization of the antenna system, better coupling does indeed occur between the test antenna and aircraft antenna when the test antenna is vertically polarized. As figure 4.2 shows, the greatest level of coupling is shown exactly near the second window location in vertical polarized testing, while the results for horizontal polarization show no significant levels of coupling. Also, similar to the trend noticed in the GS system's analysis, the coupling for TCAS is the greatest in the front of the plane, and decreases gradually as measurements were taken near the tail of the aircraft.

Also, the coupling levels are higher along the windows of the aircraft, and decrease as the measurements toward the aisle were taken. Also, since the measurements are only taken on the port side of the aircraft, it is interesting to notice that the greatest coupling occurs near the windows of the aircraft, and *not* near the aisle locations on top of which the TCAS unit is directly mounted. This observation in the plot shows that the

waves actually ‘creep’ along the aluminum surface of the fuselage and enter only through the doors and windows, instead of leaking directly into the aircraft. Such a behavior of a straight-path coupling can be predicted for future aircraft made from composite material.

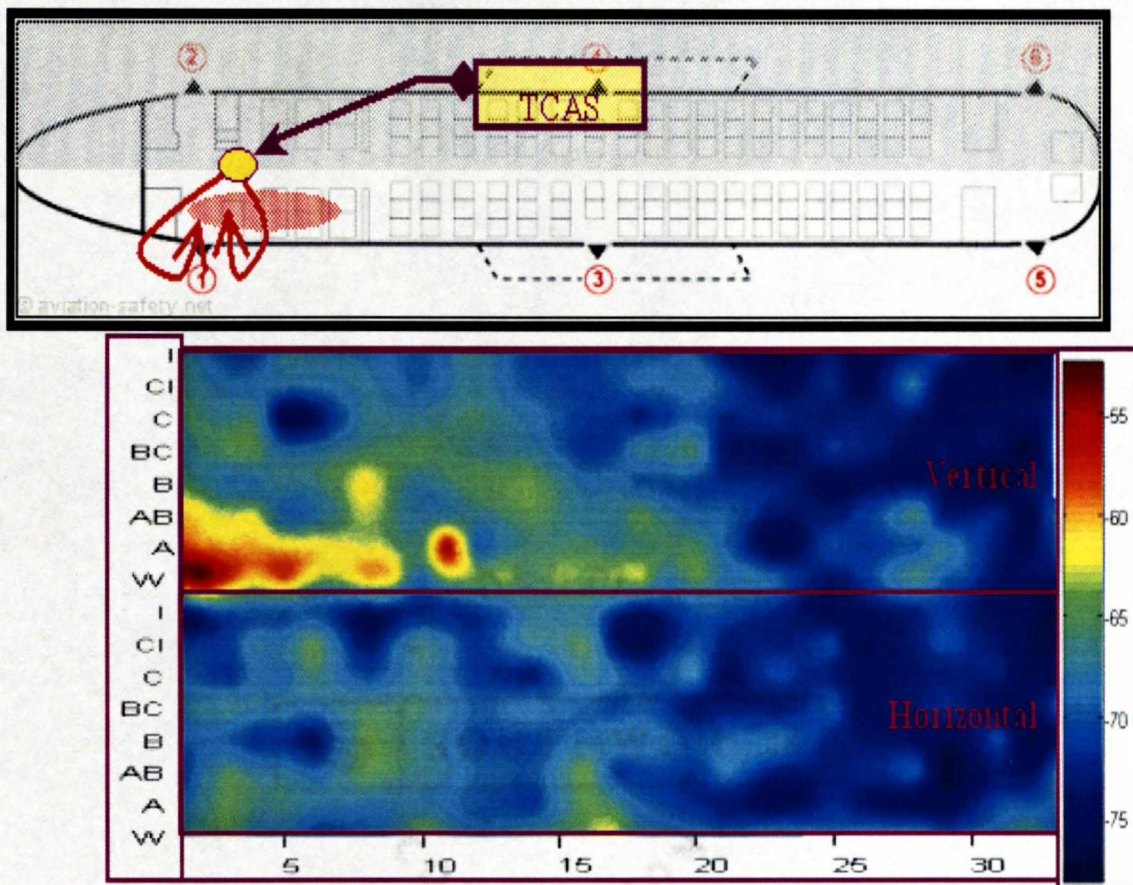


Figure 4.2: TCAS Prediction and Actual Results.

4.1.3 GPS Analysis

The GPS is located on top of window 9 of the aircraft. As mentioned earlier, the positioning of GPS is different from other systems in that there are two available slots on top of the fuselage, out of which the unit was actually installed on the slot slightly on the starboard side of the tested aircraft. Similar to TCAS, GPS is also vertically polarized. Therefore, it was predicted that the greatest levels of coupling would be noticed near window 9 in vertical polarization. Unfortunately, when performing the IPL measurements for GPS, data was only collected along the window locations of the aircraft, instead of the entire port side. However, many useful conclusions can be drawn from just the window data as well.

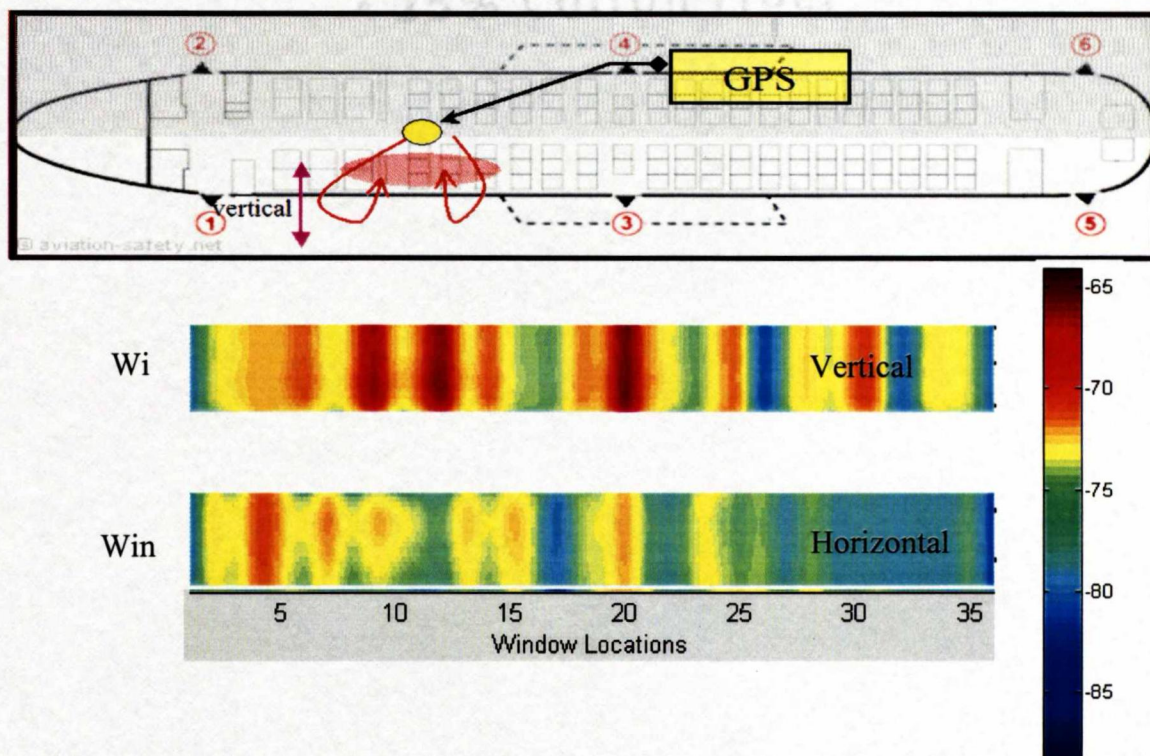


Figure 4.3: GPS Prediction and Actual Results.

Figure 4.3 shows the estimated prediction of the regions of greater coupling as well as the actual IPL results measured for GPS on the window locations in both horizontal and vertical polarizations. As predicted, the greater coupling indeed exists in the measurements in vertical polarization. However, the IPL results are not only low near window location 9, but they are also significantly low near window 12 and 20. There is also a significant peak in coupling near the tail of the aircraft on window 31. Therefore, the testing with GPS, which is thought to be one of the top systems of the aircraft in terms of EMI susceptibility concerns, shows high coupling in various regions of the aircraft, instead of concentrating the coupling regions directly beneath the installed unit around window 9.

Figure 4.4 is a simple 2-D plot of all IPL values collected for the GPS system along the rows. This method of plotting makes it easier to find the peaks of coupling levels presented. Observe that the IPL data for vertical polarization is plotted in magenta (thin line), while horizontal polarization is plotted in blue (bold line). With this method of graphing, it can be easily seen that the coupling levels in vertical polarization are greater than those in horizontal polarization. More importantly, it is interesting to note that coupling in vertical polarization is significantly greater than that in horizontal polarization only around window location 9 (on top of which the system is mounted). Otherwise, the IPL values deviate along the same level in both horizontal and vertical polarizations as measurements taken toward the rear of the aircraft are plotted.

Also in figure 4.4, observe the presence of 'L1', 'LE' and 'L2' on the x-axis that were not present in the colored plots before. These IPL measurements were obtained by

moving the test antenna along the entire circumference of a door or window exit seams, while measuring the maximum coupling over the entire sweep. These are defined as “door sweep” measurements. The tick-marks on the x-axis, labeled ‘L1’, ‘LE’ and ‘L2’, represent the “door sweeps” performed on window locations 1, 16 and 33 respectively. Door sweep was measured to understand the effects on IPL measurements due to leakage from the door seams (versus the windows). Although the IPL values taken at the door sweeps for the GPS plots were not significantly different than the values obtained directly in the surrounding windows, the necessity of taking data using the sweeping method will be emphasized in analysis in the next two chapters.

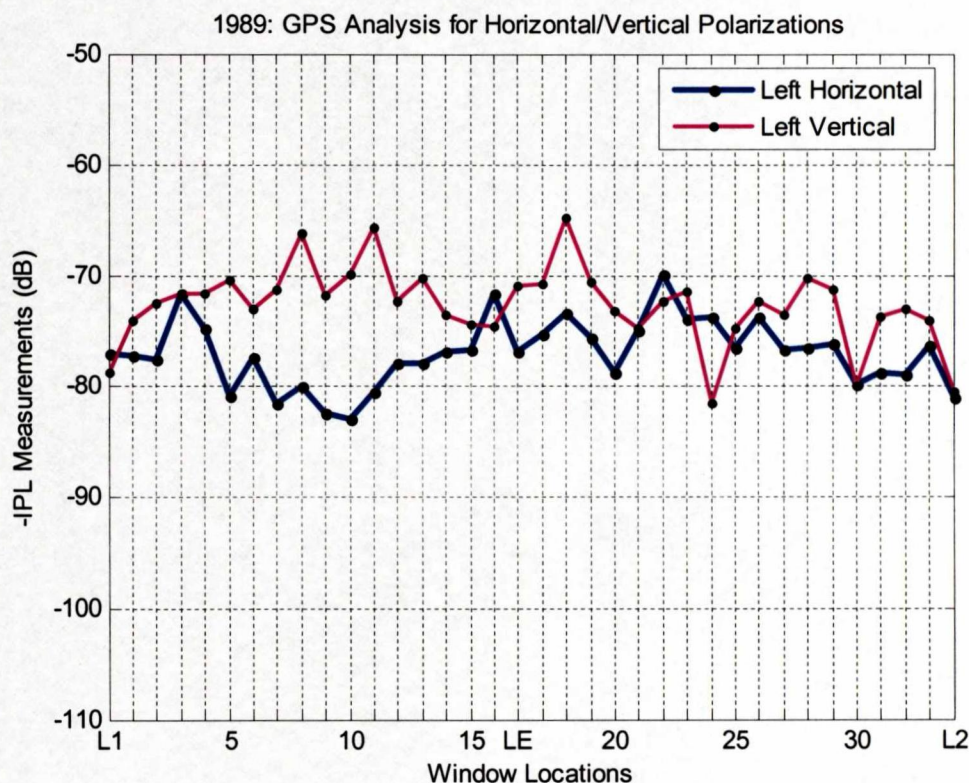


Figure 4.4: GPS results in a simpler 2D plot.

4.1.4 VHF Com. Analysis

The VHF Com. Antenna is located on top of the middle Emergency exit, precisely, window 16 of the B-737 airplane. Therefore, it was predicted that the greatest coupling would occur near window 16 (emergency exit). Also, since the aircraft antenna is vertically polarized, it was assumed that waves would couple better vertically than horizontally. The estimated and the measured result of the VHF Com. IPL pattern are shown in Figure 4.5. Graphical results confirm that the vertical polarization is dominant and the greatest coupling occurs near the emergency exit, or window location 16 of the aircraft. Just like in the previous systems of concern, the region of high coupling for the VHF are closest to the window locations, and the coupling decreases as the measurements were taken further away from the window (the emergency exit, in this particular case). Another important observation for the VHF system is that in the plots for horizontal polarization, relatively high coupling is observed throughout all windows of the aircraft, except at window location 16. This observation will be analyzed in detail later; however, it is predicted that such a pattern of high coupling near the windows may have been due to the type of transmitting antenna used. Please refer to section 5.2 to read further details on the reasoning behind the coupling along all windows in horizontal polarization for the VHF system.

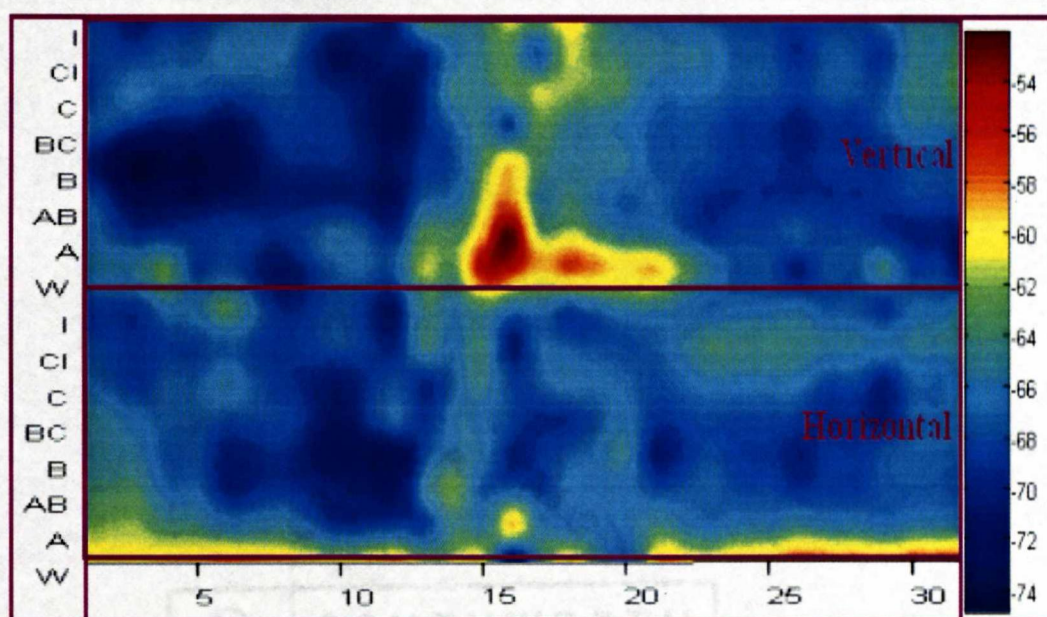
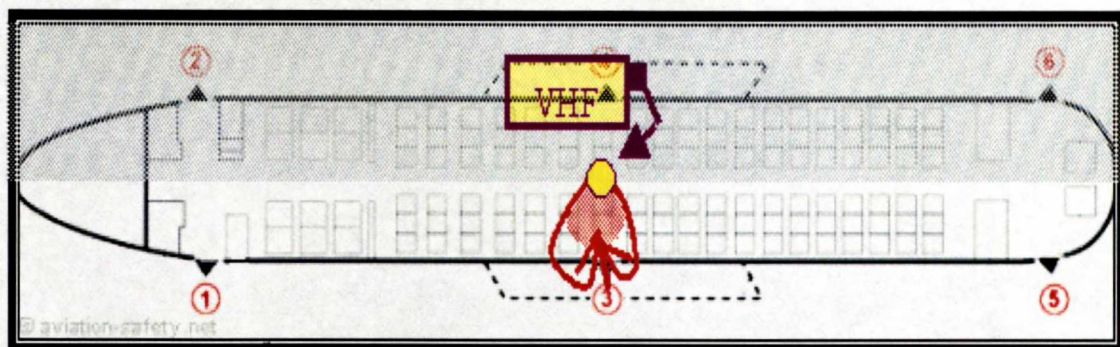


Figure 4.5: VHF Prediction and Actual Results.

4.1.5 LOC Analysis

All previous aircraft systems tested, with the exception of GS system, have been mounted on the centerline on the top of the aircrafts' fuselage. The LOC antenna is different in mounting perspective because it is located at the tip of the tail of the aircraft. Also, unlike TCAS, GPS or VHF, the LOC system is horizontally polarized. Therefore, it was predicted that the greatest coupling would occur near the rear exit of the aircraft, with the test antenna in the horizontal polarization. The estimated and the measured result of the LOC IPL pattern are shown in Figure 4.6. Graphical results confirm that the horizontal polarization is dominant, however the greatest coupling does not occur toward the rear of the airplane.

The graphical plot indicates that the L2 doorway (rear left) is not in an optimal location to allow coupling to the back of the airplane, but the over-wing exit (at window 16) is. In previous antenna systems, the couplings were the greatest near the aircraft antenna, and decreased as the distance from the antenna increased. In the case for the LOC system, however, the coupling is intense at window 16, but is also relatively large along windows 7 through 16. These graphical results cause the simple method of coupling prediction to be incorrect, as the coupling is *not* necessarily relative to the distance from test location to aircraft antenna. Since LOC system is horizontally polarized, the waves transmitted horizontally must couple better.

Also, since the antenna is mounted on the tip of the tail of the aircraft, coupling must be best at greater distances so that the horizontally transmitted signal could couple with the horizontally polarized antenna system. In case of horizontal and vertical

propagations in the rear of the fuselage, the coupling must simply not be optimum because the distance was too close. Also, the presence of the wing near the emergency exit may have also played a major role in wave reflection and coupling, making the locations near window 16 the most vulnerable to EMI effects.

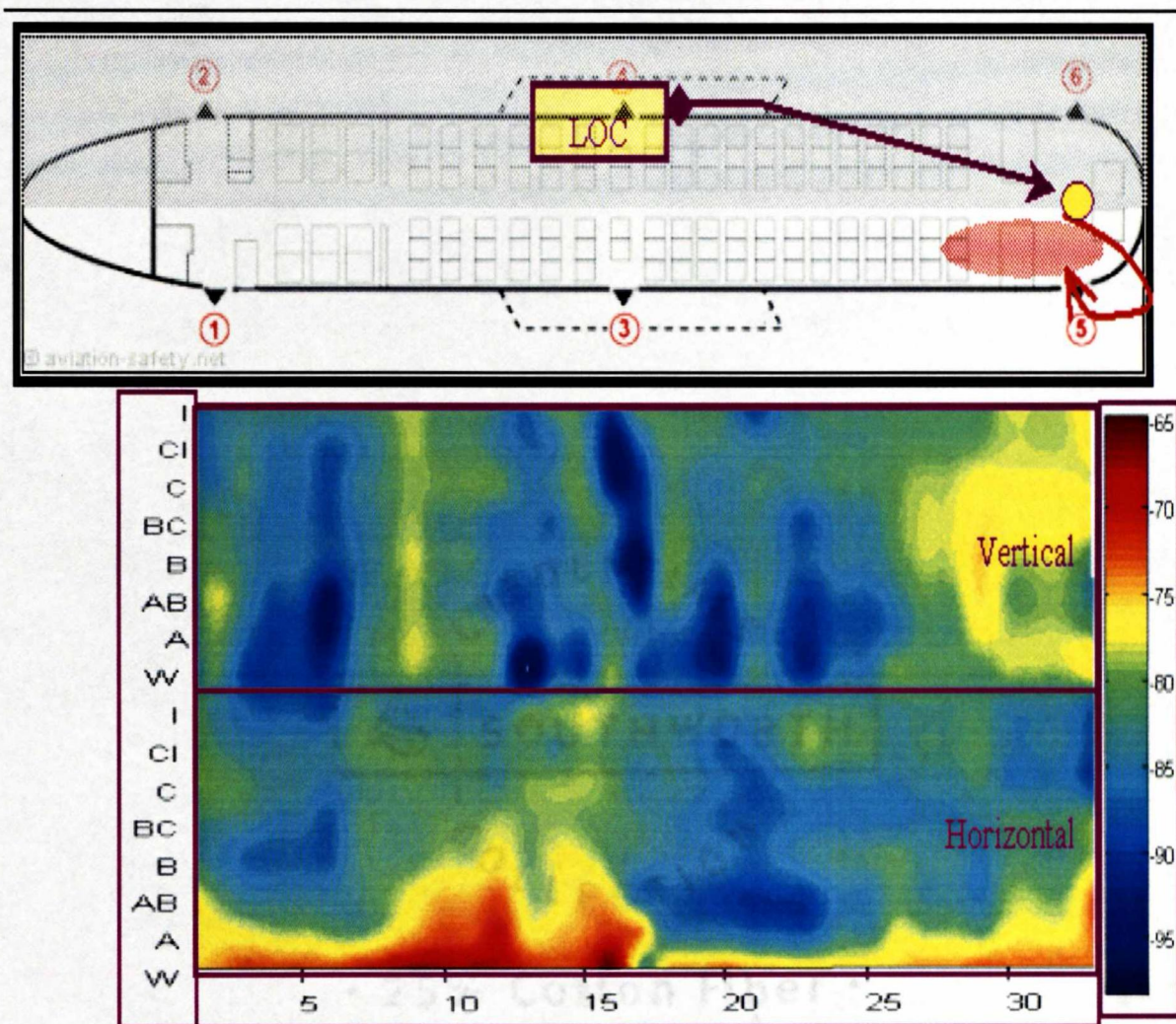


Figure 4.6: LOC Prediction and Actual Results.

4.2 Testing Airplane Symmetry on GPS

Thus far, IPL measurements analyzed have been taken only on the port side of the airplane. An important question arises that should IPL measurements taken on starboard side be similar in pattern as on the port side measurements? In terms of the schematic of a B737-200, the starboard side is very similar to the port side. Please refer to figure 4.7 for an overview of the schematic. The major differences between port and starboard side lie in the front and the tail end of the fuselage; however, due to the lack of windows in these regions, it can be assumed that not much significant impact must exist on the symmetry of IPL patterns on either sides of the aircraft.

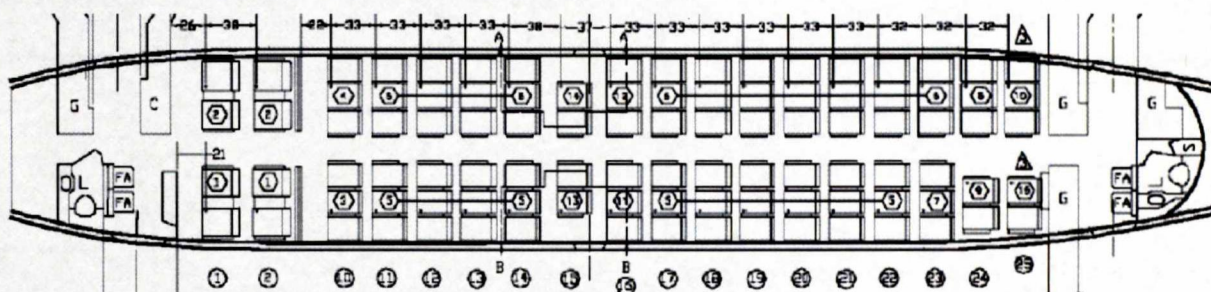


Figure 4.7: Original Schematic of B737-200.

The IPL measurements were performed using the GPS on both port and starboard side of the aircraft. With this system, the objective was not only to see whether the IPL measurements along the port side and the starboard side were symmetrical, but also whether there was any impact on the IPL values on the starboard side, since the GPS unit was installed on the starboard slot of the tested aircraft. Please refer to Figure 3.4 in previous chapter, which shows two possible locations of the GPS antenna. Since the GPS antenna was mounted on the slot toward the starboard side, it was expected that the

IPL values on the starboard side should be slightly lower than the values on the port side; therefore, the coupling on the starboard side should be a little greater than that on the port side. Figure 4.8 shows the GPS analysis for vertical polarization, while figure 4.9 shows the results for horizontal polarization taken on B737-200, #1989.

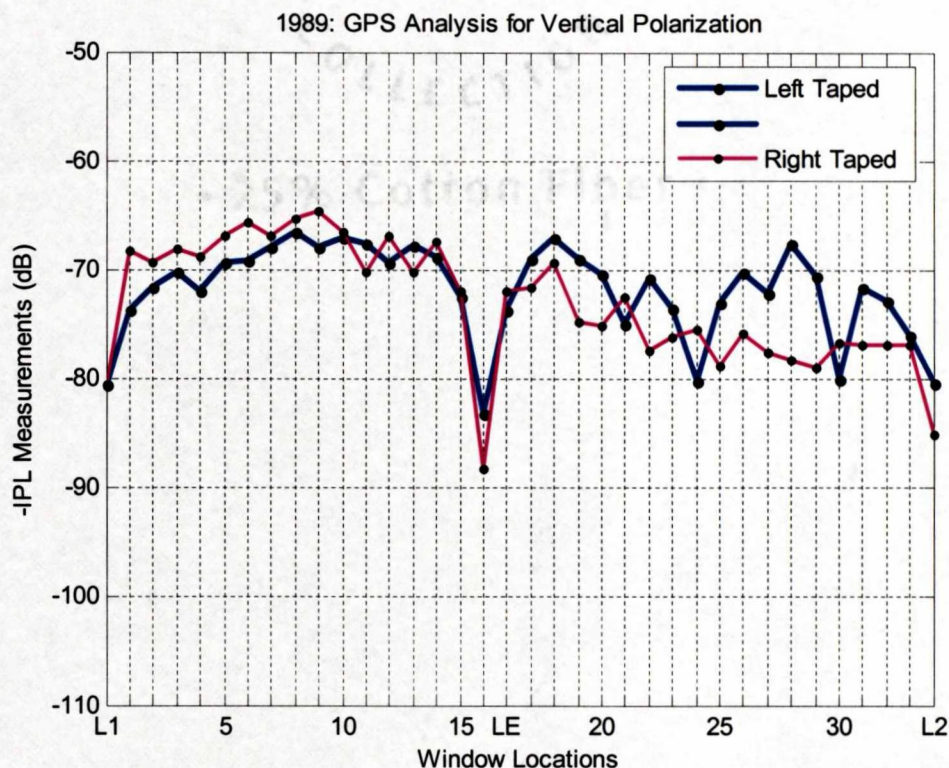


Figure 4.8: Port vs. Starboard Comparison of GPS in Vertical Polarization.

Observe in the legend that the IPL values plotted are “taped” on both port and starboard side. This testing was performed when the doors of the aircraft were physically taped (described in detail in Chapter 7). However, for this chapter, the analysis is only focused upon the aircraft symmetry and the effect on IPL pattern due to the slight shift of GPS mounting from the centerline of the fuselage. In terms of symmetry in the IPL values, the values plotted in both figure 4.8 and 4.9 for port and starboard side are very

similar in pattern. When the coupling level is increased at a particular location on the port side, it is also shown as increasing on the starboard side, and vice versa. This result shows that the IPL patterns on the aircraft are indeed symmetrical for the GPS antenna. It can also be concluded that the data should also be symmetrical for other antenna systems tested as well.

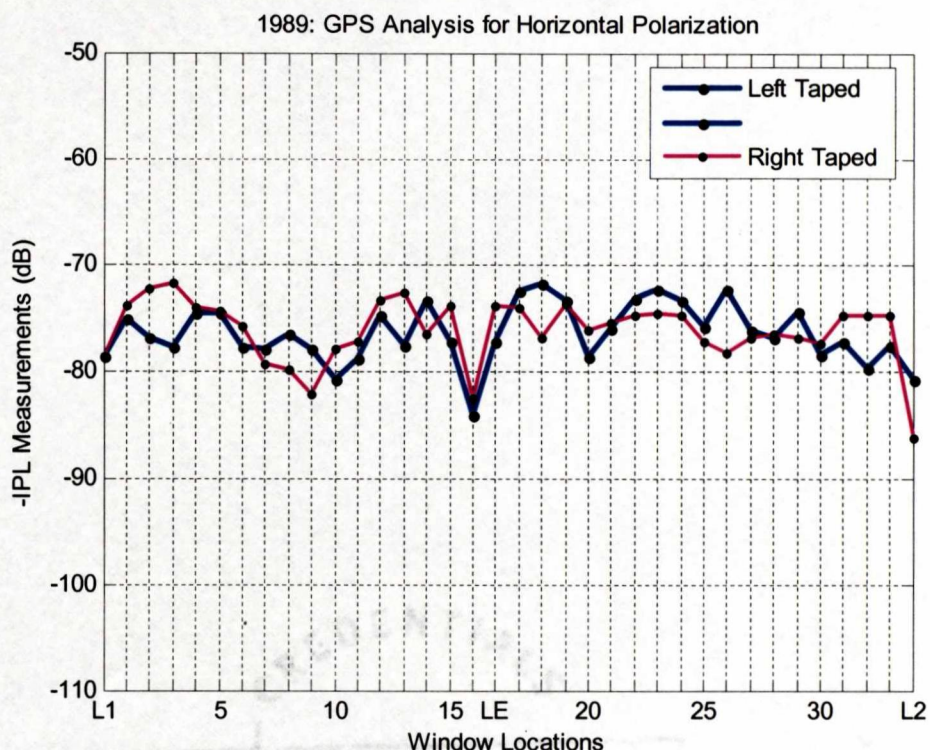
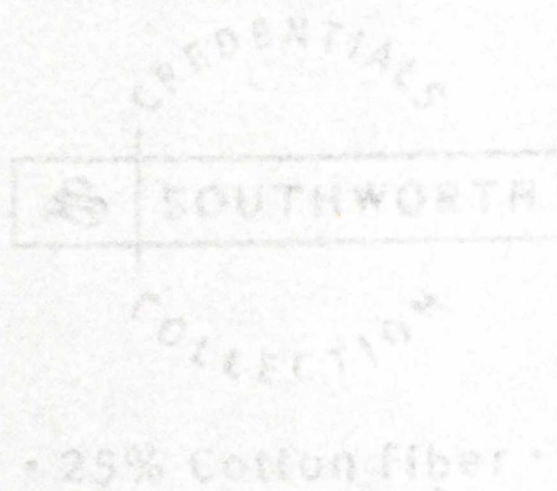


Figure 4.9: Port vs. Starboard Comparison of GPS in Horizontal Polarization.

The second concern was to study the effect on IP values due to the shift in the GPS mounting toward the starboard side. Since the GPS antenna is vertically polarized, the greater details are found in the graphical results for vertical polarization as well in figure 4.8. Due to the shift in mounting, it was predicted that the IPL values on the starboard side should be lower (greater coupling) than the values on the port side. By observing the solid magenta and blue lines in the figure, it can be seen that the starboard

side, indeed, had greater IPL measurement from windows #1 to #9; however, the measurements deviated between high and low between port and starboard side after window #10, when moving toward the tail of the aircraft. Therefore, the fact that the GPS was mounted off-centered only impacted the coupling values in the front of the fuselage, and not much in the tail end.



5 IPL VALIDATION AND COMPARISON

In previous chapters, different kind of analysis has been performed on the IPL data collected on B737-200, #1989. Since the coupling pattern and IPL levels depend on the way electromagnetic waves propagate from the transmitting antenna source and reach aircraft antenna, it raises an important question that how repeatable are the IPL measurements? When discussing wave propagations in a non-uniform environment, having a specific pattern in terms of coupling levels should be almost impossible. However, the purpose of this research is to pinpoint the locations of the highest coupling; therefore, only the repeatability of coupling levels at particular locations are of concern.

This chapter includes IPL result analysis from another aircraft of the same type as analyzed before (B737-200). The next section includes results of comparing B737-200, #1989 with B737-200, #1997. Asides from data repeatability, the effects of changing testing equipment is also analyzed in this chapter. Finally, graphical results obtained through the analysis on entire aircraft are compared with the results taken only at the window. This particular analysis is performed because taking IPL measurements on the entire plane can be very tedious, costly and time consuming.

5.1 Data Validation by Using Different Aircraft: #1989 vs. #1997

All graphical IPL data presented so far was obtained on United Airlines B737-200, #1989. Another, identical set of data was obtained using a different airplane (United Airlines B737, #1997). On this particular airplane, a different set of instrumentation, cables, and a different test team was used. This change definitely created a scenario

which made the testing of data repeatability valid. Again, it would be impossible to get the same IPL results for all systems exactly, however, for the analysis to be valid, the basic pattern of wave propagation and the spectrum of IPL values collected should be similar for both #1989 and #1997. Similar to #1989, in #1997, all windows, seats, aisles, and in between seat and aisle data was taken. Figures 5.1, 5.2 and 5.3 show the graphical plots for the GS, TCAS and VHF systems' IPL data obtained on B737, #1997, respectively. Each of the figures includes a schematic of the aircraft to show the positioning of the aircraft system of concern, the actual results on #1989 and finally the new results on #1997.

In comparing graphs, many similarities in the patterns can be observed. Most importantly, the color regions and color scale magnitudes are very similar for both the #1989 and #1997 graphs. This assures that the IPL findings were similar, regardless of the different airplanes, test equipment and personnel performing the measurements. Full seat window and aisle data was not obtained for the LOC system on #1997 due to excessive aircraft antenna/cable loss, therefore, that comparison could not be made in this analysis.

As a summary, notice that in Figure 5.1, the horizontal polarization is dominant in both the GS plots obtained from data on #1989 as well as #1997. Also, the coupling is the greatest near the front of the aircraft, since the antenna is located in the nose of the aircraft. As mentioned before, the vertical polarization is dominant for TCAS. Therefore, the highest coupling is observed when the IPL measurements were taken with the transmitting antenna in the vertical position (Figure 5.2). Also, since the TCAS is located on top of window 2 of the aircraft, the greatest levels of coupling are observed

near window 2 and L1 doorway on both #1989 and #1997. It is interesting to see that the regions of low coupling are also very similar in both graphs.

Similarly, the VHF system is also vertically polarized. As seen in figure 5.3, the VHF system is located on top of the emergency exit, precisely window 16; therefore, the regions of the greatest coupling exist near window 16 in vertical polarization for both the measurements on #1989 as well as #1997. Just like the results for #1989, the intensity of coupling decreases as the distance of the measured location from the aircraft antenna increases. Observe that for all systems analyzed above, the spectrum of the coupling also lies in the same region for the measurements on both #1989 and #1997 systems.

It was noted, however, that the measurements taken on #1997 were not as “crisp” as the measurements taken on #1989. For example, in the VHF system’s analysis, the regions of high coupling are concentrated very tightly near window 16. However, in #1997, the coupling is indeed the greatest near window 16, but it decreases gradually in the neighboring seats. Also, in the result for horizontal polarization for VHF system, it is important to observe that there is again a “wall” of high coupling next to all the windows of the aircraft for #1997. This finding led to another study in the next section, which is helpful in understanding the effects of different transmitting antennas during testing. The next section also attempts to explain the reasoning behind the regions of high coupling along all the windows in horizontal polarization for the VHF system.

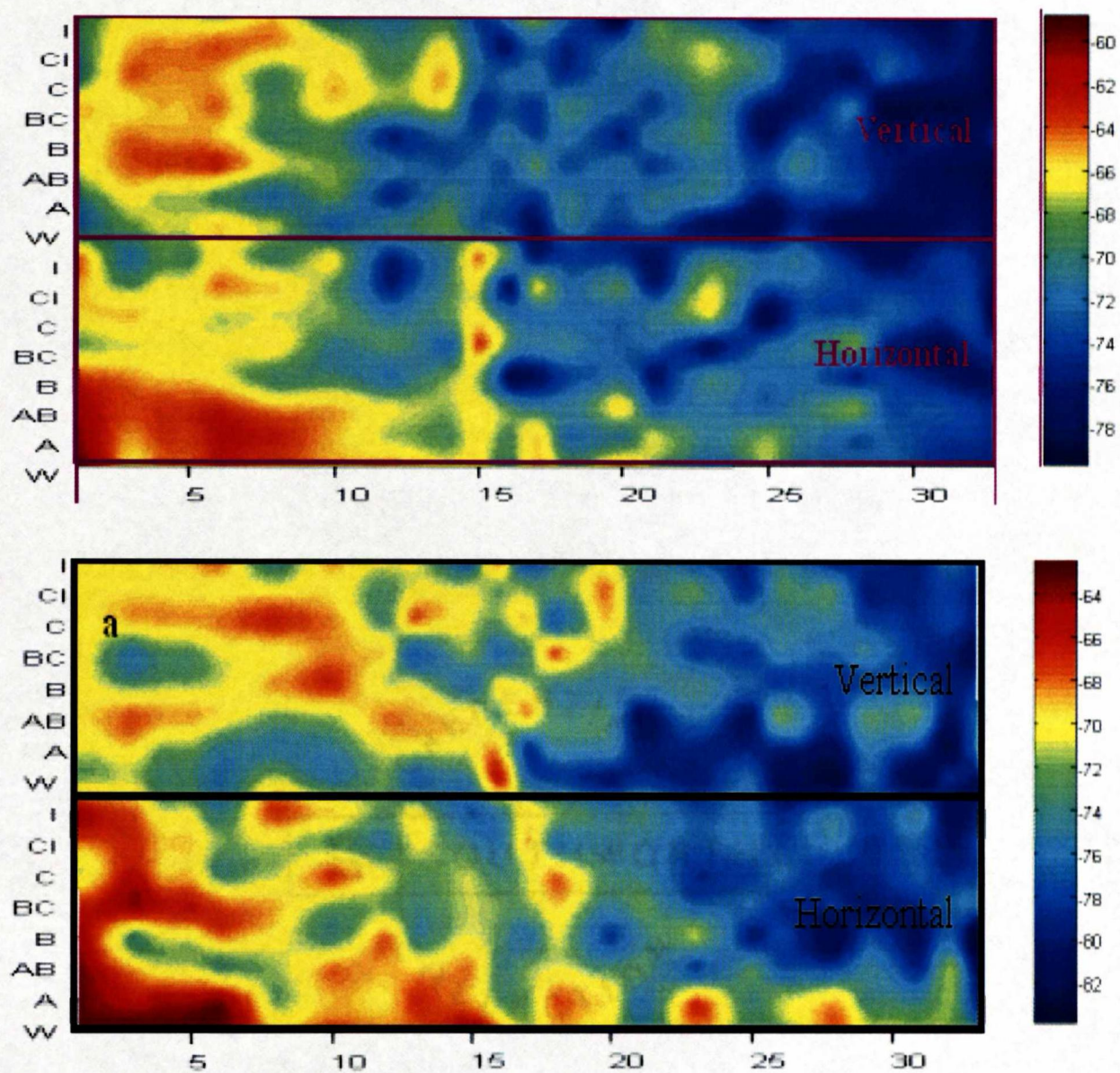
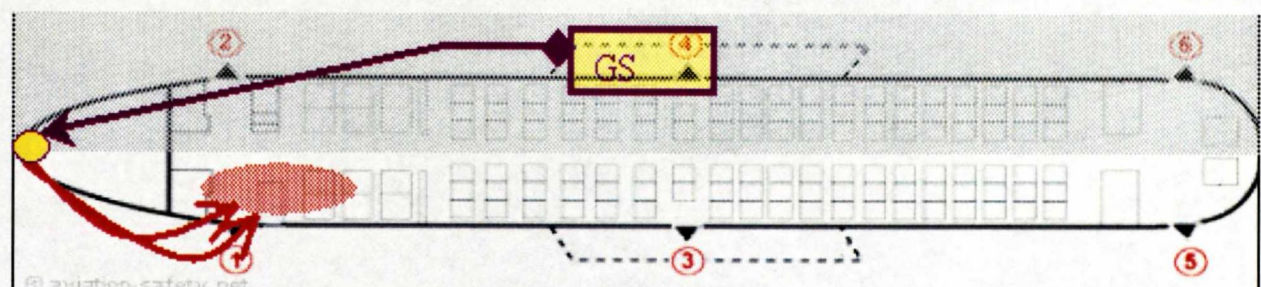


Figure 5.1: Illustration of GS location (top), results from #1989 (middle), results from #1997 (bottom) for GS.

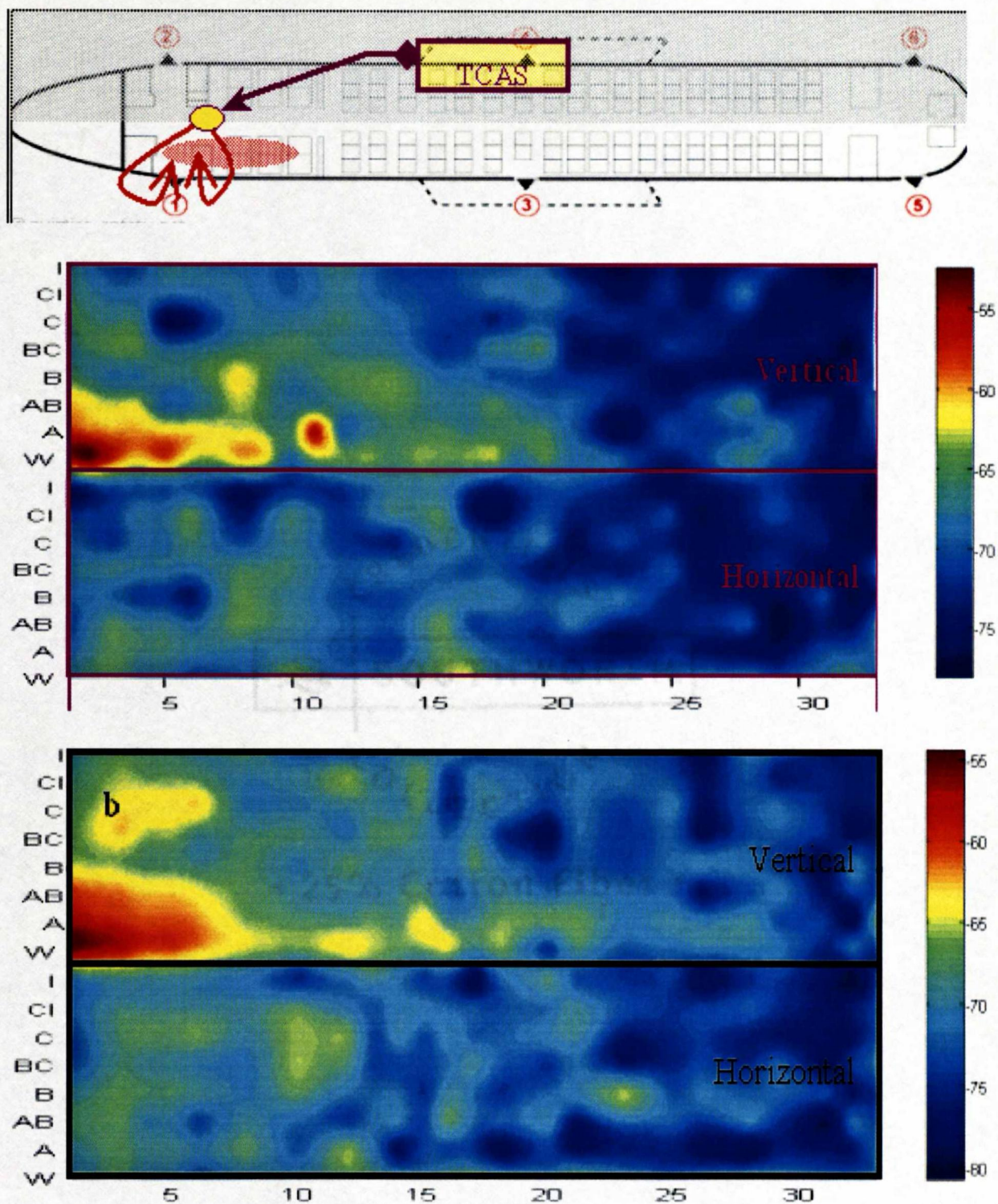


Figure 5.2: Illustration of TCAS location (top), results from #1989 (middle), results from #1997 (bottom) for TCAS.

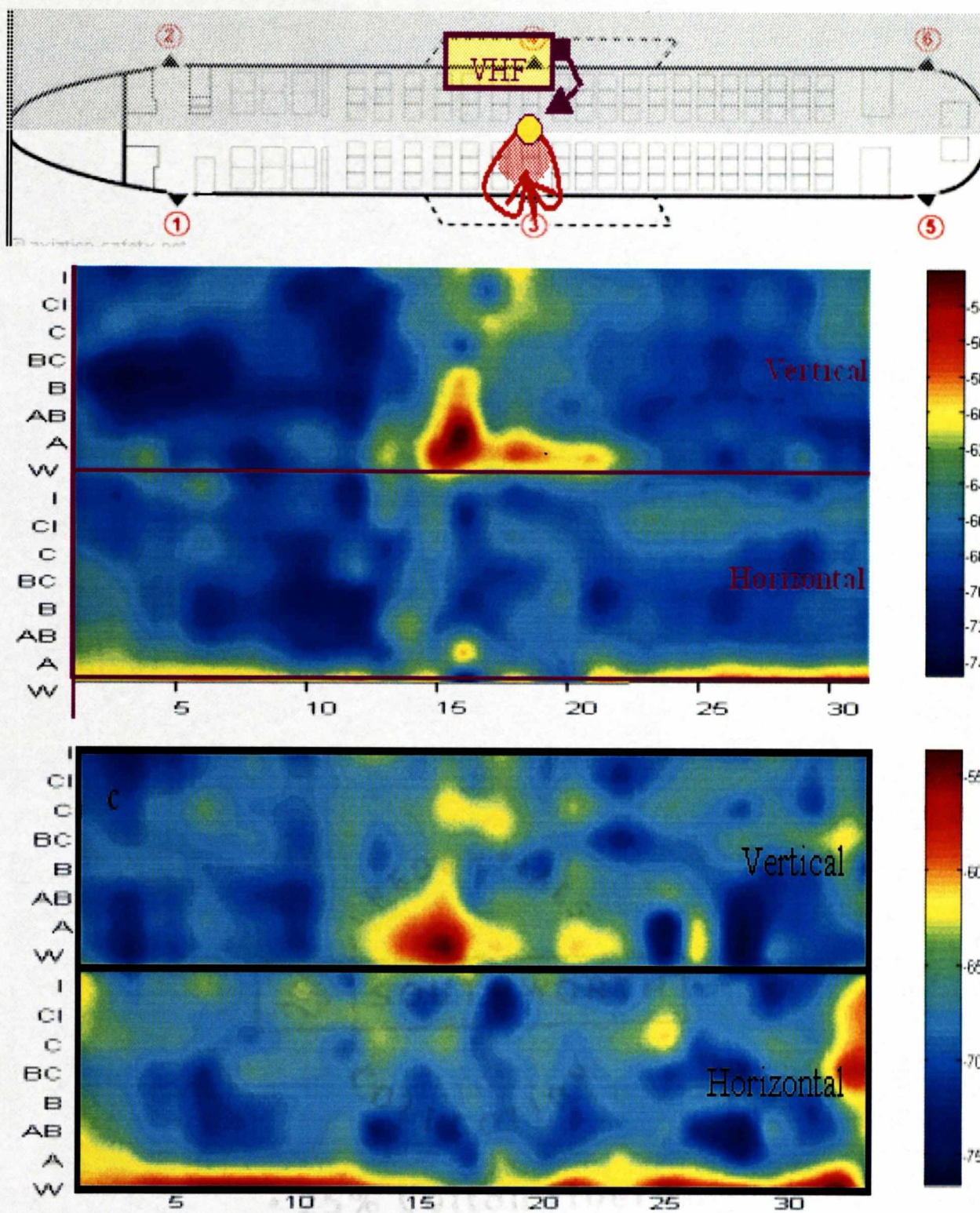


Figure 5.3: Illustration of VHF system's location (top), results from #1989 (middle), results from #1997 (bottom) for VHF.

5.2 Data Validation by Using Different Transmitting Antennae:

Dipole vs. Biconical

As described in the previous section, when analyzing the VHF system and the IPL values obtained for the system, it was discovered that there exists a region of high coupling in horizontal polarization along all the windows of the aircraft. Since the VHF system is vertically polarized, this behavior was unexpected. After much study, the reasoning behind the region of high coupling went toward the type of transmitting antenna used during testing. The VHF Com. data plotted in this paper previously utilized an ETS 3121C dipole Antenna, with antenna element lengths adjusted for optimum efficiency (54.0 cm per element in the VHF Com. frequency band). It was hypothesized that since the dipole antenna is as long as three window spans, this may be causing the unnecessary coupling along the windows even in the horizontal polarization. Also, due to the length of the antenna, it may be likely that the data obtained is not applicable in real world applications. (It is very unlikely for a passenger to carry a PED large enough to span the length of three windows.) Therefore, it was proposed that similar IPL measurements be taken on the entire airplane, using a smaller antenna, to see if the IPL patterns change for the horizontal polarization.

A Schwarzbeck UBAA9114/BBVu9135 small biconical antenna was used to repeat the entire set of IPL measurements for the VHF Com. aircraft system. The Schwarzbeck small biconical antenna is much smaller than the ETS 3121C dipole antenna (44.4 cm total length), and covers only about one window span of an aircraft, resembling a real world PED more closely. Relative to the dipole antenna, the

Schwarzbeck small biconical antenna has 10.7 dB less gain (-10.7dB) in the VHF Com frequency band. This is primarily due to reflection loss because of its small electrical size in the VHF Com frequency band. Figure 5.4 shows the two transmitting antennas used during testing. The dipole antenna is pictured on the right, while the biconical antenna is shown on the left, both in horizontal polarization. As seen, the biconical antenna is much smaller than the dipole, and is therefore, a better representation of the PEDs carried in the real-world scenarios.

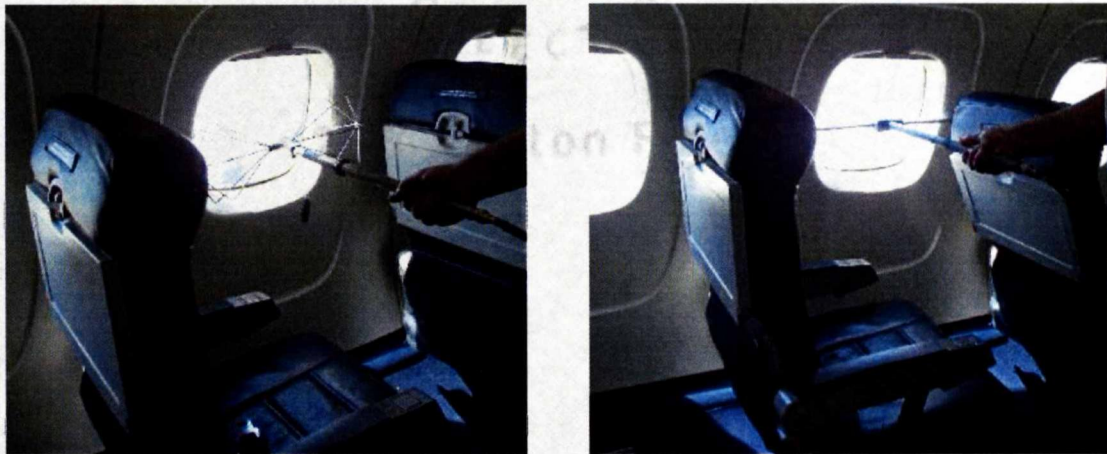


Figure 5.4: Illustration of Biconical (left) and Dipole (right) Antennae in Horizontal Testing Position.

Figure 5.5 shows schematic of the aircraft with the location of the VHF system. Also, the original graphical representation of the IPL measurements using a dipole antenna is included. Finally, the figure includes the MATLAB plot of the entire aircraft VHF Com IPL, when transmitting through the small biconical test antenna. The raw data was adjusted by +10.7 dB to account for the relative gain of the small biconical antenna to the dipole antenna.

Surprisingly, there is almost no difference in the EMI patterns of the plots. The line of greater coupling near the windows of the horizontal polarized data is still present in the plots with biconical antenna, and in fact more pronounced. This indicates that the improved horizontal polarization coupling near windows is not an artifact of the IPL measurement process, but an actual physical phenomenon. The pattern near window 16 of high coupling in the vertical polarization is also very similar. Most importantly, application of the -10.7 dB gain factor for the small biconical antenna results in a nearly identical IPL magnitude scale.

This analysis and results not only reconfirm the data repeatability, but also validate the IPL results even after using a different antenna system. Also, since the results were very identical, this can lead to the conclusion that in future, a simple biconical antenna can be used for testing to produce similar quality results after applying the gain factor. Biconical antenna is much smaller, therefore easier to transport to the testing locations. Also, this is a relatively cheaper antenna. Last but not least, using a biconical antenna as the transmitting source better resembles the real world PEDs that are usually the source of radiation during flight.

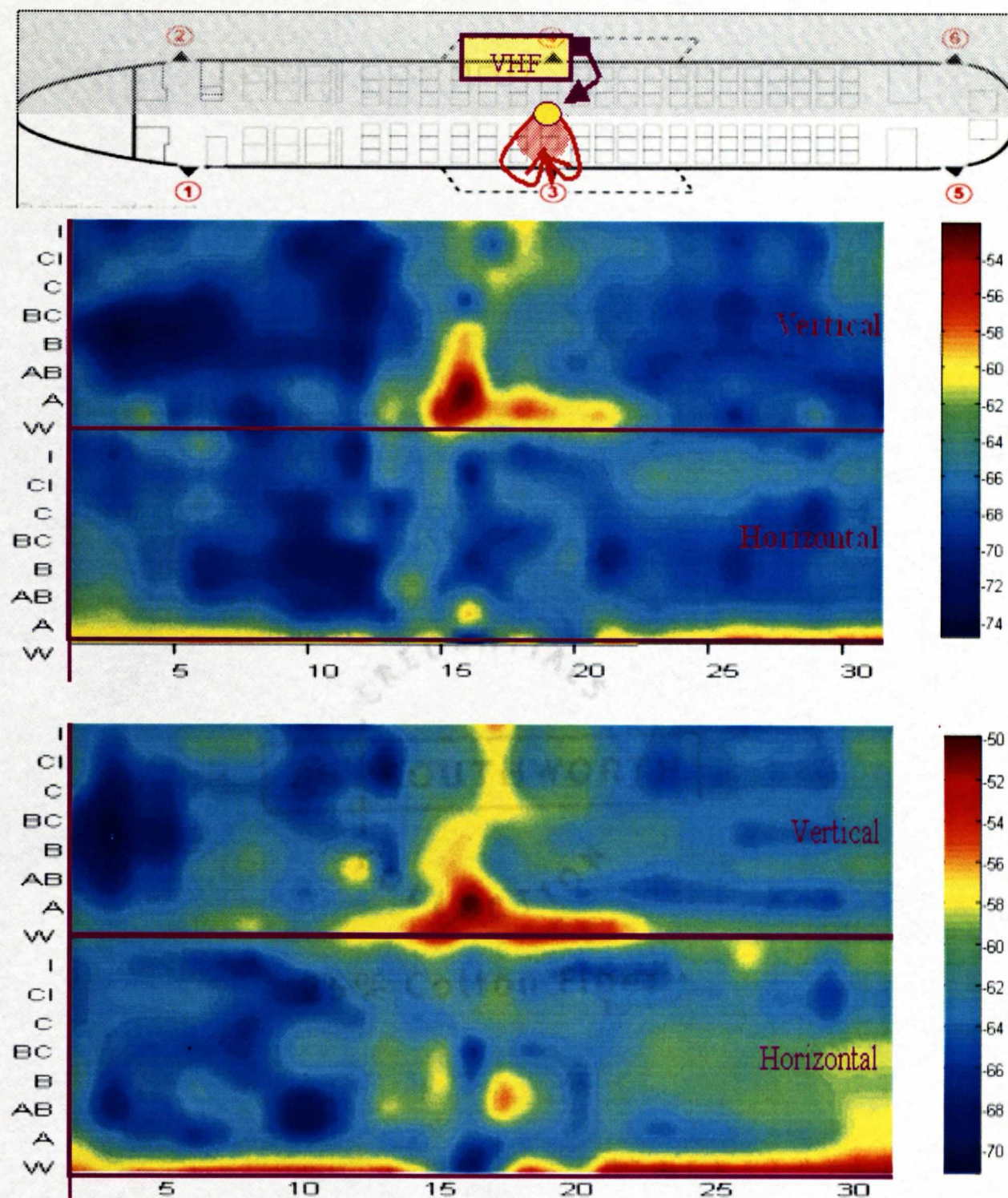


Figure 5.5: Illustration of VHF System's location (top), graphical result using Dipole Antenna (middle), graphical result using Biconical Antenna (bottom).

5.3 Data Validation by Taking Data on Windows only: Full Plane vs. Windows

Taking window, seat and aisle IPL data on an entire airplane can be tedious, time consuming and expensive. Eight sets of measurements on each row of the aircraft are required, and there are 33 rows. In addition, measurements must be made at each of these points with the transmitter once in the vertical position, then in the horizontal: leading to 528 sets of measurements (on a B-737-200 series airplane). Most IPL data reported in the past includes only window measurements. Therefore, it is helpful to find any correlation between full sets of IPL data and window-only data, to better understand and use existing IPL data sets.

In this section, graphical analysis is applied to determine whether the same characteristics and conclusions can be drawn from just the window data in comparison with the data taken on the entire aircraft. This part of the analysis will help in the understanding of whether IPL data can be just taken at the windows of the aircraft, instead of the entire rows, to determine the locations of the greatest coupling.

Graphical plots were made for only the window locations of B-737 #1989. These plots are included in Figure 5.6. After a careful comparison of these plots with the plots in Figures 5.1, 5.2, 5.5, and 5.6, in chapter 4, several conclusions can be made:

The GS graphical plots for window data show that horizontal polarization is dominant and the greatest coupling occurs in the front of the aircraft. These observations

are the same for the entire airplane data set. The vertical polarization window plot does not fully reveal the minimum IPL values obtained away from the windows.

The TCAS graphical plots show that the vertical polarization is dominant and the greater coupling occurs at the front of the aircraft. These observations are the same for the entire airplane data set observed in the previous chapters.

The VHF graphical plot results for the windows-only may be misleading, however. With a graphical plot of the entire airplane, it is clearly evident that optimal test antenna coupling is vertically polarized with the greatest coupling near the exit door. However, as seen in the window-only plot for VHF system above, the horizontal polarization appears to be dominant, and the window-only plot does not reveal that coupling rapidly diminishes when moving away from the window.

The LOC graphical plots show that horizontal polarization is dominant and that comparable coupling levels occur throughout the aircraft. These observations are the same for the entire airplane data set. The vertical polarization window plot does not fully reveal the minimum IPL values obtained away from the windows. In summary, the graphical comparison shows that taking data on the entire plane, although tedious and very time consuming, can reveal important insight into IPL coupling phenomena, which are otherwise not necessarily visible by plotting the IPL values obtained just near the window locations.

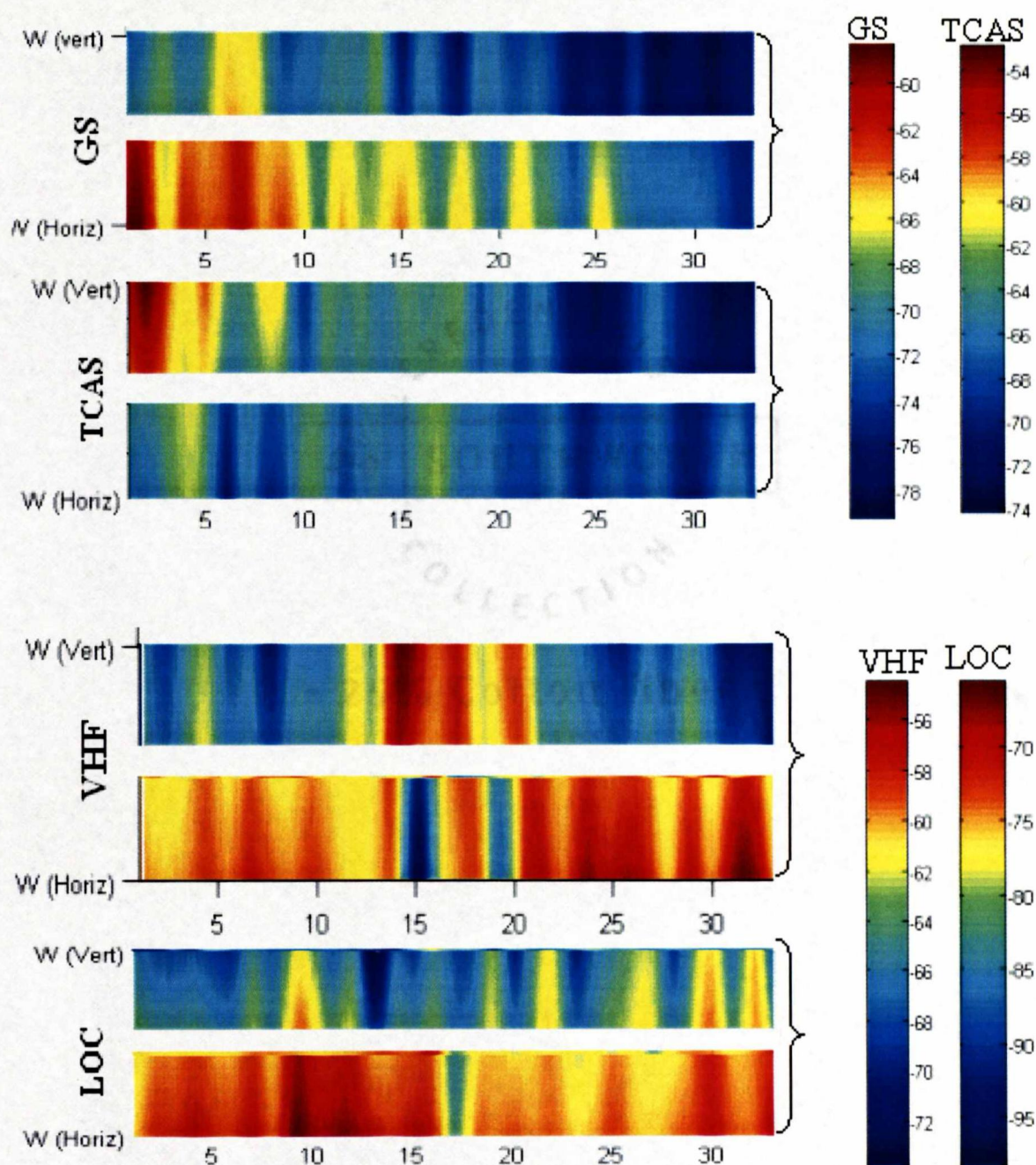


Figure 5.6: Graphical Representations of IPL data for GS, TCAS, VHF and LOC systems, taken only on window locations.

6 STATISTICAL ANALYSIS OF IPL DATA

Intense graphical analysis of IPL data has been performed in previous chapters; however, to model the electromagnetic patterns properly in later chapters, it becomes essential to analyze the collected IPL data statistically. The measurements in this research may be referred to as a statistical experiment, which describes a process by which several chance measurements are obtained [30]. The observations in an experiment are looked upon as the values assumed to be some random variable, z , which in this research represent the various coupling levels in an aircraft.

RTCA/DO-233 reported some IPL measurement data with minimums, averages, number of data points and standard deviations [26]. These quantitative statistical metrics allow tabular comparison of IPL data. Similarly, the IPL data used in the visual analysis in the previous chapters is transferred into normalized plots in this chapter so that the statistical metrics can be visualized, compared and assessed in tabular form. Statistical analysis is not only performed on the IPL data collected on the entire aircraft, but also on the measurements taken only on window locations.

6.1 Statistical Analysis on IPL Data on Entire Aircraft

The following sections include the statistical analysis of the GS, TCAS, VHF and LOC systems of the aircraft on which IPL data was measured. For all plots in each of the sub-sections below, measurement data for each aircraft system and each polarization is plotted on the x-axis while the y-axis contains the raw number of measurement locations on the airplane with a particular IPL value. The graphs for horizontal test antenna

polarization are graphed separately from the results for vertical test antenna polarization. On the top right hand corner of each graph, the histogram's mean, standard deviation and variance are shown. Each plot axis is scaled the same to facilitate comparison of polarizations and IPL measurement distributions. (i.e. x-axis IPL value ranges from 50 to 100 dB, and y-axis number of measurements ranges from 0 to 35.) These distribution plots provide quantitative comparisons of the data, while revealing minimums, maximums and distribution trends not evident in numerical metrics. Each distribution plot is accompanied by a best-fit normal statistical data distribution curve. Probability distribution analysis of IPL data will be the subject of subsequent work.

6.1.1 GS Measurement Distribution Plot

In the graphical analysis of the GS data in chapter 3, horizontal polarization coupling was shown to be dominant (meaning lower path loss). The aircraft GS antenna is horizontally polarized. The measurement distribution plot in Figure 6.1 shows the same GS data, with horizontal test antenna polarization having a slightly lower mean, higher standard deviation and therefore, higher variance than the vertical test antenna polarization. Most importantly, it can be seen that a few horizontally polarized test antenna measurements clearly define the minimum IPL locations.

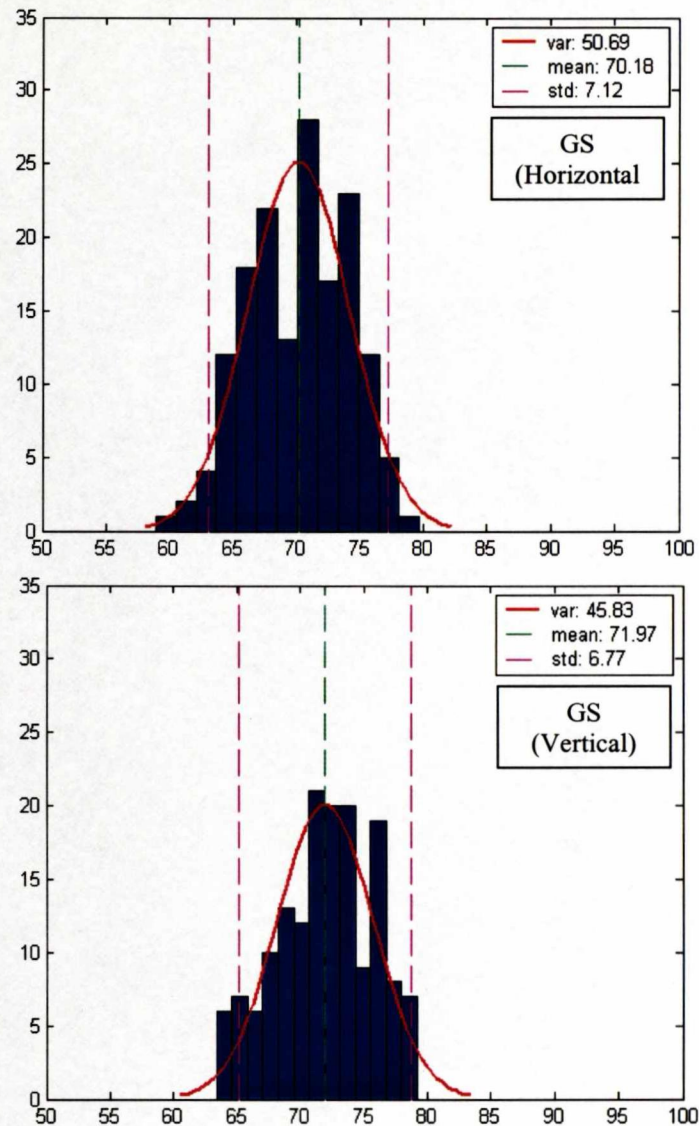


Figure 6.1: IPL Data (dBm on x-axis) vs. raw number of measurement locations (y-axis) for GS.

6.1.2 TCAS Measurement Distribution Plot

In the graphical analysis of the TCAS data (refer for chapter 3), the vertical polarization coupling was shown to be dominant. The aircraft TCAS antenna is vertically polarized. The measurement distribution plot in Figure 6.2 shows the same TCAS data, with vertical test antenna polarization having a slightly lower mean, higher standard deviation and therefore, higher variance than the horizontal test antenna polarization.

Similar to GS (but with different polarization), it can be seen that a few vertically polarized test antenna measurements clearly define the minimum IPL locations.

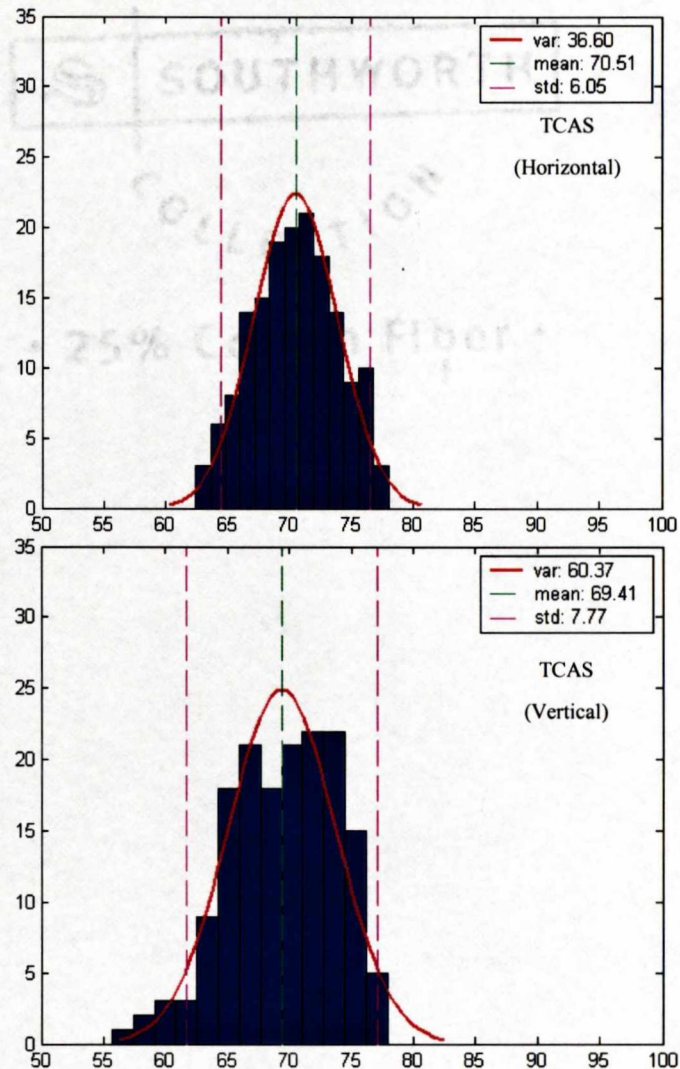


Figure 6.2: IPL Data (dBm on x-axis) vs. raw number of measurement locations (y-axis) for TCAS.

6.1.3 VHF Measurement Distribution Plot

In the graphical analysis of the VHF Com. data (please refer to chapter 3), measurements revealed optimal coupling locations (minimum IPL) for both vertical and horizontal test antenna polarizations. Similarly, in Figure 4.3, the variance, mean and standard deviation of the horizontal and vertical measurement data are very close to each other.

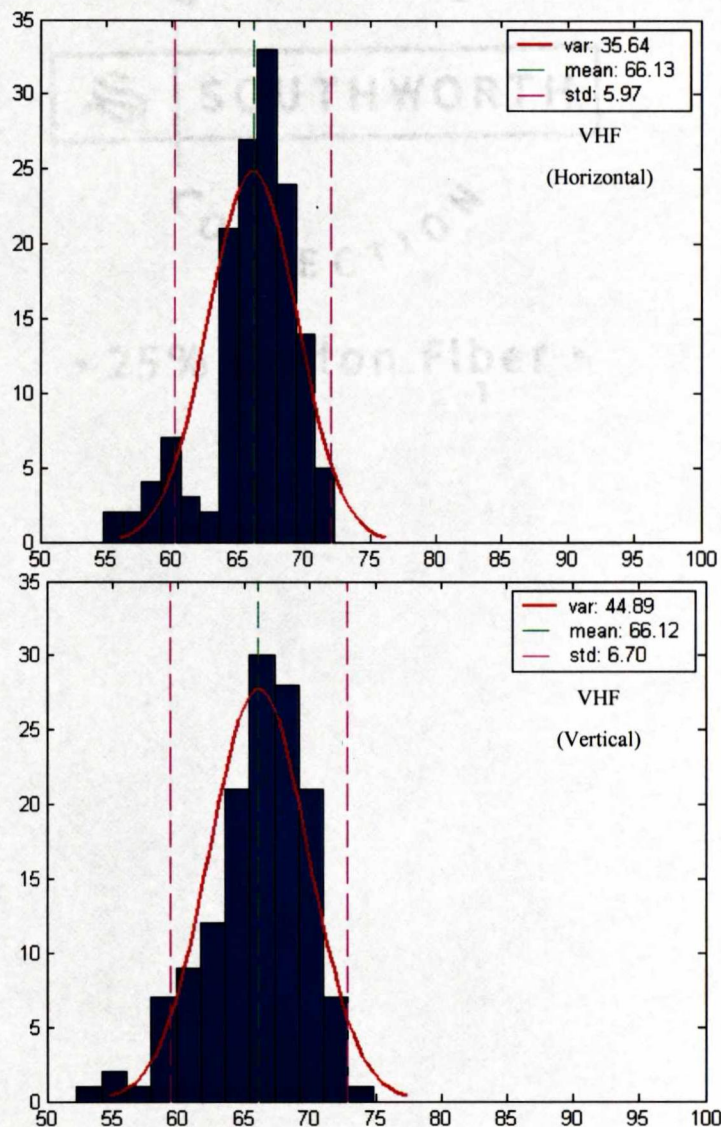


Figure 6.3: IPL Data (dBm on x-axis) vs. raw number of measurement locations (y-axis) for VHF.

The mean differs by only 0.01. However, the vertical polarization data has the (slightly) lower mean, and the higher standard deviation and variance leading to the conclusion that the test antenna couples slightly better to the VHF Com. system when it is in Vertical polarization. The aircraft VHF Com. antenna is vertically polarized. Again, it can also be seen that a few test antenna measurements clearly define the minimum IPL locations.

6.1.4 LOC Measurement Distribution Plot

In the graphical analysis of the LOC data (see Figure 4.6), horizontal polarization coupling was shown to be dominant. The aircraft LOC antenna is horizontally polarized. The measurement distribution plot in Figure 6.4 shows distinct differences in the measurement data. The horizontal test antenna polarization data clearly has the lower mean, greater standard deviation and greater variance. The minimum IPL measurement is 10 dB lower for horizontal test antenna polarization than for vertical polarization, and dominated by several specific measurement locations.



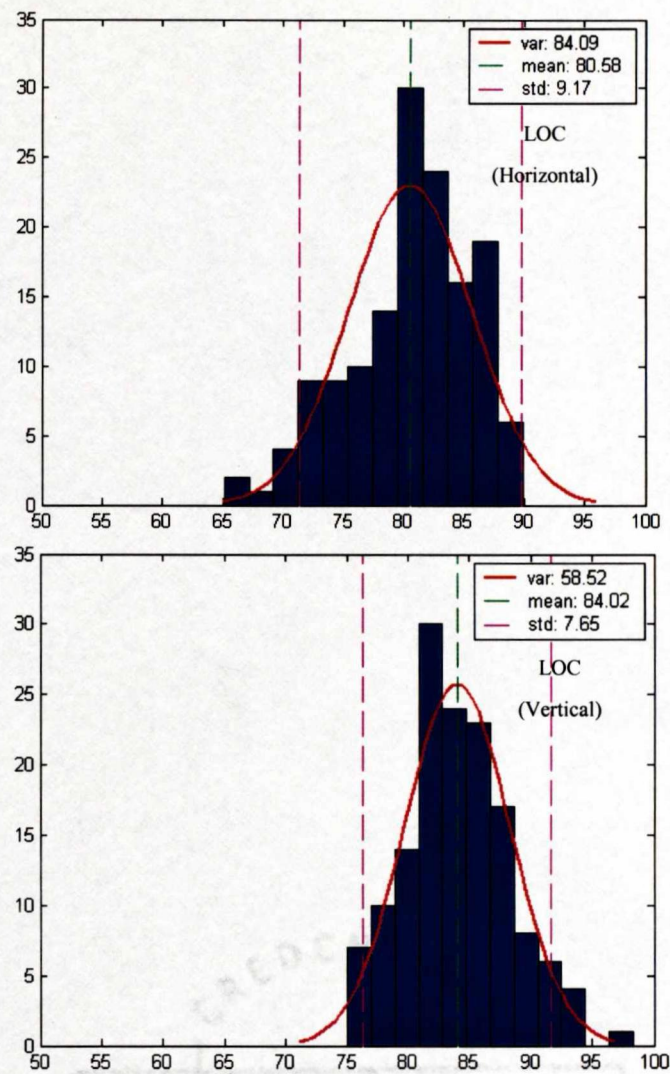


Figure 6.4: IPL Data (dBm on x-axis) vs. raw number of measurement locations (y-axis) for LOC.

6.2 Statistical Analysis on IPL Data on Window Locations only

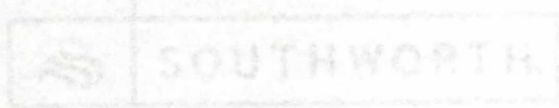
Similar to the graphical analysis, window data was separated and plotted individually for better comparison to the entire plane for a quantitative analysis. Please refer to Figures 6.5, 6.6, 6.7, and 6.8 for the measurement distribution plots of B737 #1989 window data. These plots can be compared directly to those shown in Figure 6.1, 6.2, 6.3 and 6.4 previously.

6.2.1 GS Measurement Distribution Plot for window data

Comparison of measurement data for GS (Figure 6.5 vs. Figure 6.1) clearly shows that the minimum IPL values were measured at window locations. The mean values decrease 3.0 dB for horizontal polarization and 1.1 dB for vertical polarization, indicating a fairly good level of statistical comparability between whole aircraft vs. window-only IPL measurement data.

6.2.2 TCAS Measurement Distribution Plot for window data

Comparison of measurement data for TCAS (Figure 6.6 vs. Figure 6.2) also shows that the minimum IPL values were measured at window locations. The mean values decrease 3.9 dB for horizontal polarization and 3.9 dB for vertical polarization, indicating a moderate statistical comparability between whole aircraft vs. window-only IPL measurement data.



COLLECTION

75% Cotton Fiber

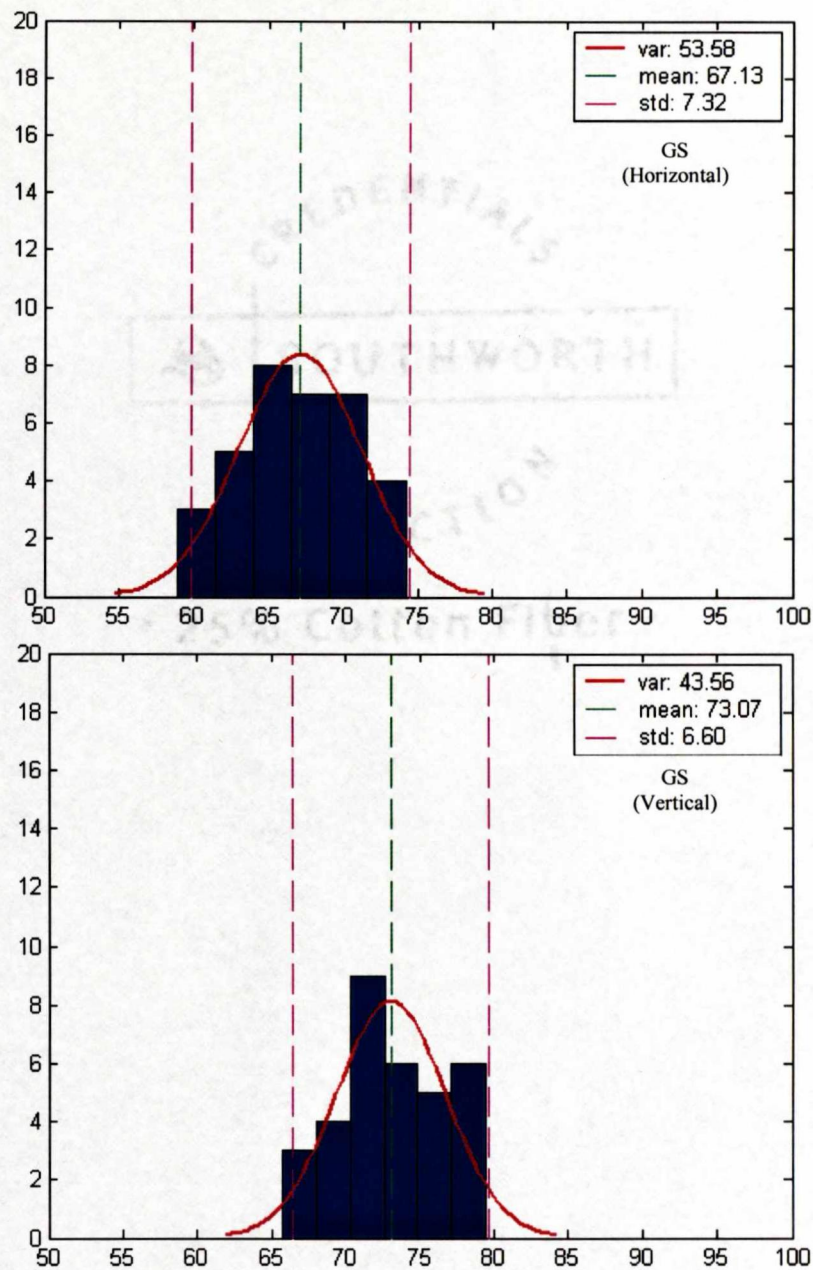


Figure 6.5: Statistical Analysis of Window Data for GS.

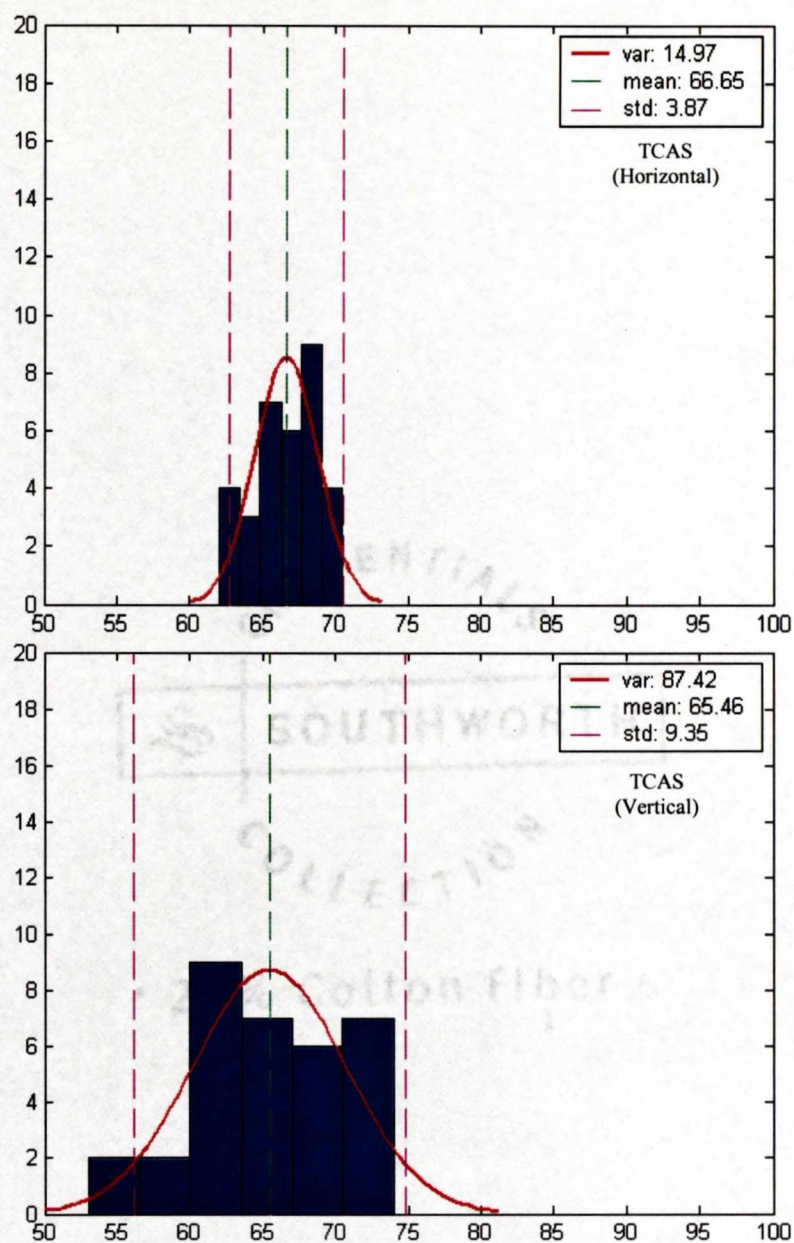


Figure 6.6: Statistical Analysis of Window Data for TCAS.

6.2.3 VHF Measurement Distribution Plot for window data

Comparison of measurement data for VHF Com. (Figure 6.7 vs. Figure 6.3) shows that the minimum IPL value was *not* measured at a window location. An IPL value 3dB less than the minimum window location was obtained when evaluating the whole aircraft data set. The mean values decrease 6.7 dB for horizontal polarization and 0.8 dB for vertical polarization, indicating a good statistical comparability between whole aircraft vs. window-only IPL measurement data, when considering vertical polarization, but not horizontal polarization.

6.2.4 LOC Measurement Distribution Plot for window data

Comparison of measurement data for LOC (Figure 6.8 vs. Figure 6.4) shows that the minimum IPL value was *not* measured at a window location. An IPL value 1dB less than the minimum window location was obtained when evaluating the whole aircraft data set. The mean values decrease 8.4 dB for horizontal polarization and 1.3 dB for vertical polarization, indicating a good level of statistical comparability between whole aircraft vs. window-only IPL measurement data for vertical polarization, but not horizontal polarization.

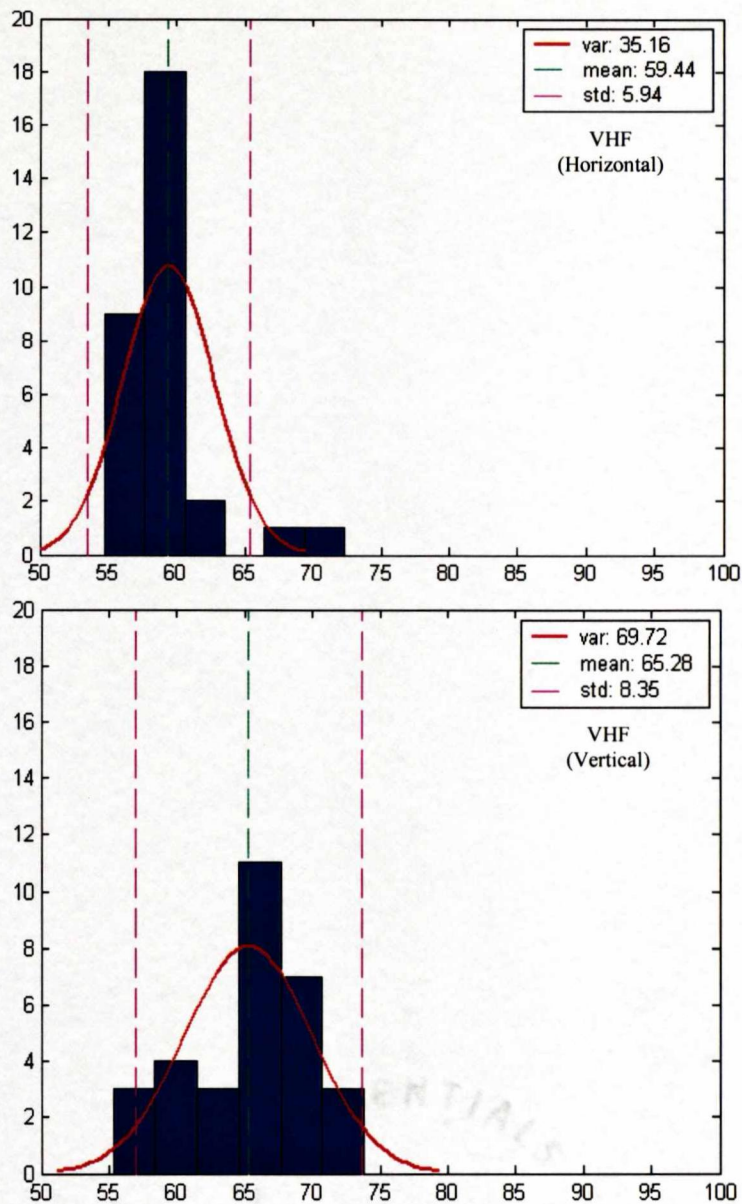


Figure 6.7: Statistical Analysis of Window Data for VHF.

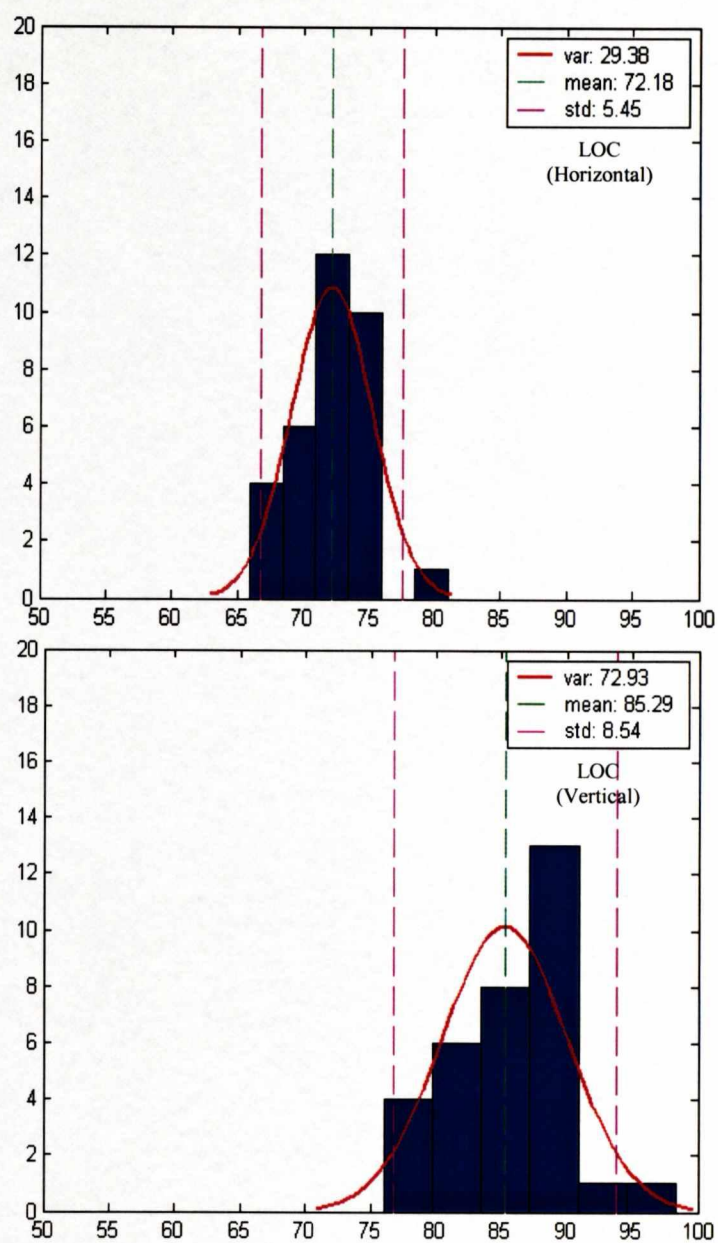


Figure 6.8: Statistical Analysis of Window Data for LOC.

Table 6.1 includes a summary of all the minimums, maximums, standard deviations, mean and variance of each antenna. It also shows a comparison of data measured on full plane vs. window locations only. From the results above, it can be concluded that IPL data sets limited to window-only locations may slightly underestimate the minimum IPL in some cases (by up to 3 dB for the VHF Com. system, in this case). Also, statistical parameters are shown to vary considerably when comparing full-aircraft vs. window-only IPL data sets. Full sets of seat and aisle data need to be evaluated from other airplane types, so that general statistical relationships may be observed and predicted in comparing full data sets with window-only data sets.

Table 6.1: Summary of Statistical Characteristics for IPL values on Full plane vs. Windows Only.

	Full Data Set		Window Data only	
	Horizontal	Vertical	Horizontal	Vertical
GS				
Minimum	59	64	59	66
Maximum	80	79	74	79
Std. Deviation	7.12	6.77	7.32	6.60
Mean	70.18	71.97	67.13	73.07
Variance	50.69	45.83	53.58	43.56
Dominant?	Yes	No	Yes	No
TCAS				
Minimum	62	53	62	53
Maximum	78	78	71	74
Std. Deviation	6.05	7.77	3.82	9.35
Mean	70.51	69.41	66.65	65.46
Variance	36.60	60.37	14.97	87.42
Dominant?	No	Yes	No	Yes
VHF				
Minimum	55	52	55	55
Maximum	72	75	72	74
Std. Deviation	5.98	6.70	5.94	8.35
Mean	66.13	66.12	59.44	65.28
Variance	35.64	44.89	35.10	69.72
Dominant?	No	Yes	No	Yes
LOC				
Minimum	65	75	66	76
Maximum	90	98	81	98
Std. Deviation	9.17	7.65	5.45	8.54
Mean	80.58	84.02	72.18	85.29
Variance	84.09	58.52	29.38	72.93
Dominant?	Yes	No	No	Yes

7 AIRCRAFT COUPLING MITIGATION TECHNIQUES USING CONDUCTIVE TAPE AND WINDOW FILMS

The previous chapters have focused on understanding the IPL patterns on an aircraft based on the locations of the aircraft doors, windows and antenna locations. The results from the graphical analysis of the IPL data imply that the regions of greater coupling are found nears the exit doors and windows majority of the time. Therefore, the next question to be considered is can the structure of the doors and windows be changed such that the level of waves transmitted through the test antenna leak significantly lesser to the aircraft antenna?

It was established in the first two chapters that it is virtually impossible to ban all PEDs, or enforce tougher measures on the PED manufacturers to spend more money in the shielding of individual PEDs. Also, it was determined that the electromagnetic waves propagated through these PEDs transmit through the doors and windows of the aircraft, creep along the fuselage, to reach the aircraft antenna systems. A simple solution to eliminate (or decrease) the EMI problem can be to start building aircraft with no windows and super sealed doors. This however, this would neither be a favored solution by the passengers, nor for the airline companies who would have to rebuild all their aircraft, costing them millions of dollars.

Therefore, the method proposed in this chapter includes shielding techniques. Previous chapters have clearly established the locations of greater coupling, and thus the windows and doors of the aircraft have proven to be the most vulnerable to electromagnetic wave leakage from the PEDs. Many techniques of shielding can be

studied; the easiest and the most cost effective being the use of conductive film and tape to shield the doors and windows. In this chapter, graphical analysis is performed with the door and exit seams sealed with conductive tape in order to better understand the effects of shielding on IPL patterns. Using this shielding method, the shielding effects are analyzed from window data for VHF and LOC systems. In addition the shielding benefit of applying electrically conductive film to aircraft windows is evaluated for GPS and TCAS systems.

7.1 Conductive Sealing of Doors and Exit Seams

This section includes graphical analysis of mitigation technique, which consisted on sealing the door and exit seam. “Aircraft taping” required conductive sealing of all door and exit seams on both sides of the aircraft using heavy-duty aluminum foil and adhesive-backed aluminum tape. Therefore, the research team taped the aircraft doors’ seams as well as the emergency exit seam. Figure 7.1 shows the image of the United Airlines with the door and exit seams taped on the starboard side. The seams of the doors and exits were also taped similarly on the port side:



Figure 7.1: Shielding of Door and Exit Seams on B737-200.

7.1.1 Analysis of Shielding of Exit Seams on GPS

In this particular testing, the starboard and port sides of the aircraft were sealed using the aluminum tape. Figure 7.2, includes the plotted IPL data, in both horizontal and vertical polarizations, obtained on the window locations of the port (left) as well as starboard (right) sides of the aircraft (B-737#1989). This plot represents the IPL data collected using the GPS antenna as the system of concern. The x-axis represents the window locations of the aircraft (window #1 being closest to the nose of the aircraft and #33 representing the window closest to the tail of the aircraft), while the y-axis represents calibrated IPL data, measured in dB. Notice in the legend that a dashed (blue, bold) line is used to represent the untaped data, while a solid (blue, bold) line is used to represent the taped data. Another solid (magenta, thin) line is used to represent the taped data on starboard side. Figure 7.2 shows that improved coupling (less loss) occurs for vertical polarization of the test antenna, rather than horizontal polarization, as predicted and verified in previous chapters. Also as a quick summary, observe that the data taken on the starboard side is slightly lower (greater coupling) than the data on the port side, due to the fact that the GPS unit is mounted slightly off-centered on the starboard side of the fuselage.

The important observation in regards to studying the effects of shielding on IPL measurements required the study between taped and untaped plots in figure 7.2. Some IPL measurements were obtained by moving the test antenna along the entire circumference of a door or window exit seams, while measuring the maximum coupling over the entire sweep. These are defined as “door sweep” measurements. The tick-marks

on the x-axis, labeled 'L1', 'LE' and 'L2', represent the "door sweeps" performed on window locations 1, 16 and 33 respectively. Door sweep was measured to understand the effects on IPL measurements due to leakage from the door seams (versus the windows). These measurements were specially performed and considered because in this part of the testing, only the door and exit seams were sealed. Therefore, the intent was to study the effect on IPL patterns throughout the aircraft by just sealing the doors.

As seen in the figure, there is not much difference between the untaped and taped results on the port side throughout the aircraft windows, except at window #16. Since window #16 is drop of about 8 dB between the taped and untaped results (taped, having the lower IPL located on the exit, where the window and door seam was sealed, there is a measurement). It was observed that although much difference was observed between the taped and untapped IPL measurement *at* the sealed window location (#16), there was not much difference in the IPL measurement taken at the door sweep. For instance, the measurements at 'LE' are very close to the measurements taken at window #15 and window #17; however, the IPL result *at* window #16 is noticeably lesser than the surrounding windows #15 and #17. This shows that sealing aircraft's exit window was indeed helpful for GPS, but not the door seam.

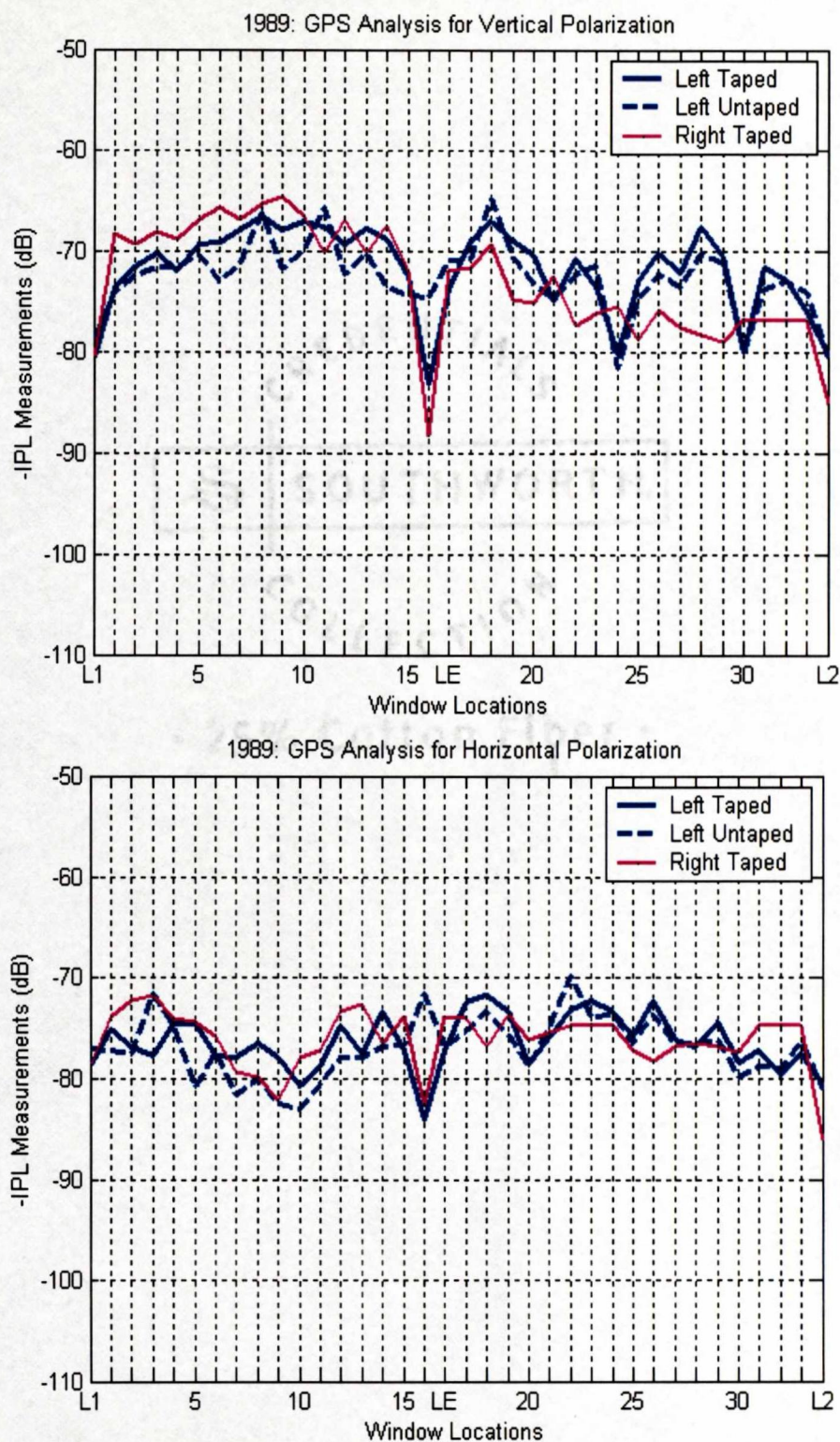


Figure 7.2: Illustration of the Effects of Shielding of Exit Seams on GPS for Horizontal and Vertical Polarizations.

7.1.2 Analysis of Shielding of Exit Seams on VHF1

The VHF1 system antenna is located on top of window #16 of the aircraft. (Most commercial transport airplanes have three VHF Com systems with separate antennas mounted on the fuselage.) Although detailed analysis of the overall IPL pattern is presented in chapter 3, the specific effects of conductive sealing of door and exit seams are shown in Figure 7.3. In this particular section, testing was performed on a B737-200 #1883. For this analysis, IPL measurements were taken at the window locations of the port side in both horizontal and vertical polarizations, both with and without taping. For the VHF system, the vertical polarization is dominant; therefore, the greater coupling is found in the IPL results with the transmitting antenna in the vertical position.

As observed in the plots in Figure 7.3, the results produced for the VHF system were much different than those from the GPS in that coupling from all passenger cabin window locations was reduced by about 5 dB, and even greater drop of up to 15 dB was observed at the door and window exit locations, where the seams were conductively sealed. In the case of testing using the VHF system, 'door sweep' was performed on the L1 and L2 doorway; however, it was not performed on the emergency exit. Therefore, the effect of applying conductive tape on the emergency exit's seam could not be studied, but shielding produced a good drop of up to 15 dB at L1 and L2 door sweep. Similar drop in coupling was also observed at the IPL measurement taken at window 16. Therefore, the application of conductive tape on the door and emergency exit seams showed significant drop in coupling levels for the VHF system.

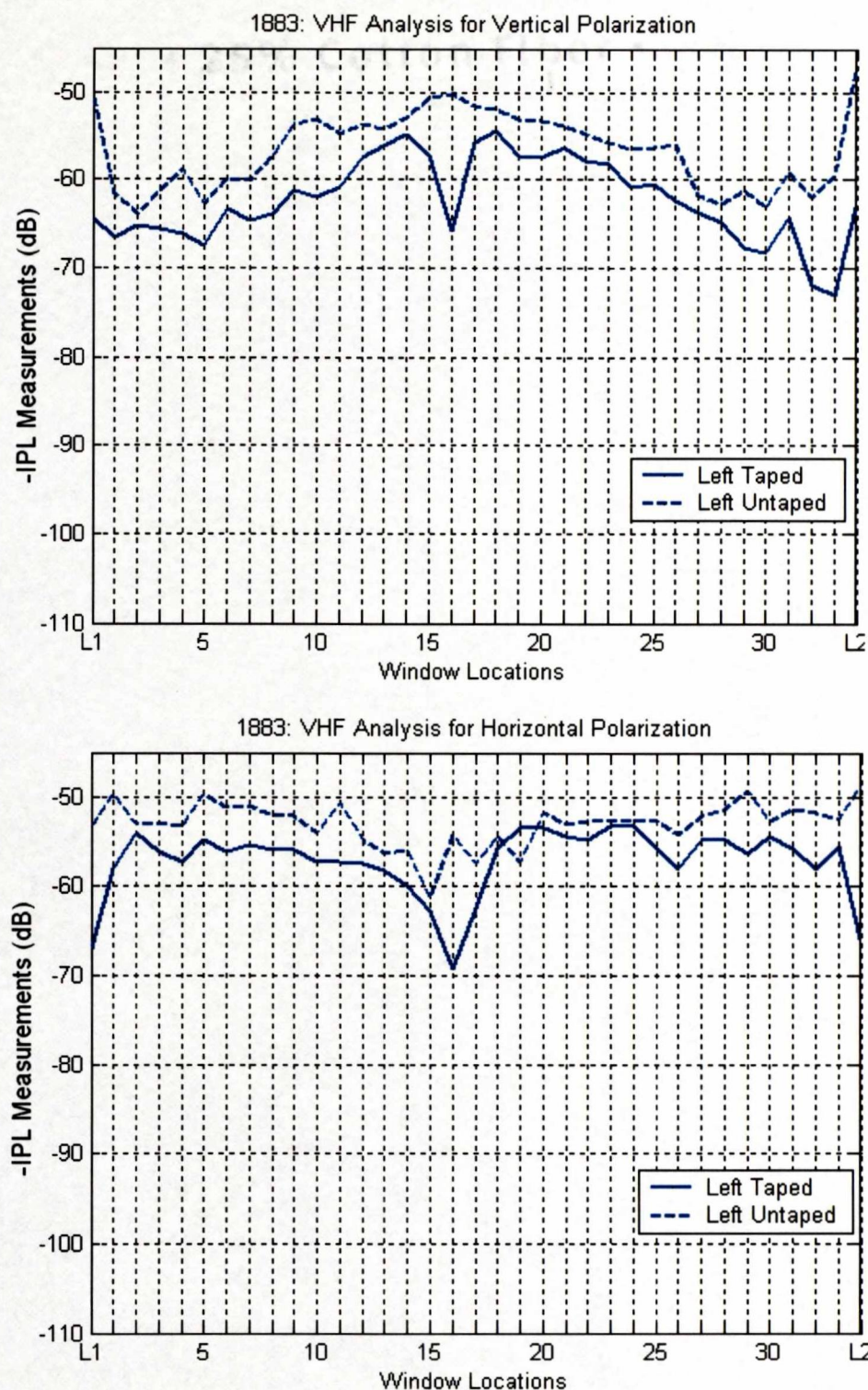


Figure 7.3: Illustration of the Effects of Shielding of Exit Seams on VHF for Horizontal and Vertical Polarizations.

7.1.3 Analysis of Shielding of Exit Seams on LOC

The VOR/LOC System antennas are located on the tip of the tail of the aircraft. Please refer to Chapter 2 for further details on IPL analysis and results derived from data taken on the entire aircraft. Similar to the taping technique used on the B737-200, #1883 in previous section, similar shielding method was applied to another B737-200, #1989 so that the LOC system could be tested for the effects of shielding. Figure 7.4 shows the effect of unshielded versus conductive sealing of door and exit seams on IPL window data taken on the port side of the aircraft in both vertical and horizontal polarizations. Unlike the testing for the VHF system on #1883 in previous section, the sealing on this aircraft was only applied to the port side, and not the starboard side; therefore, IPL measurements were also only taken on the port side of the aircraft.

The horizontal polarization is dominant for the Localizer system, so it was assumed that the shielding effects would be the most visible in horizontal polarization results. However, as seen in figure 7.4, there is not much difference between the IPL readings for taped and untaped results throughout the aircraft, except at window 16. For the LOC system (horizontal), the IPL measurement dropped about -20 dB at window 16 after the exit seams and window 16 were taped. In vertical polarization results, more than 12 dB of coupling reduction was obtained at the L1 and L2 doorways when the seams were conductively sealed. A significant drop in coupling was also observed at the LE sweep.

Coupling at window and door seams usually sets the minimum IPL used in previous PED EMI assessments to airplanes. For GPS, virtually no coupling reduction

was obtained by conductive sealing anywhere except directly at the window covered by aluminum foil. These results demonstrate an upper bound to the degree of PED EMI mitigation that may be obtained by improving the electrical bond between door and exit seams on commercial transport airplanes. It is expected that these results are representative of the level of protection that would be afforded to other aircraft radio systems operating in the VHF and "L" (1 to 2 GHz) radio frequency bands, and having similar antenna locations.

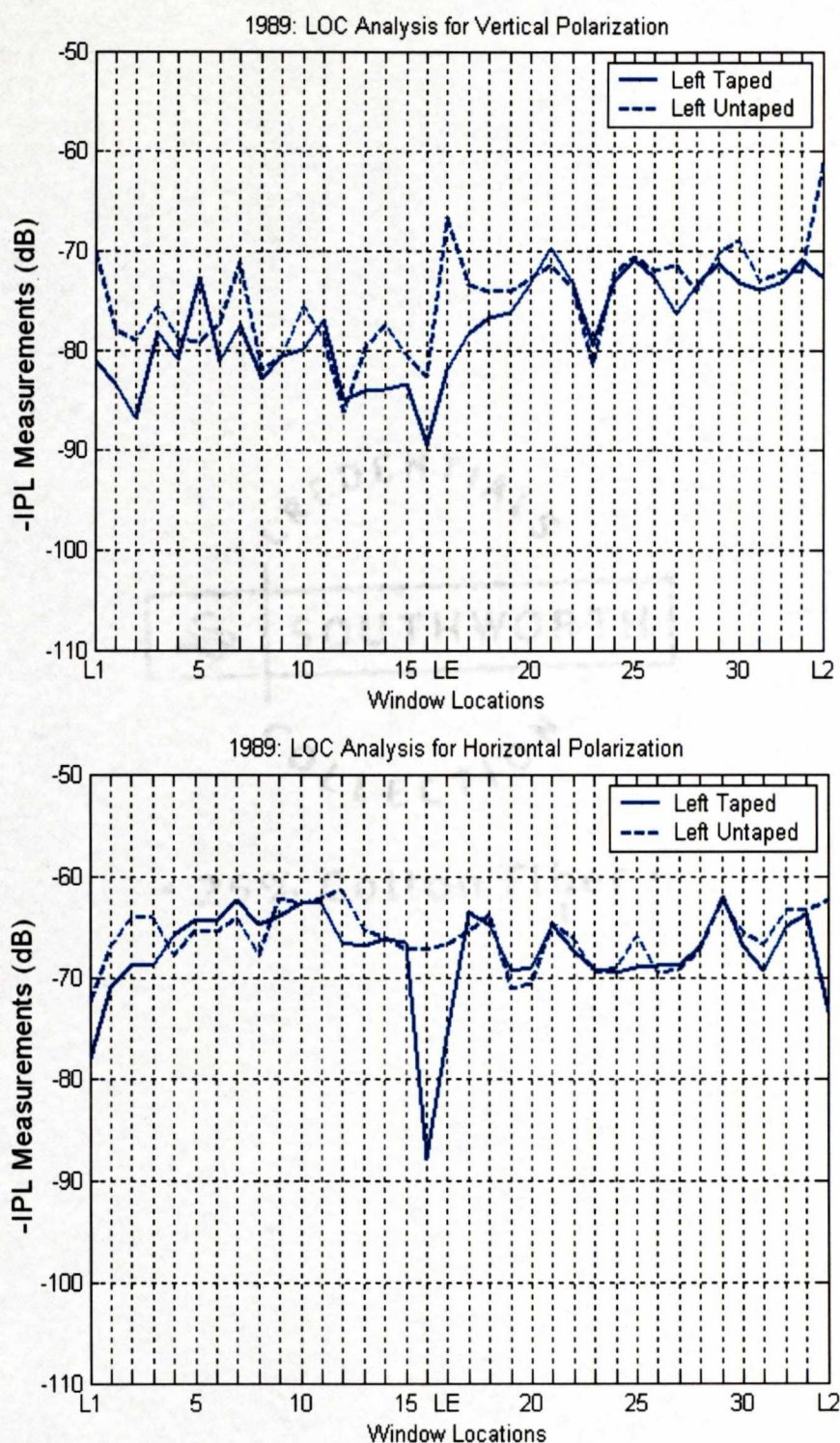


Figure 7.4: Illustration of the Effects of Shielding of Exit Seams on LOC for Horizontal and Vertical Polarizations.

7.2 PED EMI Mitigation By Conductive Window Films

The graphical analysis of IPL data in previous chapters revealed that high coupling is not only dependent on the locations of the doors, but also on the windows. The previous section focused on the sealing of only the aircraft doors. In this section, another kind of shielding technique is used for IPL measurements by taping electrically conductive window films from windows #1 to #12 on the starboard (right) side of B737-200 (#1879). Please refer to figure 7.5 for a picture of the sealed windows on the starboard side of the aircraft.



Figure 7.5: Window Films on B737 (Starboard) (W1 → W12).

The particular film used was Cortaulds VS-60 “spectrally selective” film, having a high visible light transmittance (58%), and high silver content. The film sample was obtained from the manufacturer (CPFilms), in 1998. No surface resistance data was available for the VS-60 film at the time of this analysis, but since 1998, new films with higher visible light transmittance have been introduced specifically for EMI shielding applications [34]. In this case, the film was temporarily bonded to the aircraft using 2”-

wide aluminum tape. IPL measurements were performed with and without the film installed.

7.2.1 Analysis of Window Films on GPS

As mentioned previously, the GPS is located above window #9 on B737-200. Figure 7.6 shows the IPL measurements obtained with and without window film installed on B737-200, #1987. As described in the legend, dashed line is used to represent “unfilmed” data, while a solid line is used to represent data with window films on windows #1 through #12. As seen in both graphs for horizontal and vertical polarization, the IPL measurements after window #12 are very close to each other for both filmed and unfilmed aircraft. However, there is an average of about -13 dB drop in IPL results on windows #1 through #12, where the window film was applied.

As mentioned in previous chapters, the GPS is horizontally polarized, so the continuous drop in coupling from windows 1 through 12 are observed in plots for horizontal polarizations only. In the plot for vertical polarization, although there is a drop in coupling from windows 1 through 12, there is no decrease at all at location 9, directly beneath where the GPS antenna is mounted. This analysis shows that conductive window films may be very effective in reducing coupling from the passenger cabin to aircraft GPS antennas.

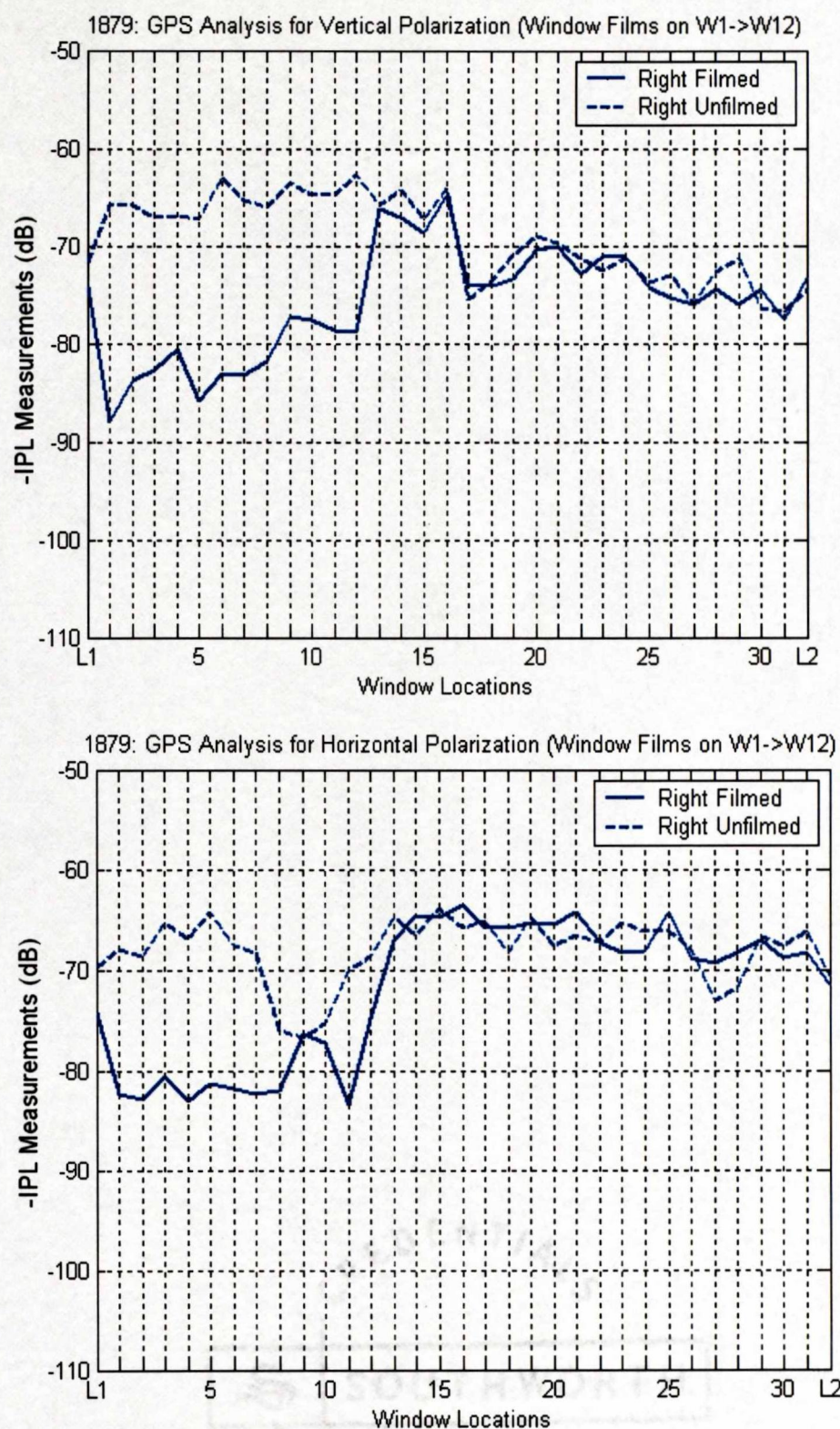


Figure 7.6: Effects of Using Conductive Window Film on GPS Results.

7.2.2 Analysis of Window Films on TCAS

The upper TCAS antenna is located above window #2 on B737-200. Additional IPL measurements were obtained with the film applied from window #1 through #12 (as shown in Figure 7.7). Measurements were taken in both horizontal and vertical polarizations from windows #1 through #16, with and without, window films. Figure 9 shows the results in both vertical and horizontal polarization. As mentioned in previous chapters, for TCAS, the vertical polarization is dominant.

As seen in figure 7.7, vertical polarization, there is about a -10 dB drop between filmed and unfilmed window coupling. The difference between the dashed and solid line actually decreases, as approaching window #12 (last taped window), and finally, the coupling levels are almost equal after windows #12. In horizontal polarization, there is not much difference between the filmed and unfilmed windows' IPL measurements. Similar to the GPS result, the use of conductive window films is shown as an effective method of reducing coupling levels from the passenger cabin to TCAS as well.

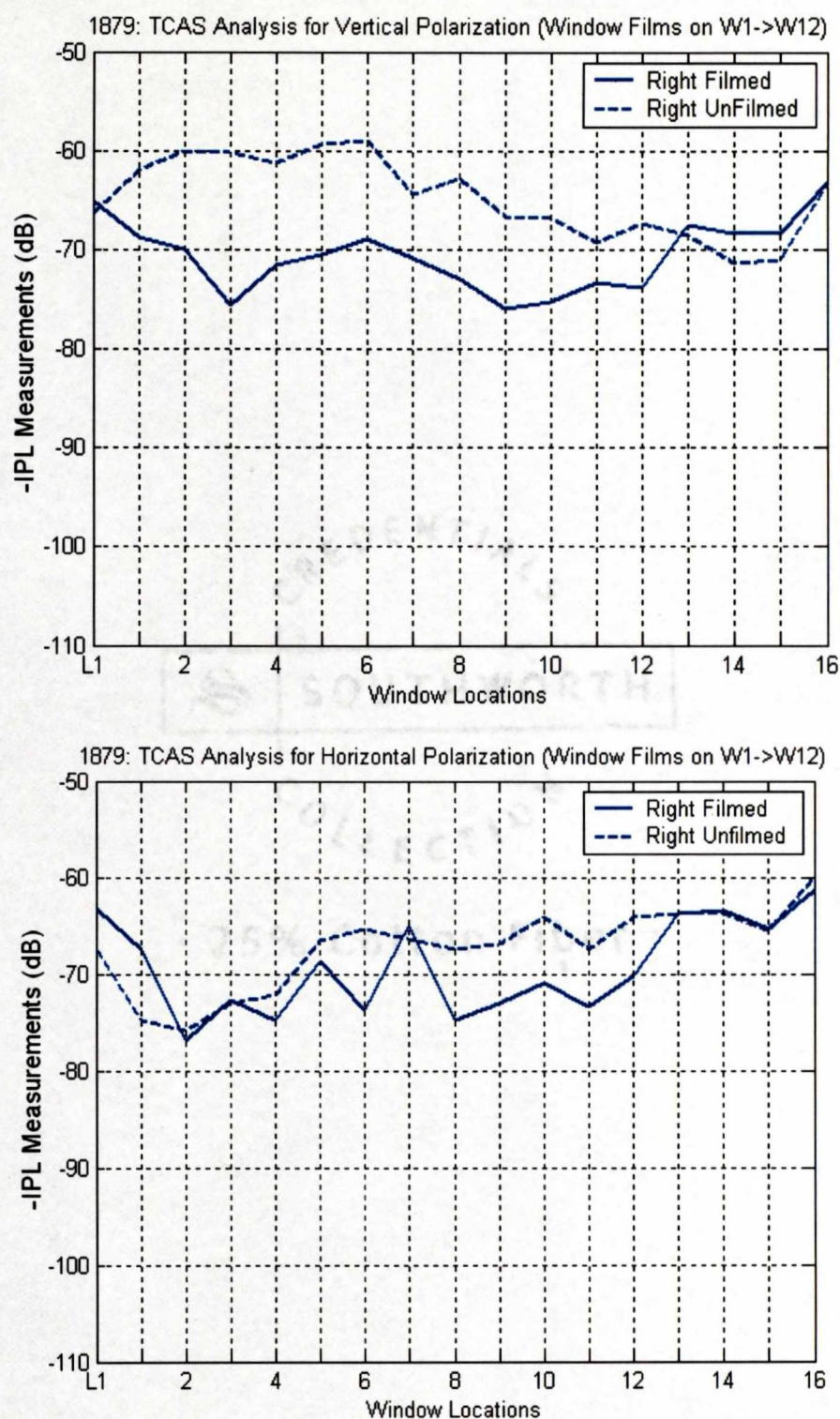
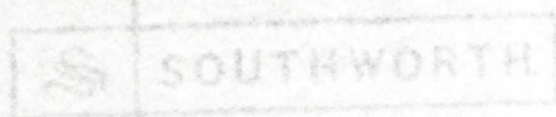


Figure 7.7: Effects of Using Conductive Window Film on TCAS Results.

In this section, the merit of PED EMI mitigation by the application of conductive window film was evaluated by measuring airplane IPL with (and without) film installed on the first 12 windows on the starboard side of the airplane. It was shown that coupling levels may be reduced by more than 15 dB for GPS and more than 10 dB for TCAS by application of conductive window film. These results demonstrate that the application of conductive films to aircraft windows may provide significant reduction in PED EMI coupling to aircraft radio systems. This testing did not evaluate the level of protection possible to aeronautical radio systems operating in the VHF and UHF radio frequency bands (ie. VHF Com, VHF Omnidirectional, LOC, Glideslope) by applying conductive window film. For future research and experimentation, it is recommended that more comprehensive evaluations of conductive sealing of door seams combined with conductive window films be performed for all aircraft radio systems. These tests should consider aging issues and maintenance strategies in the selection of materials and their installation.



COLLECTION

25% Cotton Fiber

8 Modeling EMI Patterns Using Fuzzy Logic

Extensive analysis on IPL measurements has been performed in previous chapters. The effects of shielding have also been evaluated on the path loss data collected. It has been established that although the coupling level depends on the locations of the aircraft door, windows and antenna locations, using effective shielding techniques can also drop the levels of coupling in various locations. Modeling the pattern obtained by plotting IPL data is extremely complicating. Therefore, in this chapter, the initial phases of modeling EMI patterns onboard a B737-200 have been completed for the various systems studied previously in this research. The purpose of the modeling is to enable the relocation of aircraft doors, windows and antenna systems to see the effect on coupling levels. A further detailed version of this model can enable airline companies to determine the best possible design for the aircraft to decrease the EMI problems as much as possible. Also, the modeling with shielding techniques may be used to gather the various coupling levels of concern from throughout the aircraft and forcefully group them in one place such that the airliners may be able to offer certain seat locations to passengers on which the use of PEDs would be safer, similar to an 'internet café' on the aircraft!

8.1 Introduction to Fuzzy Logic

Various modeling techniques could be used, such a ray tracing, finite element, finite difference time domain analysis, neural networks, fuzzy logic, and many more. In this research, fuzzy logic was used due to its dynamic abilities as well as its usefulness in areas in which the proper behavior of the outcome is not certain. Modeling techniques

such as neural networks expect the inputted data to be exact and accurate and also require much IPL data for better training and learning of the neural nets. Fuzzy Logic provides a simple way to arrive at a definite conclusion based upon vague, ambiguous, imprecise, noisy or missing input information. The logic extends Boolean logic to handle the expression of vague concepts. To express imprecision in a quantitative fashion, it introduces a set membership function that maps elements to real values between zero and one (inclusive); the value indicated the “degree” to which an element belongs to a set. A membership value of zero indicates that the element is entirely outside the set, whereas a one indicates that the element lies entirely inside a given set. Any value between the two extremes indicate a degree of partial membership to the set. [35]

The concept of Fuzzy Logic was conceived by Lotfi Zedah, a professor at the University of California, and presented as a way of processing data but allowing partial set membership rather than crisp set membership. Fuzzy Logic is a problem-solving control system methodology that lends itself to implementation in systems ranging from simple, small, embedded microcontrollers to large, networked, multi-channel PC or workstation based data acquisition and control systems. It can be implemented in hardware, software, or a combination of both. Fuzzy Logic’s approach to control problems mimics how a person would make decisions, only much faster.

The four-step fuzzy reasoning procedures employed by applications includes:

1. Fuzzification: establishes the fact base of the fuzzy system. First, it identifies the input and output of the system and then identifies the appropriate if-then rules and uses raw data to derive a membership function. At this point, one is ready to apply the fuzzy logic to the system.

2. Inference: As inputs are received by the system, inference, the second step, evaluates all if-then rules and determines their truth values. If a given input does not precisely correspond to an if-then rule, then partial matching of the input data is used to interpolate an answer. Several methods of answer interpolation exist.
3. Composition: Then composition combines all fuzzy conclusions obtained by inference into a single conclusion. Different fuzzy rules might have different conclusions, so it is necessary to consider all rules. There are a number of composition methods available.
4. Defuzzification: The final step of defuzzification converts the fuzzy value obtained from composition into a “crisp” value; this process is often complex since the resulting fuzzy set might not translate directly into a crisp value. Defuzzification is necessary, since controllers of physical systems require discrete signals.

8.2 Assumptions Used for Modeling

Using the rules above, a Fuzzy system was designed and implemented to model the Electromagnetic interference patterns due to PEDs onboard Boeing 737-200. Due to the complexity of the system desired to be modeled, a few major assumptions had to be made. Past measurements have revealed that electromagnetic wave propagation from the aircraft passenger cabin to aircraft antennas is primarily influenced by the presence and location of window and door apertures in the (typically) aluminum fuselage. The specific details of this propagation are not possible to measure without corrupting the propagation phenomena, and are extremely difficult to model. Figure 8.1(left) shows the propagation

problem mentioned above. A simple fuzzy logic model allows the passenger cabin propagation phenomena to be modeled by a rectangular box, with antennas located directly on top of the window locations. As seen in Figure 8.1(right), the waves are now assumed to have a straight propagation from antenna to the window, and then straight inward propagation from the window to the seat. This simple assumption helped keep the model in rectangular coordinates, instead of polar coordinates.

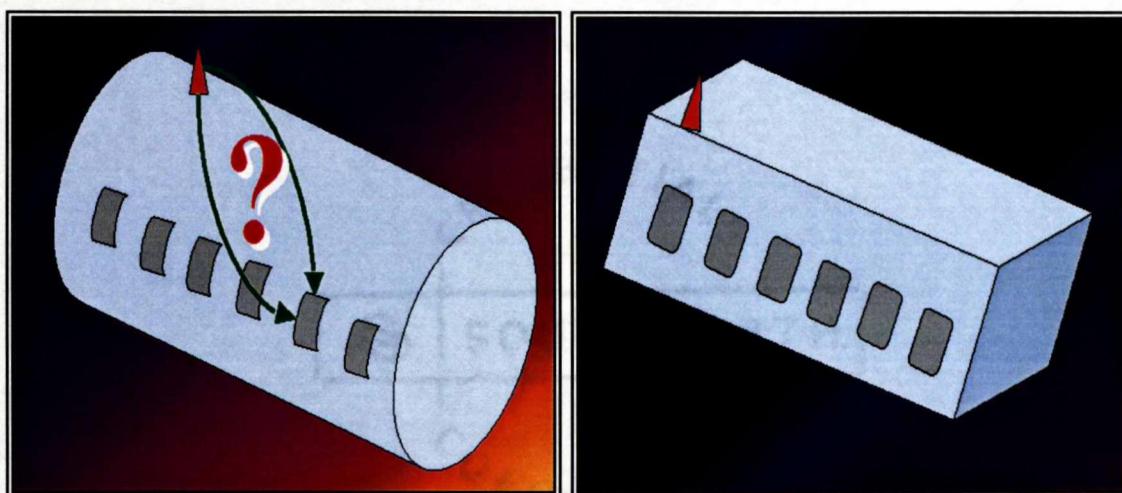


Figure 8.1: Fuselage Characteristics and Antenna placement for Fuzzy Modeling.

Another problem before modeling was the actual dimensions of the airplane were unknown. Since the entire model is based on the distance as the major factor, the author wanted to use the actual dimensions of a Boeing 737 to model the EMI patterns. Since the necessary dimensions were not available in time for this analysis, estimated “seat units” were used, where one unit represented one seat length. For the modeling performed in this paper, the height of the plane is estimated to be 5 seat units.

Also, in this particular modeling, the presence of aircraft seats or external items or human subjects is not taken into consideration. Of course, when these elements are included in the model, there will definitely be more complex wave propagation patterns.

Also, the reflection and transmission characteristics of electromagnetic wave propagation from one medium to the other depends on the relative dielectric constant of both mediums, which would determine how much of the wave actually propagates to the other medium, while how much gets lost in the process. Therefore, since the presence of 'barriers' such as seats or people are not considered, the output of the model should show more regions of greater coupling than the actual coupling levels.

Finally, since the aircraft dimensions were not known, only the systems located directly on top of the passenger section of the fuselage were considered (TCAS, GPS and VHF). In our normalized units, the fuselage height is '5 seat units'. Antenna systems such as GS and LOC (which are located in the nose and the tip of the tail of the aircraft, respectively) will be considered in future work. In particular, the output of the LOC antenna system will be impacted by wave reflection phenomenon from the aircraft wings.

8.3 Formulation of Fuzzy Rules

After observing the graphical patterns on B-737 in previous chapters, three rules are derived for the fuzzy logic system. Three factors that affect the EMI patterns include the seat's distance from the door, from the windows as well as from the aircraft's antenna. Probabilities between 0 to 1 were assigned to each seat based on the distance between the seats and the parameters (door, window or antenna). From the graphical plots, visual conclusions were drawn, such as "if the distance from the door to the seat is greater than 5 units, little to no coupling existed." With such visual understanding of the graphical plots, the following three rules were created:



Figure 8.3: Probability of Coupling (y) vs. Seat Distance (x).

$$\Rightarrow \begin{cases} 1 & 0 \leq x < 3 \\ -\frac{1}{3}x + 2 & 3 \leq x < 6 \\ 0 & x \geq 6 \end{cases} \quad (8.1)$$

The equations derived above for the various values of x were used in programming the first rule for the fuzzy logic system. Observe that x does not represent the x -axis, but instead represents the distance away from the source in *all* directions (horizontal, vertical, diagonal etc.). In this case, the source is the location of the window.

8.3.2 Seat Distance from Door

The locations of the doors have a very important role in the EMI patterns in the graphical plots. The electromagnetic waves propagate and “leak” more freely from the doors than from the fuselage or small windows of the aircraft. Figure 8.4 below shows the 8x33 matrix, representing the interior of the aircraft. According to the graphical analysis in the previous chapters, the greatest coupling occurred only about 1 seat unit away from the location of the exit doors, and then decreased as the distance from the door increased.

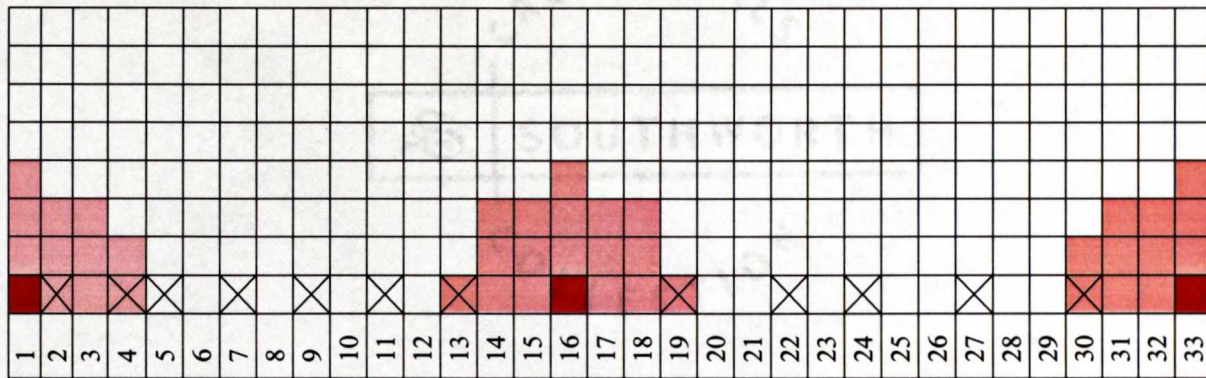


Figure 8.4: Coupling levels relative to door location for Rule 2.

The distance from door to seat equals to the slope between the seat and the door, this can be represented by the equation below, where every variable represents distance:

$$\frac{\Delta Y}{\Delta X} = \frac{|door - seat_row|}{seat_to_window}$$

From the equation, the following ranges can be derived:

$$\frac{\Delta Y}{\Delta X} = \frac{(1 \rightarrow 32)}{(1 \rightarrow 32)} = (1 \rightarrow 32)$$

The range of the numerator is from 1 to 32 from the 33 possible rows of the aircraft, the denominator has a range between 1 to 32 as well. The division of the numerator with the denominator can also range from 1 to 32. From the graphical plots, the probability of a seat to have high coupling was a 1 when the seat distance was only one unit away from the door. As the distance increased, the probability of high coupling decreased, leading to a zero probability of coupling after a distance of 4 units away from the door. Figure 8.5 shows the fuzzified coupling level between 1 and 0 based on the distance x from the exit doors.

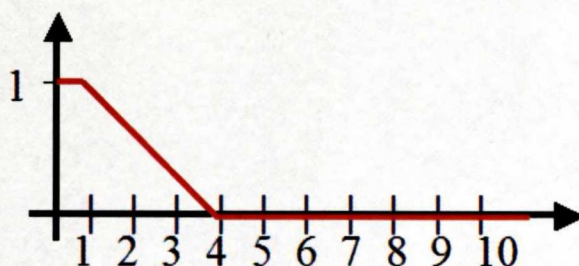


Figure 8.5: Probability of Coupling (y) vs. Seat Distance (x).

The following equation 8.2 was derived to assign the probability of coupling based on the location of the door, relative to the seat location:

$$\Rightarrow \begin{cases} 1 & 0 \leq x < 1 \\ -\frac{1}{3}x + \frac{4}{3} & 1 \leq x < 4 \\ 0 & x \geq 4 \end{cases} \quad (8.2)$$

8.3.3 Seat Distance From Antenna

The location of the antenna was the most important factor in determining the coupling intensities throughout the aircraft. As observed from the graphical plots in previous chapters, as the distance from the antenna increased, the coupling decreased. Calculating the distance from the antenna to the seats inside was a little more complex than in the previous rules because first, the distance from the antenna to window needed to be calculated, then added to the distance from window to seat. This rule also depended on the first assumption made in the previous section in which the fuselage is assumed to be rectangular. Also, in the assumption, the aircraft antenna is assumed to be placed directly on top of the windows (5 seat units high), instead of being in the center of the rectangular fuselage. Figure 8.6 shows the discretized representation of coupling based

only on the location of the antenna. In the figure, the antenna is assumed to be in top of window 16, similar to the VHF system on a typical B737-200.

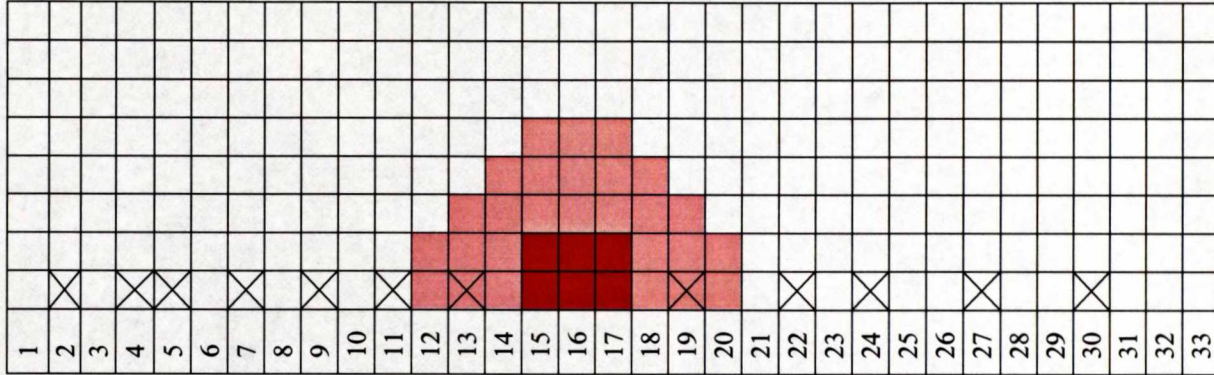


Figure 8.6: Coupling levels relative to Antenna location for Rule 3.

The coupling range can be represented by the following equation, where the variables represent distance and the variable S2W stands for the external distance from the antenna source to the window:

$$\frac{\Delta Y}{\Delta X} + S2W = \frac{|antenna - seat_row|}{height} + seat_to_window$$

According to the above equation, the following coupling ranges can be derived:

$$\frac{\Delta Y}{\Delta X} + S2W = \frac{(1 \rightarrow 32)}{5} + (1 \rightarrow 8) \Rightarrow \left(\frac{1}{5} \rightarrow 6\right) + (1 \rightarrow 8) \Rightarrow \left(1\frac{1}{5} \rightarrow 14\right)$$

From the range found above, the distance from antenna was estimated such that if the distance was less than 4 seat units, the coupling should be maximum, while if the distance was greater than 9 seat units zero coupling would exist. Figure 8.7 shows the distance from antenna to seat vs. probability of coupling graphs for rule 3.

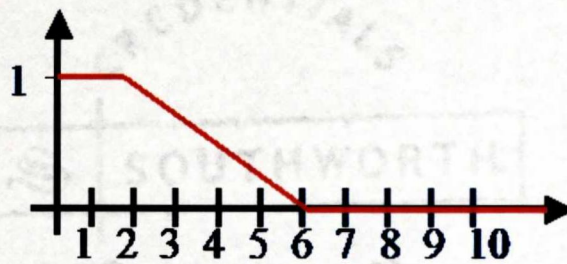


Figure 8.7: Probability of Coupling (y) vs. Seat Distance (x).

From the graph in the figure above, the following equations were derived, later used in programming the third rule in the fuzzy logic system.

$$\Rightarrow \begin{cases} 1 & 0 \leq x < 2 \\ -\frac{1}{4}x + \frac{3}{2} & 2 \leq x < 6 \\ 0 & x \geq 6 \end{cases} \quad (8.3)$$

8.4 Modeling Results and Conclusion

A MATLAB script was written to make the modeling dynamic as well as plotting the results similar to the graphs for actual IPL measurements. The user was able to define the length of the aircraft in terms of the number of rows, the number and location of doors, the location of the antenna as well as the height of the plane. Figure 8.8 below shows the user interface in which the user has specified the locations of the exit doors as well as the antenna location of the aircraft.

```
>> emag
Please Enter Antenna location: 16
Please enter location of 1st Door: 1
Please enter location of 2nd Door: 16
Please enter location of 3rd Door: 32
```

Figure 8.8: User Interface for Specifying Aircraft Characteristics.

The airplane was modeled as an 8 by 33 matrix as shown previously in the chapter. 8 represented the possible testing locations in a row, from window to aisle while 33 represented the possible number of rows of the aircraft, from the front of the fuselage, to the tail. Initially, all elements of the matrix were assigned a value of 1 to avoid division by 0 error. Once the locations of the doors and antenna were inputted, the software applied all three rules to each of the elements of the 8x33 matrix. Then the three resulting 8x33 matrices were merged together into a fourth 8x33 matrix using addition.

The results from Fuzzy Modeling are shown in Figure 8.9 (top) for the VHF system. Figure 8.9 (bottom) shows the graphical results in MATLAB from the actual IPL measurements on a VHF system analyzed in previous chapters. Similarly, Figures 8.10 (top) and 8.10 (bottom) show a close comparison of graphs derived from Fuzzy modeling vs. actual IPL plot on TCAS. As before, the x-axis represents the window locations while the y-axis represents the locations in the row where the IPL data was recorded, or interpolated. Also, the region of greatest coupling, or the lowest IPL value is colored red, while the regions of low coupling are represented by blue. The results from modeling are similar to the graphical results from the actual IPL data.

Observe the color bars for the coupling levels on the left column in both figure. While the color bar for the actual IPL plot ranges from -50's to -70's, the color bar for the plot produced by fuzzy modeling only ranges from 1 to 3. The lack of correlation in the two color bars is due to the fact that the process of defuzzification hasn't yet been applied to the modeling. The final process of defuzzification converts the fuzzy value obtained from composition into a "crisp" value. This process is often complex since the resulting fuzzy set might not translate directly into a crisp value. However, since the

process of defuzzification is very necessary, it will be accomplished in the next section.

Also observe that the regions of high coupling in the fuzzy model's output seem to be further dispersed than the regions in the actual IPL results. Again, this is due to the assumption that no seats or personnel exist in the fuzzy model. For example, the VHF plot will become much more conservative in the x-direction when the seats would be considered as the 'barriers' limiting the wave propagation in the x-direction. Therefore, the presence of obstacles would also definitely improve the fuzzy model to represent the output produced by actual results from the IPL measurements.

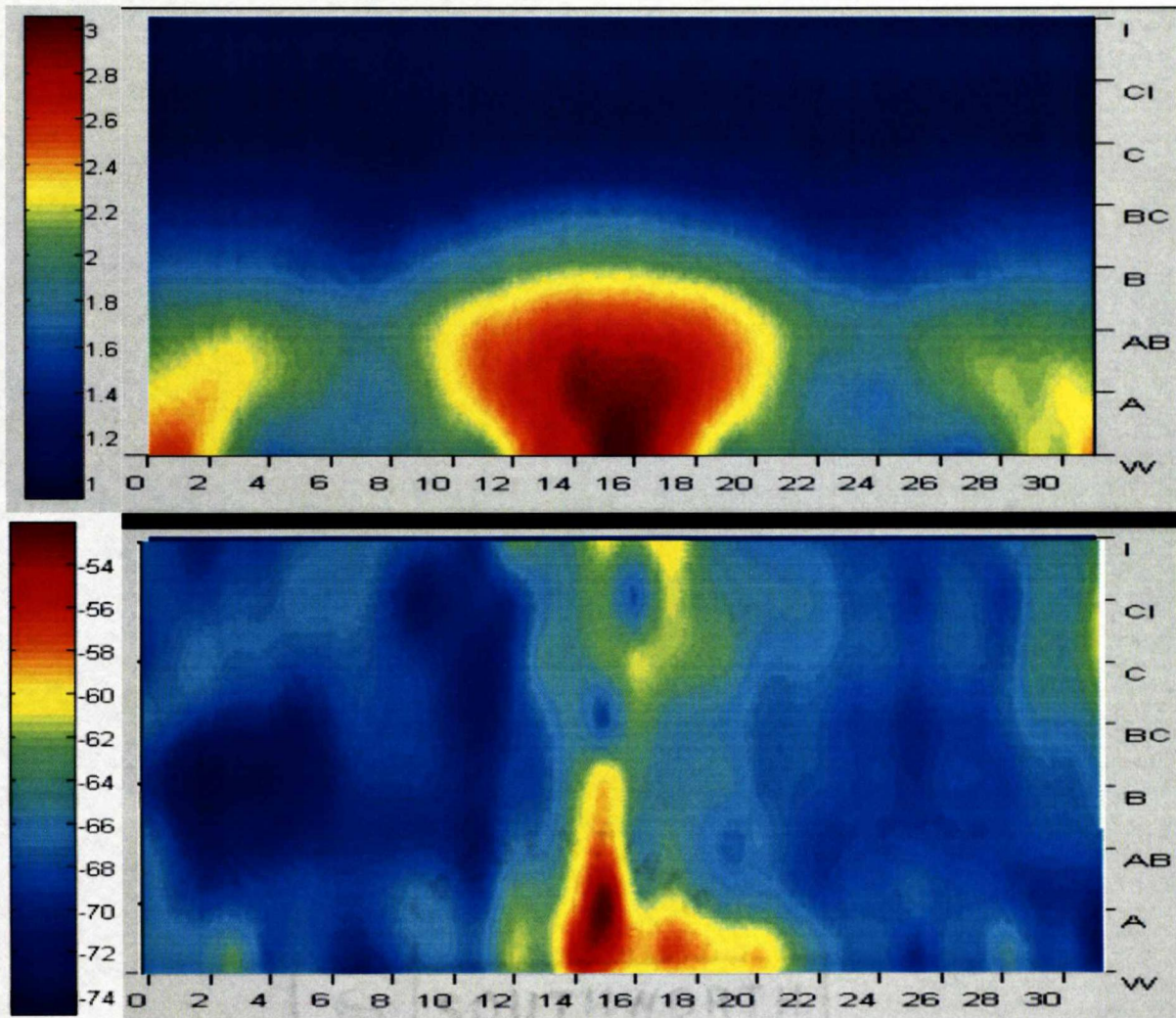


Figure 8.9: Modeled results (top) vs. Actual (bottom) IPL measurements for the VHF system (Antenna located on top of window #16).

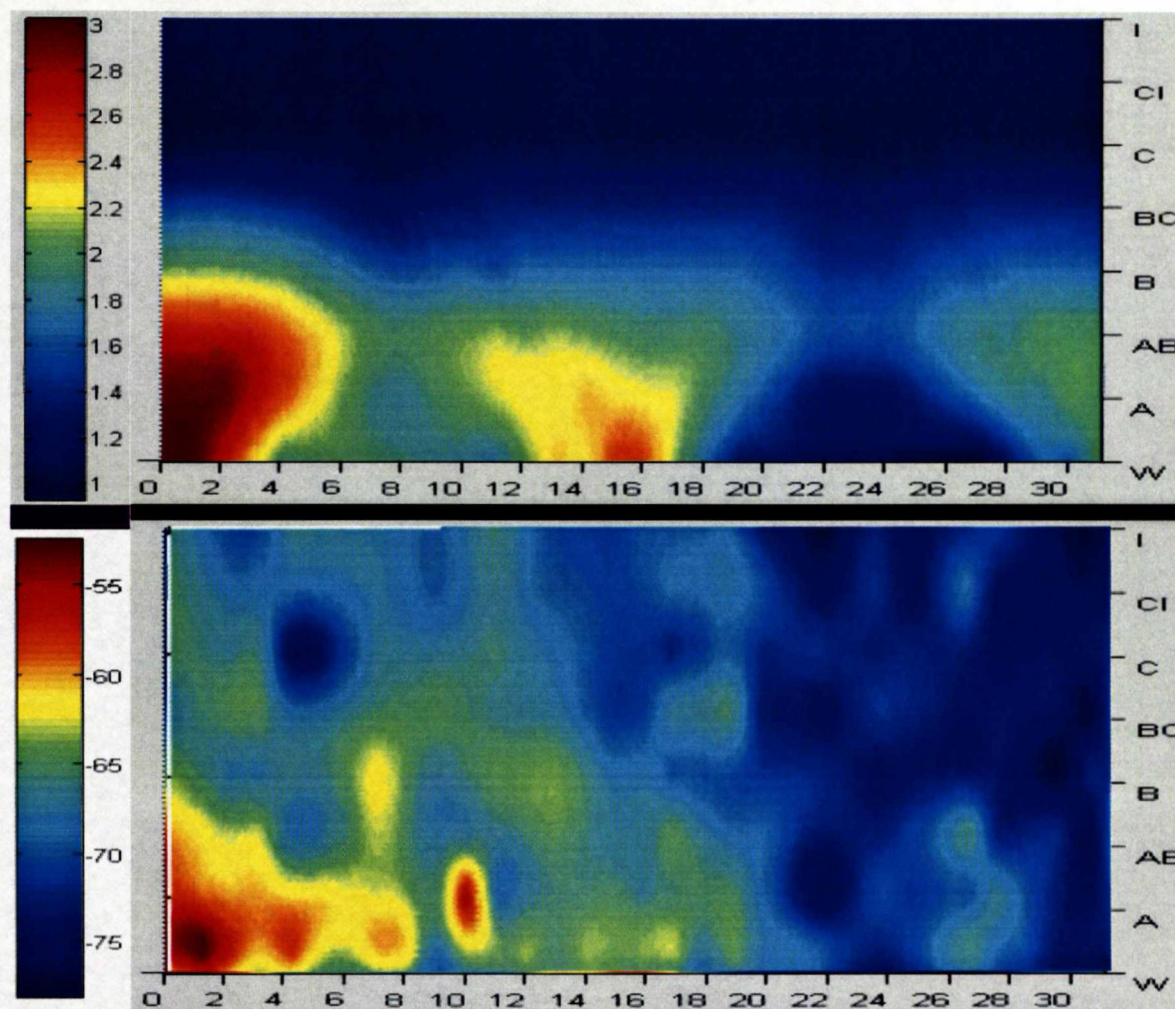


Figure 8.10: Modeled results (top) vs. Actual (bottom) IPL measurements for TCAS (Antenna located on top of window #2).

8.5 Introduction to Defuzzification

As described in previous section, regardless of the few differences, these preliminary results appear promising. However, as observed, the critical procedure of defuzzification still needs to be implemented to change the color scale of '1' to '3' to something more realistic in terms on dBm (i.e. -54 to -74 dBm). After a careful analysis, it was observed that there lies a linear relationship between the measured IPL scale and

the modeled scale of 1 to 3. Roughly, for every two values the IPL measurement increases (i.e. from -74 to -72), the modeled value increases by a factor of 0.2 (i.e. from 1 to 1.2). Therefore, the following look-up table 8.1 could be constructed to defuzzify the modeled IPL values into more realistic values resembling the units in the actual IPL measurements:

Table 8.1: Defuzzified values for the IPL data obtained through Fuzzy Modeling.

Fuzzified IPL Value	Defuzzified IPL Value
3.0	-54
2.8	-56
2.6	-58
2.4	-60
2.2	-62
2.0	-64
1.8	-66
1.6	-68
1.4	-70
1.2	-72
1	-74

The complexity of the above defuzzification method should increase as the sensitivity of the fuzzy logic system is increased. For example, in the current modeling technique, the system was assigned a linear parameterization; however, for parabolic assignment, the results should become more accurate and the defuzzified values of the

IPL measurements should be more accurate. Other type of parameterizations will be considered in future work. Also, the next step of modeling will be to improve the precision further with actual airplane measurements. The model will also be further improved to add the reflective properties as well as the effects of different polarizations, i.e. horizontal and vertical polarizations.

9 Conclusion

9.1 Summary

The use of Portable Electronic Devices (PEDs) is prohibited during take-off and landing of an aircraft because PEDs may emit signals that can interfere with the aircraft's navigation and communication systems. The coupling that may contribute to the electromagnetic interference (EMI) on the aircraft's electronics due to PEDs emissions is examined for Boeing 737 and 747 aircraft. This work, funded by the NASA Graduate Researchers Program, uses Interference Path Loss (IPL) data, collected by researchers from NASA Langley Research Center, Eagles Wings Inc. and United Airlines on several out-of-service United B737 and B747 airplanes.

In this research, IPL data was analyzed using the graphical analysis of the EMI patterns. Graphical comparisons of horizontal and vertical polarizations as well as comparison of the EMI patterns from Biconical versus Dipole antennas are made. Data accuracy was measured by comparing graphs from B737 (#1989) versus B737 (#1997). Comparisons of IPL data taken on just windows versus the entire aircraft were also made. Aircraft symmetry was tested in terms of EMI patterns on GPS. The graphical analysis of mitigation techniques, which consists of sealing the door and exit seams as well as taping of windows, was performed of GPS and VHF systems. Following the graphical and statistical analysis, a detailed model involving Fuzzy logic was examined and analyzed.

9.2 Implications

The analysis of GS, TCAS, and VHF systems resulted in the conclusion that the regions of highest coupling are directly dependant on the distance of the coupled location from the location of the windows, doors and aircraft antenna. However, for GPS and LOC system, the coupling patterns were a little unpredictable. The reasoning behind the regions of coupling in these systems hinted toward the reflection effects from the aircraft's wings, as well as the cause of different polarizations. A very significant correlation was present between the conclusions from the graphical analysis versus those from just the statistical analysis. Also, it was determined that although tedious, costly and time consuming, it is very essential to take IPL measurements on the entire aircraft versus taking measurements on just the window locations. When analyzing just the window data, several incorrect conclusions could be made had the IPL data on the entire aircraft was not present.

The positive result from testing aircraft symmetry confirmed that it is not essential to take data on *both* the port and starboard side of the aircraft. Due to the similarities in the interior structure of the aircraft, the EMI patterns found on the port side of the aircraft resembled well to the patterns found on the starboard side. Also, another observation was made in terms of the test antenna used. Although it was hypothesized that the dipole antenna should have different results from a biconical antenna, the results, after adding the gain to the biconical antenna, showed that both antennae produced very similar IPL results. This observation will be beneficial because in future tests, a simple biconical

antenna may be used, which is much easier to transport, is cheaper, and resembles a real-world PED more closely due to its smaller size.

Another major analysis performed in this thesis included understanding the effects of shielding aircraft door and exit seams as well as taping aircraft windows with conductive film. The resulting drop in coupling levels due to the shielding techniques proved the fact that most of the waves emitted from the PEDs indeed transmit through the doors and windows and find their way to the aircraft antenna. Almost 10 to 15 dB drop was observed in the tested aircraft systems by both shielding and taping techniques, which demonstrated that the application of conductive films to aircraft windows might provide significant reduction in PED EMI coupling to aircraft radio systems.

Finally, the modeling using the Fuzzy system resulted in IPL patterns very similar to those generated for actual IPL data collected. A simple model of defuzzification was applied in the end, which showed the simplicity of the entire model. However, even with the several assumptions, and lack of knowledge about the structure of the aircraft, the results of the Fuzzy model seemed very promising.

9.3 Future Work

The analysis performed in this thesis was very tedious and time consuming as most of the collected IPL data was hand written by the test team and was not available readily to be imported into MATLAB. However, now that all the IPL data is preserved in extensive data files, even more analysis can be performed to understand the patterns in depth. Also, probability distribution analysis of IPL data will need to be performed to learn more characteristics of the available data. This will include learning which

distribution the data fits best. The findings from the statistical analysis should assist in defining the fuzzy expert system more precisely.

The schematics for B737-200 were recently obtained by the courtesy of Delta Airlines. Therefore, more precise measurements of wave propagations can be made for Fuzzy Modeling. With these measurements, systems such as GS and LOC, which are not located directly on top of the aircraft's fuselage may be considered. Also, the dimensions of the aircraft's wing will assist in determining the intensity of the reflections caused for antennae on higher altitude, i.e. the Localizer on the tip of the aircraft's tail.

More IPL data is scheduled to be collected in the near future. IPL data also needs to be analyzed on B747, a relatively larger aircraft with multi-seating levels. It is hoped that with larger sets of data and after the conformation of IPL patterns' repeatability in this research, much more complex modeling will be performed, involving neural networks. The eventual goal is to understand the causes of the higher coupling patterns precisely, such that the aircraft manufacturers can either redesign the aircraft, or use the various shielding techniques proposed to provide PED access to at least a few passengers onboard a commercial aircraft.

References

- [1] T. Accardi, "Use of Portable Electronic Devices Aboard Aircraft," Advisory Circular by Federal Aviation Administration. August 20, 1993.
URL: http://www.faa.gov/avr/afs/acs/91-21_1.txt
- [2] "Data Bandplans," Cellular Services by Federal Communications Commission. June 6, 2002.
URL: <http://wireless.fcc.gov/services/cellular/data/bandplan.html>
- [3] RF LINX Home of the Antennafier: "FCC Title 47 – Part 15: Radio Frequency Devices." October 1, 1998.
URL: <http://www.rflinx.com/FCC-PART15.html>
- [4] N. Lacey, "Use of Portable Electronic Devices Aboard Aircraft," Advisory Circular by Federal Aviation Administration. October 20, 2000.
- [5] Teara's dBm Conversion Table. "RF Power Table."
URL: <http://www.ipass.net/teara/dbm.html>
- [6] C. Irving, "Federal Aviation Administration Regulations." Scanning Reference. August 4, 1996.
URL: <http://www.panix.com/~clay/scanning/rules/airlines.html>
- [7] J. Beasley, "The dB in Communications." New Mexico State University, The Technology Interface, Fall 1996.
URL: <http://et.nmsu.edu/~etti/fall96/communications/db/db.html>
- [8] "RF Power Values," CISCO Systems Inc. 1992.

- [9] P. Ladkin, "electromagnetic Interference with Aircraft Systems: Why Worry?" University of Bielefeld. Article RVS-J-97-03. October 20, 1997.
- [10] T. Nguyen, S. Koppen, J. Ely, R. Williams, L. Smith and T. Salud, "Portable Wireless LAN Device and Two-Way Radio Threat Assessment for Aircraft Navigation Radios", NASA/TP-2003-212438, July 2003, pp. 73 – 82.
- [11] T. Nguyen and J. Ely, "Determination of Receiver Susceptibility to Radio Frequency Interference From Portable Electronic Devices", 21st Digital Avionics Systems Conference, Irvine, California, October 27-31, 2002.
- [12] T. Nguyen, S. Koppen, J. Ely, R. Williams, L. Smith and T. Salud, "Portable Wireless LAN Device and Two-Way Radio Threat Assessment of Aircraft VHF Communication Radio Band", NASA/TM-2004-213010, March 2004, pp. 29 – 32.
- [13] J. Abrams. "Experts Favor Cell Phone Bans on Planes, Despite Lack of Proff Risk Exists." NewsBank InfoWeb, Milwaukee Journal Sentinal. July 21, 2000.
- [14] B. Spice. "Signal Turbulence: As wireless gadgets multiply, so does the likelihood of interference with Aviation Systems." Post-Gazette. April 21, 2003.

URL: <http://www.post-gazette.com/healthscience/20030421pedsci2p2.asp>
- [15] R. Frenzel. "Portable Electronic Devices: Do they Really Pose a Safety Hazard on Aircraft?" Hearing by Air Transport Association. July 10, 2000.

URL: <http://www.air-transport.org/public/testimony/display2.asp?nid=880>

- [16] D. Johnson. "Portable Electronic Devices Onboard Aircraft." RTCA meeting. May 2003.
- [17] J. Engle. "Trying to clear the Static on using Electronics aloft." Chicago Tribune Online, June 29, 2003.
- [18] "Wireless PDA's in Flight" TurboWx. February 15, 2004
URL: <http://www.turbopilot.com/turbowx/Airborne%20Use.htm>
- [19] D. Hatfield, Hearing on Portable Electronic Devices to the Aviation. July 20, 2000.
URL: <http://www.house.gov/transportation/aviation/hearing/07-20-00/hatfield.html>
- [20] "Why Cell Phones are Banned During Airflights." Radiocommunications Agency EMC Awareness. 2001.
URL: <http://www.compliance-club.com/Radiocomms/pages/interexpl/aviation.htm>
- [21] The Subcommittee on Aviation Hearing on "portable Electronic Devices: Do they really pose a safety hazard on Aircraft." October 20, 2000.
URL: <http://www.house.gov/transportation/aviation/hearing/07-20-00/07-20-00memo.html>
- [22] T. Perry and L. Geppert. "Do Portable Electronics Endanger Flight?" IEEE Spectrum. 2003.
URL: <http://www.airnig.co.uk/emi.htm>
- [23] "Congress Reviews EMI Threat of PED Use on Aircraft." Newslines, Compliance Engineering Magazine. 2000.

URL: <http://www.ce-mag.com/archive/2000/sepoct/2000/sepoct/newsline.html>

- [24] J. McGovern, Press Release: "Statement of U.S. Representative James P. McGovern House Subcommittee on Aviation Hearing on Portable Electronic Devices." July 20, 2000.

URL: <http://www.house.gov/mcgovern/pr72000.htm>

- [25] D. Walen. "Flying with your Mobile Phone – What's the Problem?" Presentation by FAA. February 24, 2004.

- [26] "Portable Electronic Devices Carried on Board Aircraft." RTCA/DO-233. Prepared by SC-177. August 20, 1996.

- [27] "Report on Electromagnetic Compatibility Between Passenger Carried Portable Electronic Devices (PEDs) and Aircraft Systems." ED-118. EUROCAE. November 2003.

- [28] M. Jafri, J. Ely and L. Vahala, "Graphical and Statistical Analysis of Airplane Passenger Cabin RF Coupling Paths to Avionics", 22nd Digital Avionics Systems Conference, Indianapolis, Indiana, October 12-16, 2003.

URL: <http://techreports.larc.nasa.gov/ltrs/dublincore/2003/mtg/NASA-2003-22dasc-mj.html>

- [29] "MATLAB: User's Guide: High-Performance Numeric Computation and Visualization Software." Mathworks Inc. September 1993.

- [30] R. Walpole and R. Myers. "Probability and Statistics for Engineers and Scientists." 2nd Edition. New York: NY, 1978.

- [31] M. Jafri, J. Ely and L. Vahala, "Graphical Representation of the Effects of Antenna Locations on Path Loss Data", 2003 IEEE International Symposium on Antennas and Propagation, Columbus, Ohio, June 22-27, 2003.
- [32] M. Jafri, J. Ely and L. Vahala. "Fuzzification of Electromagnetic Interference patterns Onboard Commercial Airliners Due to Wireless Technology." IEEE International Antennas and Propagation Symposium, Monterey, CA June 20-26, 2004.
- [33] M. Jafri, J. Ely and L. Vahala. "Graphical Analysis of B-737 Airplane Pathloss Data for GPS and Evaluation of Coupling Mitigation Techniques." IEEE EMC, Santa Clara, CA. August 9 – 13, 2004.
- [34] CPFilms Company Website:
<http://www.cpfindusprod.com/shielding/emi.html>
- [35] Zadeh, L and R. Yager. "Fuzzy Sets, Neural Networks, and Soft Computing." VNR Publishing, 1994.

MADIHA J. JAFRI

EDUCATION

2003 - present	<i>Old Dominion University</i> (GPA 3.62)	Norfolk, VA
2001 - 2003	<i>Old Dominion University</i> (GPA 3.53)	Norfolk, VA
1999 - 2001	<i>Virginia Tech</i> (GPA 3.56)	Blacksburg, VA
<ul style="list-style-type: none">■ Bachelor of Science in Computer Engineering. (Minor: Electrical Engineering)■ Masters of Science in Electrical Engineering (August 2004).		

COMPUTER SKILLS

Software:

- MATLAB
- TechPlot
- PSpice, OrCad
- Lab View
- Rational Rose
- Office 97, 2000, XP
- Max + Plus II
- Microsoft VISIO
- Siemen's Step 7
- ARENA
- AutoCAD R-14, 2000
- Prog. Logic Devices (PLC Shell)
- Mechanical Desktop
- Wonderware's INTOUCH
- SAS (Statistical Analysis Software)

Operating Systems:

Windows 3.x, NT, 4.0, 95, 98, 2000, ME, XP, Dos 6.x, UNIX

Programming Languages:

HTML, C/C++ (Borland, Microsoft, UNIX), Perl, PIC Assembly (68HC11, OOPic), VHDL, Ladder Logic, JAVA

Programmable Logic Controllers (PLCs):

Siemens (Step7, OPC Server), Allen Bradley, Modicon, Hirschmann, Delta V

EXPERIENCE

September 2002 - Present	NASA Langley Research Center	Hampton, VA
<ul style="list-style-type: none">■ Assisted in Research on Electromagnetic Interference (EMI) due to Wireless Technology on board Commercial Airlines■ Used MATLAB to analyze and model data measured to determine EMI patterns through out aircrafts■ Applied Statistical Analysis on results to determine the likelihood of passengers to cause interference during flight■ In process of training Neural Networks to determine EMI patterns on aircraft based on doors, windows and antenna locations		
May - August 2001/ 2002	Philip Morris, USA	Richmond, VA
<ul style="list-style-type: none">■ Assisted in Designing, Programming and Construction of Machinery used for Sample Testing■ Obtained professional training on PLCs and Ladder Logic used in demos at several events in the facility■ Gained extensive knowledge in Networking, and Upgraded most hardware in a facility		

HONORS & ACTIVITIES

Scholarships/ Fellowships/ Grants:

- Graduate Student Research Proposal Grant (NASA)
- Virginia Space Grant Consortium (NASA)
- NASA Langley Research Student Scholar
- CSEM Scholarship (National Science Foundation)
- Bradley Scholarship for Computer Engineers (VT)
- ACCESS Scholarship (VT)
- PRATT Engineering Scholarship (VT)
- Pamplin Leadership Award / Scholarship (VT)

Activities:

- Member: National Society of Collegiate Scholars
- Member: Society of Women in Engineering
- Member: National Society of Professional Engineers
- Secretary: IEEE (2002-2003)
- Member: Muslim Student Assosication
- Member: Tau Beta Pi, Engineering Honor Society
- Virginia Tech's Honors Program
- Real Estate Business: House Construction & Renovation

PUBLICATIONS & PROCEEDINGS

- September 23 - 25, 2003: IEEE International Antennas and Propagation Symposium, Columbus, OH
"Graphical Representation of the Effects of Antenna Locations on Path Loss Data"
- October 12 - 16, 2003: 22nd Digital Avionics Systems Conference, Indianapolis, IN
"Graphical and Statistical Analysis of Airplane Passenger Cabin RF Coupling Paths to Avionics"
- September 20-26, 2004: IEEE International Antennas and Propagation Symposium, Monterey, CA
"Fuzzification of Electromagnetic Interference patterns Onboard Commercial Airlines Due to Wireless Technology"
- August 9 - 13, 2004: IEEE EMC, Santa Clara, CA
"Graphical Analysis of B-737 Airplane Pathloss Data for GPS and Evaluation of Coupling Mitigation Techniques"